Atomic Energy Control Board
P.O. Box 1046
Ottawa, Canada
K1P 5S9

Commission de contrôle de l'énergie atomique
C.P. 1046
Ottawa, Canada
K1P 5S9

INFO-0087

DOSIMETRY, MEASUREMENT AND PROPERTIES OF RADON DAUGHTERS AND THORON DAUGHTERS

by

C.R. Phillips
University of Toronto

A research report prepared for the
Atomic Energy Control Board
Ottawa, Canada

RESEARCH REPORT

March 1982

SUMMARY

Chapter 1

In uranium mines, the median size of the aerosol has been found to be about 0.1 micron or less. Such small aerosols are readily deposited or "plated-out" on dosimeter interior surfaces resulting in the recording of a low dose. The "plate-out" properties of the CEA alpha dosimeter head are described with respect to aerosol properties in controlled experiments in the laboratory. A simple model is derived to estimate the amount of "plate-out" in the CEA head. Fluctuations in the radon daughter concentration in the air being sampled are shown to result in greatly increased fluctuations in plate-out.

Chapter 2

Investigation of the traps in LiF:Mg, a multi-peak phosphor, was carried out using simple phosphorescence decay analysis. Half lives at room temperature of the trapping centres (peaks -1b, -1a, -1, 0, 1, 2, 3a and 3) in the phosphor after irradiation with α radiation were found to be 3 s, 5 s, 28 s, 4 min, 15 min, 1 h, 6 h and 2 d respectively.

Justification for the method of analysis is provided and the results of measurements compared with published data. The effects of pre-annealing at 400°C for 1 h and 80°C for 24 h on the trapping configuration and on the trapping efficiencies were also studied.

Chapter 3

Fluorescence, radioluminescence, phosphorescence and thermoluminescence in TLD 100 and 700 are discussed and compared. The energy

budget in thermoluminescent material is presented in general terms. Results of measurements of radioluminescence, phosphorescence and thermoluminescence in LiF:Mg irradiated with α radiation, using simple facilities, are presented. The calculated energy budget in the exposed chips using α radiation is compared to published data using γ irradiation.

Chapter 4

An energy discriminatory thermoluminescent (TL) dosimeter system based upon successive absorption of the energy cannot be used for monitoring mixed radon daughter and thoron daughter atmospheres because of the high uncertainty in the derived thoron daughter working level. Such a dosimeter system can be used for a pure radon daughter atmosphere provided that the certainties in the efficiency of the TL readings are kept below 10%. Important considerations in choosing the TL material are: (a) the α response per incident α particle for the TL material should be nearly constant, (b) the principle of additivity of α, β and γ exposures is valid.

Chapter 5

The aqueous solubility of the thermoluminescent phosphor is the most important indicator of its performance in humid air environments. Of the common phosphors, CaF_2 shows essentially no effect of humidity, whereas LiF and $CaSO_4$ show a slight effect. $Li_2B_4O_7$ shows a large effect and is unsuitable for use in humid atmospheres.

Chapter 6

The performance of personal alpha dosimeters in mixed radon daughter and thoron daughter atmospheres in Ontario uranium mines is described together with monitoring developments which enable the radon daughter working level to be determined separately. The theoretical bases for continuous and integrated working level measurements based on individual and gross counts are presented in terms of the weighting factor for combining the thoron daughter working level with the radon daughter working level, and in terms of the in-growth time of the air. Implications for the determination of working level in the presence of thoron daughters are discussed.

Chapter 7

Radon daughter measurement methods have not previously been fully optimized in the presence of thoron daughters, the presence of which leads to an increase in the total potential alpha energy. Taking into account the fluctuations associated with flow rate and concentration as well as the statistics of decay, optimized counting schemes were determined for the daughters of radon and thoron for different sampling times over a wide range of counting intervals. The counting schemes examined were optimized for maximum precision. Counting schemes corresponding to impractically long counting intervals, and counting times which required measurements beyond an 8 hr working shift were rejected. Under these constraints the most appropriate sampling time was found to be 10 min.

Chapter 8

An optimized counting scheme for a mixture of radon daughters and thoron daughters typical of Ontario mines, developed in the previous chapter, was experimentally examined under mine conditions. The counting scheme requires a 10 minute sample and 5 1/2 hours counting instead of a 60 minute sample and more than 40 hours counting as required by a previous method. Taking into account the uncertainties associated with concentrations, flowrate and radioactive decay, the precision of the counting scheme was analyzed and found to be on average better than the 40 hour method.

Chapter 9

The precision of radon daughter measurement techniques is a complicated function of uncertainties arising from concentration and flowrate fluctuations during sampling, counting statistics and many other factors. Optimization of a measurement technique requires that all these uncertainties - not just counting statistics - be considered. In this work, the optmization procedure of Busigin and Phillips (1980) is tested against Monte Carlo experiments for the case of the modified Tsivoglou method.

Chapter 10

To investigate the variability of the charged and unattached fractions of radon daughters in uranium mines, measurements were made in two uranium mines at Elliot Lake, Ontario. Non-diesel (electric) and diesel areas of 100% relative humidity were studied. For both mines,

the charged fraction was typically in the range of 2 to 10% and the unattached fraction was typically in the range of 0 to 2%.

Chapter II

For the purposes of measurement and dosimetry of airborne radon daughters in uranium mines and elsewhere, it is important to understand their physicochemical state. This work deals with the chemical fate of ^{218}Po in air. Extensive experiments were performed to determine the rate of neutralization, diffusion coefficient and fraction born charged of ^{218}Po in air. The experiments were performed in a specially constructed apparatus of well-defined geometry. Careful control of experimental conditions made it possible to obtain more precise and detailed quantitative data than previously possible.

RÉSUMÉ

Chapitre I

On a découvert que, dans les mines d'uranium, l'aérosol a une taille moyenne de 0,1 micron ou moins. Ces petits aérosols se déposent, "se plaquent" facilement sur les surfaces internes du dosimètre qui enregistre ainsi une faible dose. Les propriétés de placage de la tête du dosimètre alpha du Commissariat à l'énergie atomique (CEA) sont décrites en fonction des propriétés des aérosols au cours d'expériences contrôlées en laboratoire. À partir de là, on a établi un modèle simple qui permet d'évaluer la quantité d'aérosol plaquée dans la tête du dosimètre du CEA. Il appert que les fluctuations de concentration des produits de filiation du radon que l'on note dans les échantillons d'air se traduisent par des fluctuations de placage beaucoup plus marquées.

Chapitre 2

L'étude des pièges du LiF:Mg, phosphore à pics multiples, s'est faite par simple analyse de décroissance de la phosphorescence. On a ainsi découvert qu'à la température de la pièce, les périodes des pièges (pics -1b, -1a, -1, 0, 1, 2, 3a et 3) du phosphore après irradiation alpha étaient respectivement de 3 secondes, 5 secondes, 28 secondes, 4 minutes, 15 minutes, 1 heure, 6 heures et 2 jours.

La méthode d'analyse est vérifiée et les résultats des mesures sont comparées à des données publiées. On étudie également les effets de la recuisson à 400° C pendant une heure et à 80° C pendant 24 heures sur la configuration des pièges et sur l'efficacité du piégeage.

Chapitre 3

Ce chapitre comprend une étude et une comparaison de la fluorescence, de la radioluminescence, de la phosphorescence et de la thermoluminescence dans les dosimètres de thermoluminescence 100 et 700. Le bilan énergétique des matières thermoluminescentes est présenté en termes généraux. On trouve aussi les résultats de mesures de la radioluminescence, de la phosphorescence et de la thermoluminescence du LiF:Mg irradié aux rayons alpha, en utilisant des appareils simples. Le bilan énergétique calculé pour les éclats exposés aux rayons alpha est comparé à des données publiées sur l'irradiation gamma.

Chapitre 4

On ne peut utiliser un système de dosimètres thermoluminescents (TL) à discrimination énergétique par absorption successive d'énergie pour contrôler les atmosphères comportant un mélange de produits de filiation du radon et du thoron, à cause de l'incertitude dans l'évaluation du niveau d'activité correspondant aux produits de filiation du radon. Cependant, ce système de dosimètres peut servir dans une atmosphère comportant uniquement des produits de filiation du radon, pourvu que l'on soit certain que les erreurs de lecture soient inférieures à 10%. En choisissant le dispositif TL, il importe de tenir compte des faits suivants: (a) le dispositif TL devrait donner une réponse alpha presque constante à une particule alpha incidente, et (b) le principe selon lequel les expositions alpha, bêta et gamma s'ajoutent les unes aux autres est valable.

Chapitre 5

La solubilité aqueuse du phosphore thermoluminescent est le meilleur indice de son rendement dans un milieu atmosphérique humide. En ce qui concerne les phosphores communs, le CaF_2 comme tel ne montre aucune réaction à l'humidité, tandis que le LiF et le $CaSO_4$ y réagissent légèrement. Quant au $Li_2B_4O_7$, il réagit beaucoup à l'humidité et ne convient pas à des atmosphères humides.

Chapitre 6

Le chapitre 6 décrit le rendement des dosimètres alpha individuels dans les atmosphères mixtes de produits de filiation du radon et du thoron qui existent dans des mines d'uranium de l'Ontario, de même que les progrès en matière de contrôle qui permettent de déterminer séparément l'unité alpha (WL) des produits de filiation du radon. Le facteur de pondération relatif à la combinaison de l'unité alpha (WL) des produits de filiation du thoron et de celle des produits de filiation du radon et le temps de croissance dans l'air sont présentés comme les bases théoriques de la mesure continue et intégrée de l'unité alpha (WL) fondées sur le compte individuel et brut. On traite de ce que signifie la détermination de l'unité alpha (WL) en présence des produits de filiation du thoron.

Chapitre 7

Jusqu'à présent, on n'avait pas optimisé complètement les méthodes de mesure des produits de filiation du radon en présence de ceux du thoron qui accroissent l'énergie potentielle alpha globale. En tenant compte des fluctuations de débit et de concentration, de même que des données statistiques sur la décroissance,

on a pu établir des modèles de comptage optimaux pour les produits de filiation du radon et du thoron dans le cas de différents temps d'échantillonnage répartis sur une gamme étendue d'intervalles de comptage. Les modèles de comptage examinés ont été optimisés afin qu'ils procurent un maximum de précision. Les modèles de comptage correspondant à des intervalles de comptage que leur longueur rend impraticables et les temps de comptage qui nécessitaient des calculs dépassant une journée de travail de huit heures ont été rejetés. Compte tenu de ces contraintes, on a évalué que le meilleur temps d'échantillonnage était de 10 minutes.

Chapitre 8

On a fait l'essai, en milieu minier, du modèle de comptage optimal élaboré au chapitre précédent et utilisé pour un mélange de produits de filiation du radon et du thoron typique des mines de l'Ontario. Ce modèle de comptage nécessite 10 minutes d'échantillonnage et cinq heures et demie de comptage, au lieu de l'échantillonnage de 60 minutes et du comptage de plus de 40 heures qu'exigeait l'ancienne méthode. Étant donné que l'on connaît mal les concentrations, le débit et la décroissance radioactive, on a analysé le modèle de comptage pour en déterminer la précision et découvert qu'elle était meilleure, en moyenne, que celle de la méthode des 40 heures.

Chapitre 9

La précision des techniques de mesure des produits de filiation du radon est une fonction rendue complexe par l'incertitude que créent les fluctuations de concentration et de débit en cours d'échantillonnage, les données statistiques sur le comptage et de nombreux autres facteurs. L'optimisation d'une technique de mesure oblige à tenir compte de tous les éléments d'incertitude, plutôt que des seules données statistiques sur le comptage. Dans ce travail, la méthode d'optimisation Busigin et Phillips (1980) est confrontée aux expériences de Monte Carlo relativement à la méthode Tsivoglou modifiée.

Chapitre 10

Pour étudier la variabilité de fractions chargées et libres des produits de filiation du radon dans les mines d'uranium, des mesures ont été prises dans deux mines d'uranium d'Elliot Lake (Ontario). On a donc étudié des zones d'humidité relative de 100% où se trouve de la machinerie non diesel (électrique) et

d'autres où fonctionne de la machinerie diesel. Dans les deux mines, la fraction chargée variait en général de 2% à 10%, tandis que la fraction libre variait en général de 0% à 2%.

Chapitre 11

Aux fins de mesure et de dosimétrie des produits de filiation du radon en suspension dans l'air des mines d'uranium et ailleurs, il importe de comprendre leut état physico-chimique. Ce document traite du comportement chimique du Po^{218} en suspension. Des expériences exhaustives ont été effectuées pour déterminer le taux de neutralisation, le coefficient de diffusion et la fraction de Po^{218} chargée dès l'origine. Les expériences ont été effectuées dans un appareil qui a été spécialement construit à cet effet et dont la géométrie est bien déterminée. Le contrôle attentif des conditions de l'expérience a permis d'obtenir des données quantitatives plus précises et détaillées qu'auparavant.

DISCLAIMER

The Atomic Energy Control Board is not responsible for the accuracy of the statements made or opinions expressed in this publication and neither the Board nor the authors assume liability with respect to any damage or loss incurred as a result of the use made of the information contained in this publication.

TABLE OF CONTENTS

		Page No.
	SUMMARY	
CHAPTER 1.	RADIOACTIVE AEROSOL PLATE-OUT IN ALPHA DOSIMETER HEADS	1-1
	1.1 Introduction	1-1
	1.2 Experimental	1-2
	1.3 Theoretical	1-5
	1.4 Results and Discussion	1-9
	1.5 Conclusions	1-14
CHAPTER 2.	INVESTIGATION OF TRAPPING CENTRES IN THERMO-LUMINESCENT DOSIMETRY MATERIALS WITH APPLICATION TO LiF:Mg	2-1
	2.1 Introduction	2-1
	2.2 Theory	2-4
	2.3 Experimental Aspects	2-13
	2.4 Results	2-15
	2.5 Conclusions	2-22
CHAPTER 3.	INVESTIGATION OF RADIOLUMINESCENCE, PHOSPHO-RESCENCE AND THERMOLUMINESCENCE IN DOSIMETRY MATERIALS WITH APPLICATION TO LiF:Mg	3-1
	3.1 Introduction and Theory	3-1
	3.2 Experimental Details	3-4
	3.3 Results	3-5
	3.4 Summary and Conclusions	3-8

		Page No.
CHAPTER 4.	DESIGN CONSIDERATIONS FOR AN ENERGY DISCRIMINATORY THERMOLUMINESCENT DOSIMETER TO MEASURE SEPARATELY RADON DAUGHTERS AND THORON DAUGHTERS	4-1
	4.1 Introduction	4-1
	4.2 Design of an Energy Discriminatory TL System	4-1
	4.3 Efficiency of the Energy Discriminatory TL System	4-2
	4.4 TL Readout Procedure	4-7
	4.5 Uncertainty Analysis and Conclusions	4-11
CHAPTER 5.	THE EFFECT OF HUMIDITY ON THERMOLUMINESCENT MATERIALS	5-1
CHAPTER 6.	WORKING LEVEL MEASUREMENT OF RADON DAUGHTERS AND THORON DAUGHTERS BY PERSONAL DOSIMETRY AND CONTINUOUS MONITORING	6-1
	6.1 Introduction	6-1
	6.2 Dosimeter and Monitoring Developments	6-1
	6.3 Theoretical Procedure	6-6
	6.4 Results and Discussion	6-10
	6.5 Conclusions	6-15
CHAPTER 7.	AN OPTIMIZED SCHEME FOR MEASUREMENT OF THE CONCENTRATIONS OF THE DECAY PRODUCTS OF RADON AND THORON	7-1
	7.1 Introduction	7-1
	7.2 Analysis Technique	7-1
	7.3 Results	7-9
	7.4 Discussion and Conclusions	7-9

		Page No.
CHAPTER 8.	OPTIMIZED COUNTING INTERVALS FOR CONCENTRATION MEASUREMENT OF THE DECAY PRODUCTS OF RADON AND THORON IN A URANIUM MINE	8-1
	8.1 Introduction	8-1
	8.2 Experimental Procedure	8-3
	8.3 Data Analysis	8-5
	8.4 Discussion	8-7
	8.5 Conclusions	8-10
CHAPTER 9.	OPTIMIZATION OF RADON DAUGHTER MEASUREMENT TECHNIQUES	9-1
	9.1 Introduction	9-1
	9.2 Monte Carlo Simulation of Cascading Radioactive Decays	9-3
	9.3 Application of the Monte Carlo Method to Evaluate the Precision of the Modified Tsivoglou Method	9-4
	9.4 Conclusions	9-9
CHAPTER 10.	MEASUREMENT OF CHARGED AND UNATTACHED FRACTIONS OF RADON AND THORON DAUGHTERS IN TWO CANADIAN MINES	10-1
	10.1 Introduction	10-1
	10.2 Charged Fraction Measurements	10-1
	10.3 Unattached Fraction Measurements	10-3
	10.4 Conclusions	10-6
CHAPTER 11.	THE CHEMICAL FATE OF ^{218}Po IN AIR	11-1
	11.1 Introduction	11-1
	11.2 Experimental Investigation	11-1
	11.3 Theoretical Model for the Collection of ^{218}Po Species in an Electric Field	11-3

		Page No.
11.4	Calculation of Flux in a Positive Electric Field	11-5
11.5	Calculation of Flux in a Negative Electric Field	11-6
11.6	Calculation of Flux in Zero Electric Field	11-7
11.7	Calculation of Electric Mobility	11-8
11.8	Experimental Results	11-10
11.9	Discussion	11-14
11.10	Conclusions	11-15

REFERENCES

ACKNOWLEDGEMENTS

CHAPTER 1

RADIOACTIVE AEROSOL PLATE-OUT IN ALPHA DOSIMETER HEADS

1.1 Introduction

The energy discriminatory track etch alpha dosimeters produced by the Commissariat à l'Energie Atomique (CEA) of France are designed to monitor the exposures of workers to radon gas and its air-borne daughters in uranium mines. The chemical activity and the mobility of the daughters before attachment to airborne particles are both usually higher than the corresponding properties of radon itself. Radon daughters in the air can be depleted either by ventilation or by deposition from the gas phase onto solid surfaces in the mine. The ratio of the two mechanisms can vary from 1 to 100 depending on the degree of ventilation and the surfaces that are available for attachment (Holub and Droullard, 1980). Holub and Droullard (1979) studied the effects of condensation nuclei, humidity and turbulence on the plate-out of radon daughter activity on chamber walls. They found that the activity was not deposited on the walls by the turbulent flow from the fan but was deposited on the fan blades themselves.

The mechanisms that govern plate-out of aerosols include: deposition by convective diffusion, deposition by inertial mechanisms, collision, and coagulation. The particle size, d_p, at which convective diffusion is effective depends on the velocity and the external force fields and is usually in the range $d_p < 1$ µm. The efficiency of collection by diffusion for particles smaller than about 0.5 µm increases with decreasing particle size. Particles substantially larger than 1 µm are unable to follow the motion of an accelerating gas stream and deposit on

surfaces by inertial mechanisms. Particles smaller than about 1 μm may collide as a result of their Brownian motion or as a result of differential sedimentation, that is, the sweeping out of small particles by larger ones falling through them. Brownian motion controls for particles smaller than 1 μm.

The purpose of the present work is to estimate the extent of plate-out in the CEA dosimeter head. The particle size of aerosols used was less than 1 μm, consistent with the size of aerosols observed in uranium mines (Busigin, van der Vooren and Phillips, 1981).

1.2 Experimental

Figure 1 shows the internal aerosol plate-out surfaces in the CEA head. Plate-out was measured by comparison with open face filter sampling. The effect of pump speed was studied using MSA pumps (Model C-210). The flowrate through the dosimeters was varied over the range 0.01 L/min to 0.22 L/min, a range which spans the normal operating flowrate (0.05 L/min) of the dosimeter.

Zinc aerosols of median diameter 0.02 μm < d_p < 0.15 μm were generated and introduced into the radon chamber after passing through a Kr-85 neutralizer to remove any pre-existing charge. The experiments were performed in two ways. In the first procedure, six replicate samples were taken using three pumps: for the first part of the experiment, each pump was fitted with CEA dosimeter heads and allowed to run for 10 minutes of sample collection; for the second part of the experiment, the three pumps, each operating at a flowrate identical to its respective flowrate in the previous (dosimeter) measurements in the first part of the experiment were fitted with open face filter holders

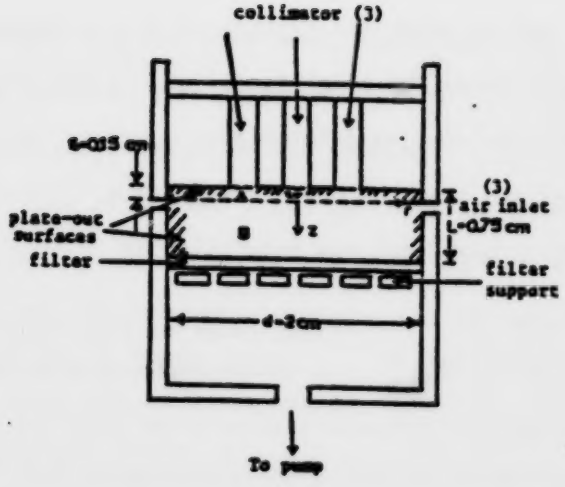

Figure 1. Schematic Diagram of the CEA Dosimeter Head.

and also allowed to run for the 10 minutes of sample collection. Thus the dosimeter and open face filter samples in the radon chamber were taken at different real times. In the second procedure, side by side measurements were taken with the dosimeter and the open face filter. The sampling time was also 10 minutes. The waiting time before counting was 5 minutes, and the (total alpha) counting time was 6 minutes. A 10 minute sampling time was chosen in order to accumulate enough counts to provide good counting statistics. The 5 minute waiting time was necessary to allow the CEA heads and filters to be disassembled for counting, and to allow the setting up of a consecutive experiment. Tri-mat counters (Model TM 372A) fitted with a ZnS scintillator and a photo-multiplier tube were used for alpha counting the filters from the dosi-meter heads and from the open face filters.

The % plate-out was calculated as

$$\% \text{ plate-out} = \frac{(\text{total count on open face filter}) - (\text{total count on CEA head})}{(\text{total count on open face filter})} \times 100\%$$

Diffusion battery measurements were made for activity size distributions and atmospheric concentrations of RaA, RaB and RaC inside the radon chamber according to the method of Busigin, van der Vooren and Phillips (1980). The unattached fraction was obtained using the wire screen method (van der Vooren, Busigin and Phillips, in press).

Experimental data on plate-out were compared with theoretical predictions based upon a simple model.

1.3 Theoretical

The CEA dosimeter head can be modelled in two regions: the region between the bottom of the collimator and the air inlet (region A), and the region between the air inlet and the filter (region B) (see Fig. 1). The following assumptions are made:

1. Diffusion is the dominant mechanism. Since the mean activity size is <1 μm, inertial deposition is unimportant.

2. Collection by electrostatic mechanisms is negligible. The unattached fraction was found to be very small, <0.2%. Although no measurements on charged fraction were made, it is expected to be small since the plate-out surfaces were grounded.

3. Collision and coagulation are ignored.

4. Laminar flow is assumed since the Reynolds number is <20.

5. The aerosol is described by its activity size distribution. In the experiments, the activity size distribution was measured, and the mean activity diameter determined.

6. The surface acts as a perfect absorber for the aerosols, that is, at the surface, the concentration is zero.

I. Region A - Stagnant Flow Condition

The diffusion equation is given by

$$0 = D_{iB} \frac{\partial^2 N_i}{\partial z^2} \qquad (1)$$

where N_i = activity size distribution function

$i = 1$ for RaA; $i = 2$ for RaB; and $i = 3$ for RaC

D_{iB} = diffusivity of i-member of radon decay chain through air, cm^2/s

$= 1.15 \times 10^{-15}(2r)^{-1.95}$ for $0\ \mu m < 2r < 1\ \mu m$ (Friedlander, 1977)

z = axial coordinate

r = activity size, cm

The boundary conditions are

at $z = 0,\ N_i = 0$

$z = \delta,\ N_i = N_{i\infty}$

where δ = thickness of the stagnant region, cm

A solution is obtained as

$$N_i = N_{i\infty} \frac{z}{\delta} \tag{2}$$

The mass transfer rate in the region A is then given by

$$\left|(M_i)_A\right| = 2.98 \times 10^{-16} \frac{\pi}{\delta} N_{i\infty} \int_{r_1}^{r_2} r^{-1.95} N_{i\infty}(r)dr \tag{3}$$

where $(M_i)_A$ = mass transfer rate in region A, atoms/s.

II. Region B - Laminar Flow through Short Pipe

Since the Schmidt number is very large, $\sim 10^4$, a thin concentration boundary layer exists. The convective diffusion equation for the region near the surface becomes:

$$u \frac{\partial N_i}{\partial z} = D_{iB} \frac{\partial^2 N_i}{\partial r^2} \tag{4}$$

where u = velocity, cm/s

r = radial coordinate measured from the surface.

The boundary conditions are:

at $r = 0,\ N_i = 0$

at $r = \infty,\ N_i = N_{i\infty}$

Axial diffusion is negligible since the Peclet number is large, $\sim 10^4$.

A solution to equation (4) is given by Friedlander (1977) as:

$$Sh_i = 1.077 \left[Re_i \, Sc_i \, \frac{d}{z} \right]^{1/3} \tag{5}$$

where Sh_i = Sherwood number, $\frac{k_z d}{D_{iB}}$

Re_i = Reynolds number, $\frac{u_{av} d}{\nu}$

Sc_i = Schmidt number, $\frac{\nu}{D_{iB}}$

d = diameter of the pipe, cm

ν = kinematic viscosity, cm^2/s

k_z = local mass transfer coefficient, cm/s

u_{av} = average flow velocity, cm/s.

A similar solution is obtained by Lévêque (1928):

$$Sh_i = 1.615 \left[Re_i \, Sc_i \, \frac{d}{z} \right]^{1/3} \tag{6}$$

Equation (6) is used to obtain the mass flux

$$|J_i| = D_{iB} \left| \frac{\partial Q_i}{\partial r} \right|_{r=0}$$

$$= 1.615 \frac{D_{iB}}{d} \left[Re_i \, Sc_i \, \frac{d}{z} \right]^{1/3} Q_{i\infty} \tag{7}$$

The mass transfer rate in region B is given by

$$|(M_i)_B| = 3.396 \times 10^{-10} \, L \left[\frac{d^2 u_{av}}{L} \right]^{1/3} N_{i\infty} \int_{r_1}^{r_2} r^{-1.3} \, n(r) dr \tag{8}$$

where $(M_1)_B$ = mass transfer rate in region B, atoms/s

L = length of the tube (dosimeter), cm

d = diameter of the tube (dosimeter).

The total mass transfer rate to the surface is thus obtained as

$$M_1 = |(M_1)_A| + |(M_1)_B| \tag{9}$$

In order to compare with the experimental results, the build-up on the surface in the sampling time and the decay after sampling have to be considered. Raabe and Wrenn (1969) have solved the build-up and decay equations for radon daughters. The total α-disintegrations in a given counting period are given by

$$A = \bar{N}_1 \left[- \left(1 + \frac{R_2}{\lambda_1}\right) R_4 - \frac{R_1 R_5}{\lambda_2} + \frac{(R_1 + R_2)}{\lambda_3} R_6 \right] + \bar{N}_2 \left[- \frac{R_3 R_5}{\lambda_2} + \frac{R_3 R_6}{\lambda_3} \right] + \bar{N}_3 \left[-R_6 \right] \tag{10}$$

where A = total α-disintegrations in a given counting period

λ_i = decay constant, min^{-1}

$$R_1 = \frac{\lambda_1 \lambda_2 \lambda_3}{(\lambda_1 - \lambda_2)(\lambda_3 - \lambda_2)}$$

$$R_2 = \frac{\lambda_1 \lambda_2 \lambda_3}{(\lambda_1 - \lambda_2)(\lambda_1 - \lambda_2)}$$

$$R_3 = \frac{\lambda_2 \lambda_3}{\lambda_3 - \lambda_2}$$

$$R_4 = e^{-\lambda_1 \beta} - e^{-\lambda_1 \alpha}$$

$$R_5 = e^{-\lambda_2 \beta} - e^{-\lambda_2 \alpha}$$

$$R_6 = e^{-\lambda_3 \beta} - e^{-\lambda_3 \alpha}$$

α = the beginning of a counting interval, min

β = the end of a counting interval, min

$\bar{N}_i$ = number of atoms of i-isotope on the surface at the end of the sampling period.

The $\bar{N}_i$ are given by

$$\bar{N}_1 = \frac{M_1}{\lambda_1}(1 - e^{-\lambda_1 T})$$

$$\bar{N}_2 = \frac{(M_1 + M_2)}{\lambda_2}(1 - e^{-\lambda_2 T}) + \frac{M_1}{(\lambda_2 - \lambda_1)}(e^{-\lambda_2 T} - e^{-\lambda_1 T})$$

$$\bar{N}_3 = \frac{(M_1 + M_2 + M_3)}{\lambda_3}(1 - e^{-\lambda_3 T}) + \frac{(M_1 + M_2)}{(\lambda_3 - \lambda_2)}(e^{-\lambda_3 T} - e^{-\lambda_2 T})$$

$$+ \frac{M_1\lambda_2}{(\lambda_2 - \lambda_1)(\lambda_3 - \lambda_1)}(e^{-\lambda_3 T} - e^{-\lambda_1 T})$$

$$+ \frac{M_1\lambda_2(e^{-\lambda_2 T} - e^{-\lambda_3 T})}{(\lambda_2 - \lambda_1)(\lambda_3 - \lambda_2)} \qquad (11)$$

where T = sampling period, min.

The plate-out can therefore be obtained as:

$$\% \text{ plate-out} = \frac{A}{\text{total counts on open face filter corrected for counter efficiency}} \times 100\% \qquad (12)$$

The diffusivities for RaA, RaB and RaC are functions of the respective particle diameters. Busigin, van der Vooren and Phillips (1981) found that the mean activity sizes for RaA, RaB and RaC were almost the same in the mine. The diffusivities can then be estimated from the mean activity size assuming that all of the radon daughters attach to the aerosols.

1.4 Results and Discussion

Detailed experimental and theoretical results on the plate-out of attached radon daughters inside the CEA dosimeter head are presented

in the Appendix. Figure 2 shows the effects of the pump speed and the mean activity size on the plate-out of attached radon daughters. Each data point represents the average of six repeated experiments. Since the experimental data are scattered, the effect of mean activity size is uncertain. This uncertainty is due to difficulty in controlling the aerosol size distribution within the radon chamber. The activity size varies locally and from time to time.

The data points are fitted by least mean squares (solid line in Figure 2). The maximum plate-out is 15%; plate-out decreases as the pump speed is increased. At the normal operating pump speed (0.05 L/min), plate-out is estimated to be 13% (higher than would be expected theoretically).

The theoretical results for particle sizes corresponding to those determined in the experiments (and listed in Table 1) show little plate-out on the surface due to diffusion (dotted line in Figure 2). Figure 3 is a more detailed representation of the theoretical data. The maximum calculated plate-out is 6%. The discrepancy between the experimental and theoretical results is in part due to the large uncertainty in the low flowrates, in part due to local and transient variations of the activity size and bulk concentrations of RaA, RaB and RaC inside the radon chamber, in part due to the statistical nature of the counting process, and in part due to the assumptions used in the theoretical analysis. In the analysis of the effect of fluctuations in radon concentration and pump speed on percent plate-out (Fig. 4), it is found that a given change in concentration affects the measurement of plate-out to a much larger extent than the same percent change in pump speed. A 5% change

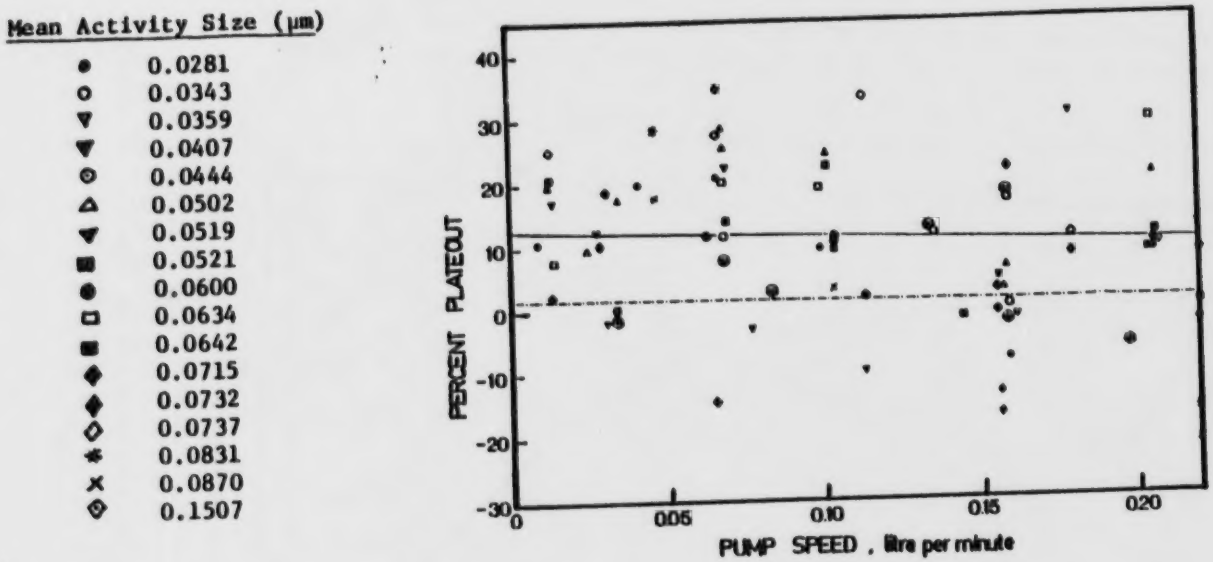

Figure 2. The effect of pump speed and mean activity size on the plate-out of attached radon daughters inside the CEA dosimeter head. (———) experimental; (- - - -) theoretical.

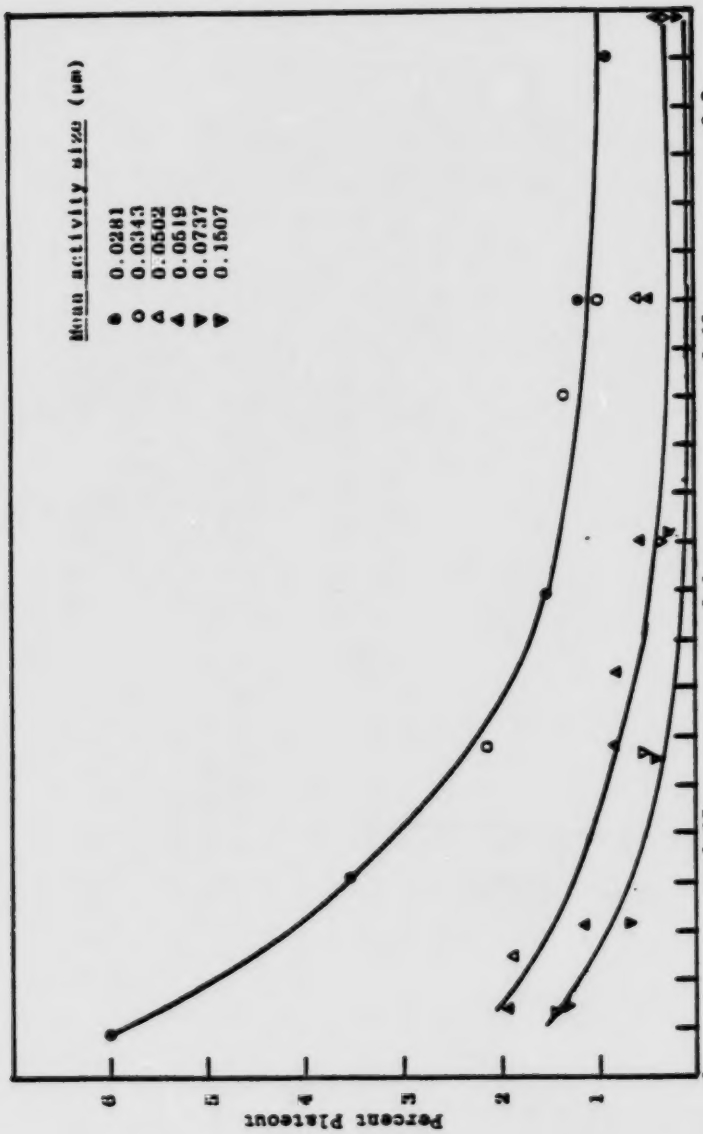

Figure 3. The effect of pump speed and mean activity size on the plate-out of attached radon daughters inside the CEA dosimeter head (theoretical results).

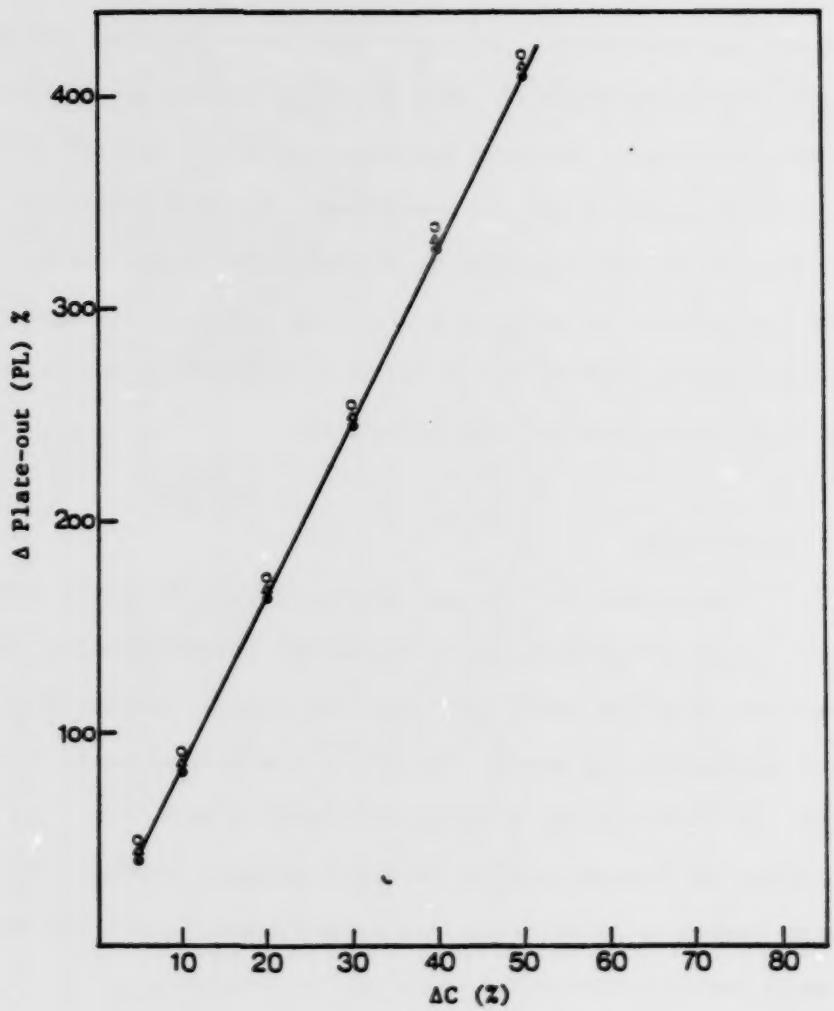

Figure 4. Effect of fluctuations in radon daughter concentration and pump speed on % change in plate-out.

in radon daughter concentration and a 10% change in pump flow both result in a 40% change in percent plate-out. For aerosols, the change in percent plate-out should be proportional to the change in aerosol concentration; however, for radioactive aerosols measured by count rate, the effect is much more pronounced because of the decay. The uncertainty resulting from the concentration fluctuations could account for the discrepancies between the experimental and theoretical data. Further, Brownian coagulation inside the dosimeter head may exist so that the inertial mechanism becomes important. Detailed investigation of the possible effect of Brownian coagulation was not undertaken. At the surface, the recoil energies of RaA and RaB might be sufficient to detach the host aerosol from the surface, at which an equilibrium concentration may develop. Such a process, however, would result in a lower concentration gradient and thus lower plate-out than calculated.

1.5 Conclusions

Theoretical calculations predict little plate-out (6%) on the inner dosimeter surfaces due to diffusion. Experimentally, the maximum plate-out found was about 15%. The data show a decrease in plate-out with increasing pump speed. Because of the scattering in the experimental data, the effect of the mean activity size is uncertain. The effect on plate-out of fluctuations in the radon daughter concentration in the radon chamber is shown to be very large; concentration fluctuations make a major contribution to the experimental uncertainty.

APPENDIX

TABLE 1. Experimental and Theoretical Results on Plate-out of Attached Radon Daughters in the CEA Dosimeter Head

Expt. No.	Mean Activity Size (μm)	Activity Size (μm)			Concentration (pCi/L)			Pump Speed (L/min)	Open[1] Face Count	% Plateout	
		RaA	RaB	RaC	RaA	RaB	RaC			Experimental	Theoretical
1	0.0343	0.0390	0.0380	0.0282	250.1	189.3	162.6	0.068	3151	11.3	2.14
								0.14	8499	11.8	1.31
								0.16	6585	0	0.98
								0.16	9676	16.9	0.89
2	0.0502	0.0194	0.0514	0.0591	213.2	140.4	91.1	0.025	867	9.1	1.88
								0.068	2615	25.1	0.84
								0.16	5228	2.6	0.54
3	0.0444	0.0242	0.0505	0.0498	290.7	154.6	113.0	0.034	1774	-1.9	1.69
								0.068	2903	7.9	1.26
								0.083	3723	2.9	1.00
								0.13	7037	12.5	0.63
								0.16	6941	17.7	0.68
								0.16	6226	-2.7	0.76
								0.20	6377	-6.5	0.79
4	0.0281	0.0222	0.0317	0.0247	237.6	191.2	166.4	0.0098	880	10.2	6.00
								0.041	2166	19.4	3.56
								0.066	5244	20.9	1.68
								0.099	6525	9.2	1.52
								0.16	10008	-8.7	1.14
								0.21	13676	8.3	0.90

Expt. No.	Mean Activity Size (μm)	Activity Size (μm)			Concentration (pCi/L)			Pump Speed (L/min)	Open[1] Face Count	% Plateout	
		RaA	RaB	RaC	RaA	RaB	RaC			Experimental	Theoretical
5	0.0519	0.0509	0.0549	0.0493	270.8	204.8	164.6	0.014	1197	17.8	1.92
								0.031	2525	-1.1	1.14
								0.077	4527	-3.0	0.83
								0.11	7539	-9.2	0.56
								0.16	10624	5.2	0.44
								0.18	17206	30.9	0.28
								0.22	14676	12.9	0.35
6	0.1507	0.0957	0.0227	0.1653	403.8	144.3	81.6	0.014	1076	3.0	1.35
								0.031	2580	19.3	0.70
								0.065	4885	-13.6	0.46
								0.11	7246	2.2	0.36
								0.18	15785	8.4	0.19
								0.22	17783	8.8	0.18
7	0.0737	0.0284	0.0732	0.1141	301.0	172.0	71.5	0.013	736	26.0	1.45
								0.066	3331	28.0	0.51
								0.11	6179	34.2	0.32
								0.18	10054	11.5	0.23
								0.22	10059	-2.5	0.24
8	0.0642	0.0399	0.0586	0.0752	354.9	189.2	93.6	0.012	1107	21.7	1.24
								0.034	2469	0.77	0.75
								0.069	4427	14.3	0.52
								0.10	6726	22.8	0.38
								0.21	14379	11.9	0.22
								0.23	16233	0.63	0.20
9	0.0359	0.0207	0.0193	0.2607	455.0	281.8	160.8	0.028	2205	12.4	2.55
								0.068	5144	35.2	0.34
								0.10	6499	10.3	0.30
								0.16	11489	22.2	0.19
								0.21	13825	9.9	0.18

Expt. No.	Mean Activity Size (μm)	Activity Size (μm)			Concentration (pCi/L)			Pump Speed (L/min)	Open[1] Face Count	% Plateout	
		RaA	RaB	RaC	RaA	RaB	RaC			Experimental	Theoretical
10	0.0732	0.0354	0.0714	0.1087	252.6	171.0	92.1	0.028	2192	11.0	0.61
								0.068	5144	35.2	0.34
								0.10	6499	10.3	0.30
								0.16	11489	22.2	0.19
								0.21	13825	9.9	0.18
11	0.0407	0.0240	0.0373	0.0726	430.1	299.4	178.3	0.012	1141	20.9	2.88
								0.034	2780	17.9	1.56
								0.066	4900	28.8	1.08
								0.10	6723	24.6	0.89
								0.16	11507	6.5	0.60
								0.21	14074	20.6	0.53
12	0.0634	0.0478	0.0646	0.0752	251.8	168.2	121.4	0.014	972	8.2	1.42
								0.068	3770	21.4	0.58
								0.099	4576	19.8	0.54
								0.21	10656	29.5	0.29
13[2]	0.0831	0.0584	0.0897	0.1011	431.6	291.1	198.0	0.047	1829	28.4	0.84
								0.103	3405	9.9	0.58
								0.239	6521	-17.0	0.39
14[2]	0.0840	0.1108	0.0794	0.0713	367.6	364.3	287.8	0.047	3622	17.5	0.75
								0.103	9522	3.0	0.37
								0.239	16163	-22.2	0.28
15[2]	0.0600	0.0498	0.0718	0.0618	493.8	374.4	293.4	0.063	6662	11.2	0.52
								0.103	9508	10.0	0.43
								0.265	19977	15.5	0.27
								0.497	32625	-29.4	0.21

Expt. No.	Mean Activity Size (μm)	Activity Size (μm)			Concentration (pCi/L)			Pump Speed (L/min)	Open[1] Face Count	% Plateout	
		RaA	RaB	RaC	RaA	RaB	RaC			Experimental	Theoretical
16[2]	0.0521	0.0515	0.0641	0.0668	516.1	371.7	271.7	0.144	8765	-1.6	0.58
								0.203	16694	8.0	0.34
17[2]	0.0775	0.0779	0.0657	0.0680	397.1	312.4	250.6	0.155	4352	-0.46	0.97
								0.157	4000	-16.1	1.06
								0.157	4183	2.5	1.01
								0.159	3987	-13.5	1.07

[1] The CEA dosimeter filter count is not shown but can be obtained from this column and the experimental % plateout column using the definition:

$$\% \text{ Plateout} = \frac{(\text{total count on open face filter}) - (\text{total count on CEA head})}{(\text{total count on open face filter})} \times 100\%$$

[2] Measurements were made simultaneously on the CEA dosimeter and the open face filter operated side by side; measurements for experiments 1-12 were made using first the dosimeter and then the open face filter.

CHAPTER 2

INVESTIGATION OF TRAPPING CENTRES IN THERMOLUMINESCENT DOSIMETRY MATERIALS WITH APPLICATION TO LiF:Mg

2.1 Introduction

Thermoluminescence is commonly used as a technique for recording integrated gamma dose in environmental surveys and in occupational health and safety. Although thermoluminescence has also been applied to record working level from radon daughters in uranium mines and related areas, less is known about its alpha dose-response characteristics than about its gamma dose-response characteristics. This work is aimed at broadening the alpha response data base.

Of the many thermoluminescent materials available, LiF is the most widely used. LiF:Mg, (TLD 100 or TLD 700 from Harshaw), which contains Mg as a modifier, has been investigated by many workers. Data on the activation energy, E, and on the frequency factor, S, of the various traps in LiF:Mg and in other phosphors may be derived from the Randall-Wilkins basic thermoluminescent glow curve equation (Randall and Wilkins, 1945). This equation is based on a one trap model and assumes that the retrapping process is negligible compared to the detrapping process, that is, that the kinetics involved are first order. Further, thermal quenching is not taken into account. The Randall-Wilkins equation is:

$$\phi(T) = Ch(t_1) \quad (T) \exp\left[- \frac{1}{q} \int_{T_1}^{T} \alpha(T')dt' \right] \qquad (1)$$

where $\alpha(T)$ is the transfer probability given by

$$\alpha(T) = S \exp\left[-\frac{E}{kT}\right] \tag{2}$$

The light intensity has a maximum at T_m. The following relation between E, T_m and S is easily derived:

$$\frac{E}{kT_m^2} = \frac{S}{q}\left[-\frac{E}{kT_m}\right] \tag{3}$$

Equation (3) holds for a constant heating rate, q, where $T = T_1 + qt$. For a hyperbolic heating rate, q', where $1/T = 1/T_1 - q't$, equation (3) simplifies to:

$$\frac{E}{k} = \frac{S}{q'} \exp\left[-\frac{E}{kT_m}\right] \tag{3a}$$

or equivalently

$$E = (1.461\ kT_{i_2}\ T_m)/(T_m - T_{i_2}) \tag{3b}$$

where T_{i_2} is the temperature at which the thermoluminescent intensity reaches half of its maximum value.

For the special case of $q = 0$, the phosphor is held at constant temperature T, and the number of filled traps h(t) decays exponentially with time:

$$h(t) = h(t_o) \exp(-\alpha t) \tag{4}$$

where t_o is the time at the end of the irradiation of the phosphor. Therefore, a phosphor kept at a constant temperature T gives a delayed luminescence as a result of the recombination of the detrapped carriers with emitting centres. This luminescence which decays exponentially with time, according to equation (4), is called phosphorescence. Equation (4) can be written as

$$-\frac{1}{t}\ln\left[\frac{h(t)}{h(t_o)}\right] = S\exp\left[-\frac{E}{kT}\right] \qquad (4a)$$

The parameters E and S of the individual traps have been determined by applying the basic thermoluminescent glow curve, equation (1), or its derivatives, equations (2)-(4), directly to the experimental glow curves or to their derivatives.

Garlick (1949), Harris and Jackson (1970a) and Webb (1967) plotted theoretical thermoluminescent glow curves for a constant heating rate. From a comparison of the experimental glow curve with the theoretical one, approximate values for E and S were determined. This method is known as the glow curve method.

Another well-known method (Webb, 1967; Zimmerman and Cameron, 1966; and Gorbics et al., 1967) is the so-called isothermal decay method. The phosphors are kept at a constant temperature, T, for a variable time, t, then read, and the relative peak height or the total output light measured. Comparison of the relative peak height or the relative total light output with the theoretical value (equation (4) or (4a)) allows E and S to be determined.

Moran and Podgorsak (1971), Zimmerman and Cameron (1966) and others (Webb, 1967; Ziniker et al., 1973) used the peak shape method to determine the parameters E and S. Measurement of the relative peak height of the total light output for different temperatures yields values of E and S. From a plot of the relative peak height or the total light output vs 1/T, values of E and S are derived using equation (4) or equation (4a). Mayhugh et al. (1970) used the peak shape method to determine the values of E and S for peak 5 in TLD 100.

Another method is based on the variation of T_m with the heating rate. Using equation (3), the constants E and S can be determined by measuring the temperatures of the maximum emissions at various heating rates. Thus Moran and Podgorsak (1971) analyzed the data of Gorbics et al. (1967) to determine values of E and S for peak 5 of LiF:Mg. Hickmott (1972) used a hyperbolic heating rate and applied equation (3a) to determine values of E and S for some of the peaks of rf-sputtered SiO_2 films deposited on silicon.

Hill and Schwed (1955) calculated the activation energy E in sodium chloride from the initial rise of the glow peak, using the relation

$$\ln \phi = -\frac{E}{kT} + \text{constant}$$

which is a good fit to the rise of the glow curve. This method is called leading edge analysis.

Evaluation of the trapping parameters can also be made from conductivity glow curves (Nicholas and Woods, 1964); instead of measuring the thermoluminescent emission, the electrical conductivity is measured. From the resultant plot of the current vs temperature (called the thermally stimulated current or conductivity glow curve), the parameters E and S can be derived.

2.2 Theory

The methods described above are subject to a number of uncertainties. They assume measurement of one peak, whereas because of the complexity of the thermoluminescent glow curve, the measurement is a superposition of several peaks. This complexity is particularly troubling in

the LiF:Mg case, in which about 14 peaks are found in the range of temperature between 30°C and 400°C. It is evident that the larger the number of glow peaks, the more difficult it is to determine the thermoluminescent kinetics. Much work has been carried out in order to try to resolve close peaks by annealing and by bleaching processes, by using a slow heating rate, and by optical repopulation; complete resolution is impossible. Podgorsak et al. (1971) and later Cooke (1978) identified the peaks in LiF:Mg but an inevitable discrepancy is found between their results. Podgorsak et al. reported a peak at 375 K, which Cooke could not resolve in the regular glow curve, although he could in a photobleached glow curve. Further, while Podgorsak et al. reported a large peak at 267 K, Cooke reported three peaks at 235, 250 and 270 K. Fairchild et al. (1978) used special apparatus to measure simultaneously the light intensity, the temperature of the phosphor and the emitted wavelength, and through the kinetic equations describing each glow peak were able to determine the kinetic parameters E and S in TLD 100. As thermal quenching is not taken into account because of its complexity, any method which uses a variable temperature is subject to a further uncertainty: if thermal quenching of a certain band occurs at a temperature T which is in the range of the experimental temperatures, emission from that band is partially eliminated giving rise to misleading interpretation. The variations of the phosphor temperature with time, the actual heating rate, q, the maximum temperature, T_m, and other parameters are difficult to determine, and allow large uncertainties to be introduced in the determination of E and S. Even after isolation of a single peak and assessment of relevant parameters, it is still a complex process to determine values of E and S, primarily because of lack of sensitivity to variation in S. Table 1 shows data for LiF:Mg

Table 1

Summary of LiF Data from Previous Investigators

PEAK NUMBER	I « 1 » α: 2^{π}s T_m(°c)	E(ev)	$t_{1/2}$	II «1,2,3» α: 2πs T_m(°c)	E(ev)	S(s⁻¹)	III « 2 » E(ev)	S(s⁻¹)	$t_{1/2}$(25°)	$t_{1/2}$(37°)	$t_{1/2}$(124°)	$t_{1/2}$(136°)
-4												
-3												
-2												
-1b -1a -1												
0												
1	65	0.9	5min									
2												
3a				—	--	---						
3	120	1.04	20h									
4	160	1.11	20d				1.19±0.05	140^{+}-540^{++}	[7-433y] 6.85y	1.25y	0.77h	0.285h
5	195	1.19	12 y	220	[9-2300 y] 1.25±0.07	$8\times10^{+}$	1.25±0.05	540^{+}-4410^{++}	[80-220 y]		5.25h	2.33h
5a												
6	210	1.25	150y				2.3	[$\geq 1.0^{5}$y] 1×10^{22}				
7												
8												
9												
10												
11												

Table 1 (continued)

PEAK NUMBER	IV «2,4» T_m(°C)	IV «2,4» $E_{(ev)}$	IV «2,4» q = 25% $S_{(s)}$	V «2» T_m (°C)	V «2» $t_{1/2}$	VI «3,4» T_m (°C)	VI «3,4» $E_{(ev)}$	VI «3,4» q = 35% $S_{(s)}$	VII «3» T_m(°C)	VII «3» $E_{(ev)}$	VII «3» q = 1340% $S_{(s)}$	VIII «3» $E_{(ev)}$
4												
3												
2												
-1b -1a -1												
0												
1				80	5 mn	59	[55mn] 1.16	3×10^{15}				
2				105	10 h	102	[55 d] 1.47	5×10^{18}	57	[10 d] 1.1	1×10^{13}	
3a												
3				118	0.5 y	137	[31 y] 1.77	4×10^{21}	137	[2,3y] 1.21	1×10^{13}	
4				160	7 y							
5	235	1.25	[304y] $226\,10^{11}$	195	80y	183	[36×10^{2}y] 2.2 ± 0.2	$1\times10^{23\pm2}$	197	[3.7×10^{-5}] 1.97	1×10^{20}	1.24±0.7
5a												
6				230	–							
7												
8									265	1.96	1×10^{17}	
9												
10												
11												

Table 1 (continued)

PEAK NUMBER	IX $s=\ q=s\,T_{stab}$	X $s=\ q=s\,T_{stab}$		XI $s=1.1\times$		$q=10^{13}\,T_{stab}$
	T_m(°C)	T_m(°C)	T_m^+(°C)	T_m(°C)	E (ev)	S (s^{-1})
-4	-128 (t_{stab}=30min at 75°C)	-131	-133			
-3	-109	-117	-118			
-2	-88	-84	-82			
-1b		-38				
-1a	-6	-23	-20			
-1		- 3	+ 5			
0	14	13	-			
1	59	53	46	62	[2.2h] 1.04	1×10^{16}
2	102	-	90	94	[31d] 1.07	1×10^{13}
3a				112	[112d] 0.987	1×10^{11}
3	137	137	129	137	[140d] 1.05	1×10^{11}
4	164	162		170	[310By] 1.54	4×10^{13}
5	186	182	175	190	[1.6×10^8 y] 2.2	1×10^{12}
5a				210	[2×10^8 y] 1.61	1×10^{15}
6				235	[7.5×10^7 y] 1.7	1×10^{14}
7				260	[27×10^8 y] 1.79	1×10^{15}
8				285	[4.9×10^10 y] 1.96	5×10^{15}
9				315	[6.6×10^10 y] 2	1×10^{16}
10				345	[2.4×10^14 y] 2.19	1×10^{16}
11				370	2.27	1×10^{16}

Code for References

I Harris and Jackson (1970a)
II Webb (1967)
III Zimmerman, Rhymer and Cameron (1966)
IV Gorbics, Attix and Pfaff (1967)
V Zimmerman and Cameron (1964)
VI Moran and Podgorsak (1971)
VII Ziniker, Rusin and Stoebe (1973)
VIII Mayhugh, Christy and Johnson (1970)
IX Podgorsak, Moran and Cameron (1971)
X Cooke (1978)
XI Fairchild, Mattern, Langweiber and Levy (1978b)

Code for Methods

1 Glow Curve Method
2 Isothermal Decay Method
3 Peak Shape Method
4 Variation of T_m with q
5 Others

Footnotes

[ ] $t_{\frac{1}{2}}$ values calculated from E and S values = $t_{\frac{1}{2}} = \frac{\ln 2}{S} \exp\left(-\frac{E}{kT}\right)$

T_m^+ from photobleached curves

peaks as published by various investigators. Some discrepancies exist, particularly in values of S.

To overcome difficulties encountered in the methods described above, it was determined in the present work that emissions at constant temperature could be used to identify trapping centres and to determine their half lives.

According to the Randall-Wilkins formula (equation (4)), the number of filled traps, h(t), decays exponentially with time when temperature is kept constant. As the thermoluminescent output, I(t), is proportional to h(t), the same exponential decay applies:

$$I(t) = I(o) \exp\left[- S \exp\left[-\frac{E}{kT}\right] t\right] \qquad (6)$$

where I(o) is the light intensity at time t = 0. Therefore, irradiated thermoluminescent material emits some light at constant temperature (called phosphorescence if T is room temperature (Mayhugh et al., 1970; Fairchild et al., 1978). The mean half-life of the trap is

$$\tau = \frac{1}{S} \exp\left[\frac{E}{kT}\right] \qquad (6a)$$

The total light output of the thermoluminescent material at constant temperature is the sum of contributions from the various traps each decaying exponentially with time. This light can in principle be resolved into separate peaks by a simple decay analysis. In the series of measurements conducted here, the total light output vs time is measured using a manual Harshaw reader. Since the phosphor is held at constant temperature, quenching is not a problem. It is however necessary to justify the assumption of first order kinetics and to ascertain that

emission spectra from the various traps are identical or at least that the response of the reader is the same to all emissions.

First order kinetics are observed when the intensity of the thermoluminescence is proportional to the concentration of thermally released charges, that is,

$$I = (\text{constant}) \cdot \frac{dh}{dt} = -\alpha h \tag{7}$$

If the thermally released charges are retrapped once or more before initiating a light emission process, second order kinetics are observed. In that case, equations (1)-(6) do not apply, and second (or higher) order equations must be used. For the second order kinetics, the differential equation is:

$$\frac{dh}{dt} = -\frac{\alpha h^2}{N} \tag{7a}$$

where N is the trap concentration. The solutions for equations (7) and (7a) are similar and accurate glow curve data are required to differentiate between the two processes. Equation (7a) predicts a wider glow curve but methods of measuring widths at half maximum can hardly distinguish between the two processes. Townsend et al. (1967) demonstrated that the glow peaks of LiF from 25 K to 255 K are described by first order kinetics. Hickmoth (1972) used a hyperbolic heating rate to measure thermoluminescence in rf-sputtered SiO_2 films and found that the shapes of the glow curves are independent of the hyperbolic heating rate, q', an expected result only if the process is first order. Fairchild et al. (1978) found that first order kinetics adequately describe all of the glow peaks. On the other hand, Grant and Cameron (1966) found a correla-

tion between peak 2 and the other peaks in LiF:Mg, and Harris and Jackson (1970a) and Jackson and Harris (1970) found a correlation between peaks 2 and 3 as well as between peaks 4 and 5. Booth et al. (1972) found evidence that supports their results. Their investigations indicate that high temperature traps result from an aggregation of simple low temperature traps. A growth in the 200°C peak as a function of time within, before or after an exposure was found, indicating that retrapping of escaping charge carriers is not responsible. A more likely cause is migration of low temperature trapping centres into higher temperature centres. The effect (growth of peaks 4-5) results in about a 25% increase for storage at room temperature for a month and about a 30% increase at 100°C for storage for one hour or so. Later measurements by Mason et al. (1976) indicate that the effect is really negligible, being significant only for very high cooling rates (>10^3 °C/min). It therefore seems that the retrapping or migration effect, if it exists, is quite small and negligible for short periods. Results from the present experiments shed some light on this "sensitivity transfer" from shallow to deep traps and vice versa.

The second effect that should be considered is whether or not the emission spectra are almost identical for all traps of the phosphor. If the spectra are indeed identical, then the simple method proposed of measuring the total light output using a photomultiplier and a reader can be applied; if the spectra are significantly different, the emitted light should be measured in its various bands, which is quite a difficult task. Pearson and Cameron (1966) found no difference in the emission spectra of sensitized and unsensitized LiF:Mg. Klick et al. (1967) observed emissions from various LiF samples all having a band at 400 nm; only pure

LiF had an additional weak band near 265 nm. Harris and Jackson (1970b) found that the thermoluminescent output for LiF:Mg shifted slightly to shorter wavelengths (from 470 to 400 nm) for high temperature glow peaks, and that no variation of the emission spectra of any peak was observed over the dose range 1 krad to 1 Mrad. Deverd and Stoebe (1972) confirmed Harris and Jackson's findings. Fairchild et al. (1978) provided further confirmation, but with some exceptions: they resolved the emitted spectrum between 500 and 10^5 rads γ for peaks 1 to 5 into three separate emission bands, namely 3.01, 2.09, and 2.71 eV. The 2.9 eV band is a relatively low intensity band. These three close bands satisfactorily account for all the thermoluminescent emission observed for samples exposed to 10^5 rads or less. For higher exposures, two additional narrow bands at 2.98 and 2.5 eV are introduced. The existence of more than one band can then explain the shift in λ observed by some authors. Podgorsak et al. (1971) found that the emission spectra of the dosimetry peaks 1 to 5 have only one maximum at 400 nm in the range 190-510 nm. They found that only peak -4 shows UV emission (around 210 nm) whereas peak -1 shows several weak maxima at 310, 250 and 210 nm together with a strong maximum at 400 nm. Cooke (1978) found that all of the thermoluminescent peaks, except the complex peaks at 142 and 162 K (peaks -4 and -3), show the same emission spectrum with a maximum at 400 nm. Despite small discrepancies in the findings of the various workers, the small shift found by some investigators to a shorter wavelength for higher temperature glow peaks, and the possibility that LiF:Mg could have some close bands for some of its peaks, it is likely that the simple method proposed of isothermal kinetic decay analysis is applicable. The response of the photocathode of the reader

used (EMI, S-11) is almost flat in the range 150-450 nm (from a plot of quantum efficiency vs wavelength for various photocathodes issued by EMI Electronics Ltd), a range that covers the wavelengths of the various peaks of LiF:Mg.

From the above discussion, it appears possible to apply the proposed method to investigate trapping centres in LiF:Mg. The measurements are intended to provide data on the peaks -1b to 3 of TLD 100 and 700 and to shed light on the effect of the regular annealing treatment on the trapping configuration and on efficiency.

2.3 Experimental Aspects

New LiF:Mg chips, TLD 100 and 700, 1/8" x 1/8" 0.035" and 0.015" thick, manufactured by Harshaw Chemical Corp. were used in the measurements reported here. The LiF crystals contained approximately 100 ppm of Mg according to the manufacturer. They were used in two batches, one with no preannealing and the other after annealing for one hour at 400°C followed by 24 hours at 80°C. (This annealing protocol has been used for thermoluminescent LiF chips in radon daughter dosimeters.) The chips were selected to have uniform sensitivity with less than 2% standard deviation after a test exposure to 100 rads. The chips were exposed to foil alpha sources of Am-241 and Po-210 (Amersham). No collimator was used as the chips were placed directly on the foil source, always exactly on the same location. The sources were not uniform (measured by α spectroscopy using a collimator), but no exact calibration was required and the exposure R to the chip, delivered to a layer of thickness 30 μm, was approximated by using the derived equation:

$$R\ [rads] = (50 \pm 5)t \qquad (8)$$

(for Am source, activity of 2 $\mu Ci/cm^2 \cdot 2\pi$)

where t is the exposure time in minutes. As the irradiation time varied between 15 s and 60 min, the exposure varied in the range 10 rads to 3 x 10^3 rads.

To check the effect of annealing, chips were given the standard annealing treatment before being irradiated. After irradiation, the chips were immediately (delay of few seconds) viewed by means of the photomultiplier of a manual Harshaw reader (Model 2000 A). This procedure avoided measuring "fast phosphorescence" due to forbidden transitions in some ion impurities, with half periods of a few milliseconds, and usually temperature independent; rather the traps were measured involving the release of carriers from the traps by heat quanta supplied from the thermal vibrations of the phosphor. For each measurement, the sample was placed on the reader pan, and kept at a constant temperature using the external position of the heating cycle. The reader was flushed with nitrogen at a flowrate of 4 L/min. The chips were read with the irradiated face toward the photomultiplier tube to avoid variation in thermoluminescence due to differences in geometry. The whole emission spectrum was detected, recorded and plotted.

The decay of the luminescence signal at room and higher temperatures was determined by measuring the total output light as a function of time. When the phosphorescence intensity decayed to almost the background intensity $(8 \pm 4)\ 10^{-4}$ nC/s, the dosimeters were read using the regular readout cycle with a linear heating rate of 10°C/s. T_1, T_2 and T_{max} were set at 120°C, 250°C and 370°C respectively. The response of

the system was calculated at 0.7 ± 0.1 ncoulomb/rad. The plot of the total output light was then analyzed and resolved into separate peaks by a simple decay analysis. From the plot, the appropriate half lives of the traps were found at the measured temperature. For a single trap, the plot of ln I vs t is a line of slope $m = \tau^{-1} = S \exp(-E/kT)$. From the mean life time τ_1 and τ_2 at two different temperatures, T' and T", values of E and S can be calculated.

2.4 Results

The measurements reported here were made on annealed and unannealed chips of TLD 100 and TLD 700 exposed to various dose levels. Figure 1 depicts a typical phosphorescence decay curve of an annealed chip irradiated for 15 s (12.5 rads) and read at room temperature.

Figure 2 shows the phosphorescence from one TLD 100 chip irradiated for 1 min (approximately 50 rads) and read at room temperature. The experimental points lie on average between the glow curve obtained through the plotter and measurements of charge made through the photomultiplier tube over short intervals of time, and subjected to background subtraction. The bars represent one standard error; the accuracy of the measurements was better than ±10%. The luminescence is resolved by least squares into exponential components which are represented by the straight lines. The background subtracted was $(8 \pm 4) \times 10^{-4}$ nC/s.

The three lines obtained are related to traps with half lives at room temperature of 4.2 min, 32 s and 7 s. It is important to note their intersection with the current axis, i.e., the current at t = 0. This value is a characteristic of the trap: the efficiency of trapping the hole

FIGURE 1. Typical Phosphorescence Decay Curve of an Annealed LiF:Mg Chip (Irradiation 13 s, Corresponding to 12.3 rads) Read at Room Temperature.

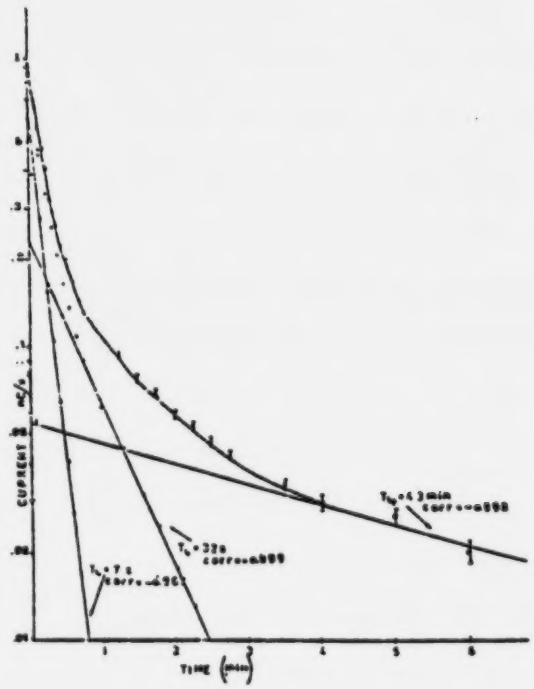

FIGURE 2. Phosphorescence Decay Curve for an Annealed TLD 100 LiF:Mg Chip (Irradiation 60 s, Corresponding to 30 rads) Read at Room Temperature. The bars represent one standard error. Correlation coefficients are shown for the least squares resolution of the curve into three straight lines.

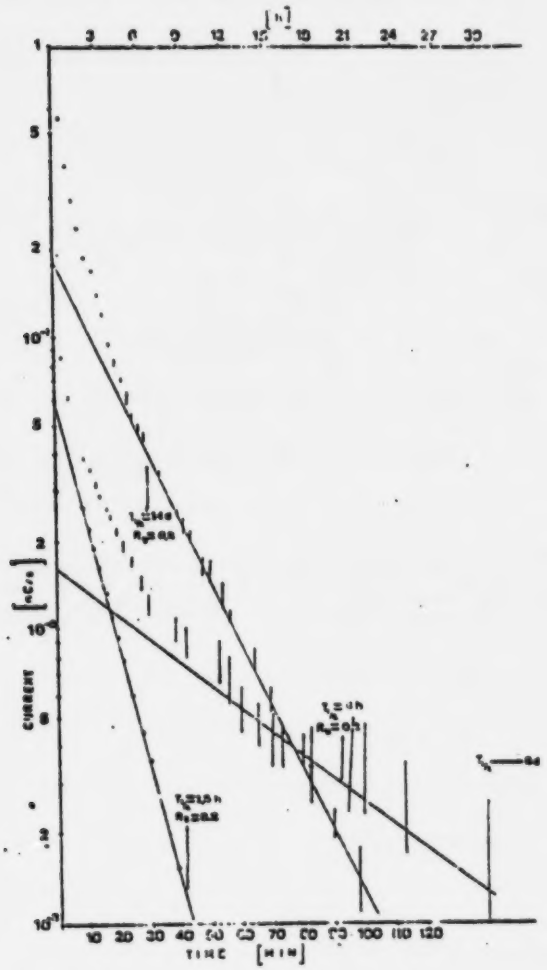

FIGURE 3a. Average Phosphorescence Decay Curve for a Large Number of Annealed CiF:Mg Chips (irradiation 60 min, corresponding to 3 x 10^3 rads) Read at Room Temperature. The luminescence is resolved into exponential components (straight lines) as in Fig. 2. The bars represent ranges of values. No difference was found between TLD 100 and TLD 700.

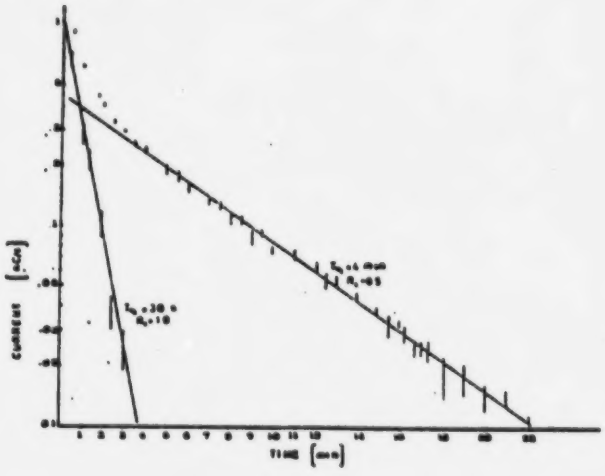

FIGURE 3b. Average Phosphorescence Decay Curve for a Large Number of Annealed CiF:Mg Chips (Irradiation 60 min, Corresponding to 3 x 10^3 rads) Read at Room Temperature. The luminescence is resolved into exponential components (straight lines) as in Fig. 2. The bars represent ranges of values. No difference was found between TLD 100 and TLD 700 chips.

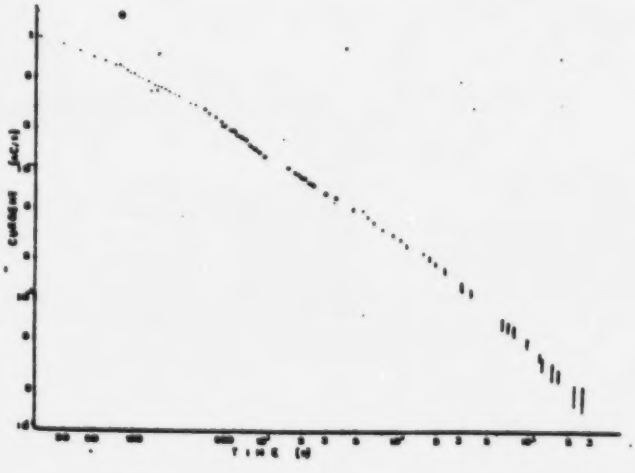

FIGURE 4. Average Phosphorescence Decay Curve for a Large Number of Unannealed LiF:Mg Chips (Irradiation 60 min, Corresponding to 3 x 10^3 rads) Read at Room Temperature. The bars represent the ranges of values. No difference was found between TLD 100 and TLD 700 chips.

(electron) liberated by α irradiation in the specific trap and of the emission of light when the charge is freed. The value obtained for R is related to the saturated value R_S by the simple relation

$$R = R_S \left[1 - \exp - \left(\frac{\ln 2 \cdot t_{irr}}{T_{\frac{1}{2}}} \right) \right]$$

As a consequence, R_S for the above 3 traps is 0.37, 0.35, 0.7 nC/s respectively.

Figures 3a and 3b show the average phosphorescence of a large number of annealed chips irradiated for 60 min (exposure of 3×10^3 rads), and read at room temperature. Each point is an average of several readings of different chips since it was found that measurements on different chips were the same within experimental limits. Although a variation in sensitivities was sometimes found (up to ±10%) due to different chip sensitivities, chip history, or the experimental limits, not much variation in $T_{\frac{1}{2}}$ values was found. No differences were found between TLD 100 and TLD 700. The luminescence was resolved into exponential components as represented by the straight lines. The bars represent the range of readings for the various chips.

Figure 4 shows the average phosphorescence decay of a large number of unannealed phosphors up to 3×10^5 s. The data are resolved in Figs. 5a to 5d.

A summary of the half lives at room temperature determined by the present method is given in Table 2. The accuracy of the established values of $T_{\frac{1}{2}}$ depends on the peak but lies between 10 and 40%. A comparison between these results and those of Table 1 lead to the identification of the peaks as peaks #-1b to #3. Values of R_S are also shown in Table 1.

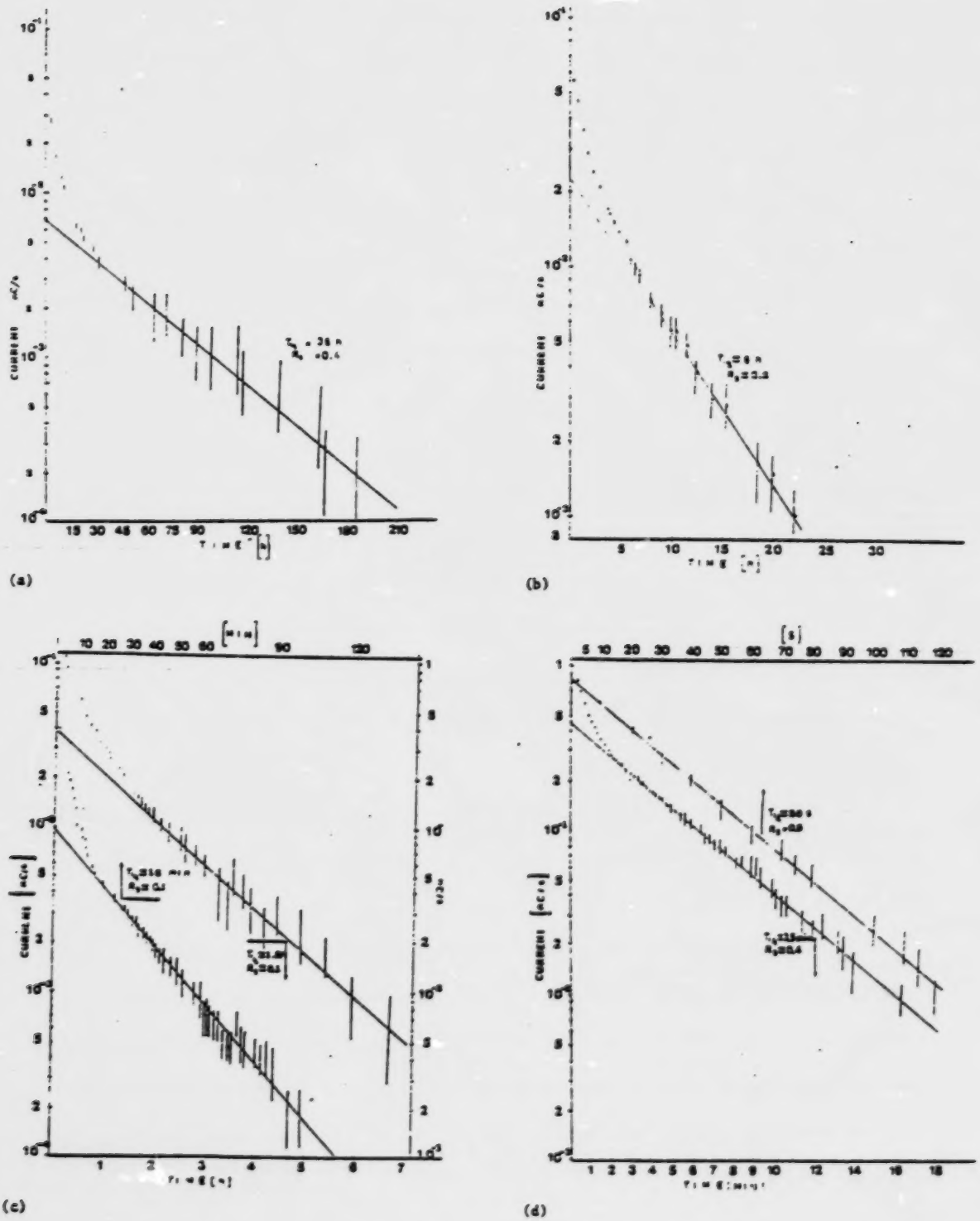

FIGURE 5. Resolution of the Data of Figure 4 into Exponential Components. The bars represent ranges of values.

Table 2

Summary of Values of T_m and $T_{1/2}$ Found in This Work Compared with Those Determined from the Literature

	The present method						References[a]											
	annealed		unannealed		average		(a)	(b)	(c)		(d)		(e)		(f)		(g)	
Peak #	$T_{1/2}$	E_a	$T_{1/2}$	E_a	$T_{1/2}$	E_a	T_m	T_m	T_m	$T_{1/2}$	T_m	$T_{1/2}$	T_m	$T_{1/2}$	T_m	$T_{1/2}$	T_m	$T_{1/2}$
- 1b	-	-	3 ± 1 s	1.6 ± 0.2	3 s	1.6	-38	-	-	-	-	-	-	-	-	-	-	-
- 1a	5 ± 2 s	-	5 ± 2 s	0.5 ± 0.2	5 s	0.6	-20	-	-	-	-	-	-	-	-	-	-	-
- 1	30 ± 5 s	1.0 ± 0.1	20 ± 8 s	0.8 ± 0.1	28 s	0.8	15	-	-	-	-	-	-	-	-	-	-	-
0	4 ± 1 min	0.5 ± 0.1	3.5 ± 0.5 min	0.45 ± 0.05	4 min	0.4	13	14	-	-	-	-	-	-	-	-	-	-
1	14 ± 2 min	0.2 ± 0.05	16 ± 2 min	0.1 ± 0.05	15 min	0.1	46	59	62	2.2 h	65	5 min	80	5 min	80	5 min	59	55 min
2	1.3 ± 0.2 h	0.2 ± 0.05	1.2 ± 0.2	0.1 ± 0.05	1 h	0.1	90	102	94	3.1 d	-	-	105	10 h	102	55 d	97	10 d
3a	6 ± 1 h	0.2 ± 0.05	6 ± 1 h	0.2 ± 0.05	6 h	0.2	-	-	112	11.2 d	-	-	-	-	-	-	-	-
3	2 ± 1 d	-	1.5 ± 0.5 d	0.4 ± 0.2	2 d	0.4	129	137	137	14.0 d	120	20 h	118	0.5 y	137	31 y	137	2.3 y

Notes:

1. T_m obtained by various workers through the use of different heating rates.
2. Most of the $T_{1/2}$ values given in this table are calculated using the equation $T_{1/2} = S \exp\left(\frac{-E}{kT}\right)$ and using published values of S and E.
3. Temperatures in degrees Celsius.

[a]References:

(a) Cooke, D.W., J. Appl. Phys., 49(7), 4206-4215, 1978.

(b) Podgorsak, E.B., Moran, P.R. and Cameron, J.R., J. Appl. Phys., 42(7), 2761-2767, 1971.

(c) Fairchild, R.G., Mattern, P.L., Lengweiler, K., Levy, P.W., J. Appl. Phys., 49(8), 4523-4533, 1978.

(d) Harris, A.M. and Jackson, J.M., Health Physics, 18, 162-164, 1970.

(e) Zimmerman, D.W. and Cameron, J.R., TID-25160, 1964.

(f) Moran, P.R. and Podgorsak, E.B., USAEC Report No. C001005-164 (1971).

(g) Zimker, W.M., Rusin, J.M. and Stoebe, T.G., J. Mater. Sci., 8, 407-412, 1973.

Values of T_m and $T_{\frac{1}{2}}$ measured or calculated by other investigators are also shown.

2.5 Conclusions

1. TLD 100 and 700 have similar trapping configurations since the half lives and R_S values of the trapping centres -1 to 3 were found to be the same. Moreover, the half lives and R_S values involved are independent of the exposure level in the range up to 5 x 10 rads.

2. There is no change in the half life values of the traps between annealed and unannealed chips, but there is a noticeable change in the intensity of light emitted (a change in the value of R_S), which indicates probably a difference in the trapping efficiency or a difference in the quenching process or a survival of new luminescent centres due to the annealing process, but not a change in the values of S and E or the addition of new trapping centres.

3. The 8 traps found in this work are identified with peaks -1b to 3. The existence of certain of these peaks (-1a, -1b, 2, 3a) was previously questionable as they have been resolved by only some investigators. The present results confirm the existence of these peaks.

4. The total light output as a function of time exhibited first-order kinetics with distinct decay rates whose half lives were established. The results here support the hypothesis that retrapping processes are insignificant or not measurable and the findings by several investigators that the glow peaks of TLD 100 and 700 may be described by first order kinetics.

5. The discrepancy between the present results and some published data on T_m and on $T_{\frac{1}{2}}$ for the peaks -1b to 3 is quite large. The values

obtained in the present work however agree with some of the published data.

6. Deeper traps are currently under investigation. The procedure outlined here is applied at constant temperatures >20°C, and values of E and S for the peaks 3, 3a, 4 and 5 are derived.

List of Symbols

C	characteristic constant of a phosphor
E	activation energy
h(t)	number of filled traps at time t
I(t)	thermoluminescent intensity at time t
k	Boltzman constant
N	trap concentration
q	linear heating rate
q'	hyperbolic heating rate
R	measured current extrapolated to t = 0
R_S	saturation current level of a specific trap
S	frequency factor
T	temperature
T_1	initial temperature at time t
t	variable time
t_1	time at commencement of heating
T_m	temperature when the light intensity is maximum
$T_{\frac{1}{2}}$	temperature when the light intensity reaches half of its maximum value
t_o	time at the end of the irradiation

$t_{\frac{1}{2}}$	time when the peak height or the total light output decays to half of its value, at room temperature
T_1	temperature at commencement of readout cycle (set in reader)
T_2	temperature at end of readout cycle (set in reader)
T_{max}	temperature at end of heating cycle
$a(T)$	transfer probability at temperature T
$\phi(T)$	light intensity at temperature T
τ	mean lifetime of trapped electron or hole.

CHAPTER 3

INVESTIGATION OF RADIOLUMINESCENCE, PHOSPHORESCENCE AND THERMOLUMINESCENCE IN DOSIMETRY MATERIALS WITH APPLICATION TO LiF:Mg

3.1 Introduction and Theory

Energy absorbed in matter is converted into heat, into chemical bonds, into emitted light as fluorescence, radioluminescence and phosphorescence, and into storage in metastable states. Solid state dosimetry is based on material having a large ratio of metastable states. LiF:Mg is widely used as a thermoluminescent material for radiation dosimetry, an application of interest being measurement of the alpha radiation of radon daughters. The present work concerns the energy budget of LiF:Mg exposed to α radiation.

Several light emission processes take place in the phosphor during and after irradiation. As a result of the direct interaction of the (α or γ) radiation with the crystal, light is emitted by atomic transitions, in a process called fluorescence, which has a characteristic time of 10^{-10} to 10^{-7} seconds. During irradiation of the crystal, the electron-hole pairs created may find their way to a luminescence centre and result in radioluminescence. The time involved in this process is less than one second. Another important light emission process which occurs in the crystal is fast and regular phosphorescence. Fast phosphorescence is due to forbidden transitions in some impurities in the crystal. This process, which is not a trap process, is temperature independent, and has a characteristic time of a few milliseconds. Regular or trap type phos-

phosphorescence is temperature dependent and the life time involved is characteristic of the activation energy E and the transfer probability $\alpha(T)$. Delayed luminescence decays with time as a sum of several exponential processes resulting from the release of carriers from shallow traps by heat quanta supplied from the thermal vibrations of the phosphor and their recombination with luminescent centres (Mourad and Phillips, 1981). Carriers from deeper traps are released by heating the phosphor, which then liberates some of the energy as thermoluminescence.

The intensity of the total luminescence from the crystal during and after the irradiation is time dependent. When the temperature of the phosphor and the absorbed dose rate are both held constant, the luminescence intensity increases with time to an equilibrium value, I_{max}, and then decays after the exciting irradiation has been cut off. Since the fluorescence intensity does not vary with time during irradiation, the increase is due to phosphorescence and radioluminescence only. Phosphorescence arises mainly from shallow traps in the phosphor which capture and release carriers. For each trap, the phosphoresence intensity, R, at time t is given by the equation (Mourad and Phillips, 1981):

$$R = R_S (1 - e^{-t/\tau}) \qquad (1)$$

where R_S is the saturation value and τ is the mean life of the trap. Thus the phosphorescence intensity increases with irradiation time until a saturation level is reached at which most of the separate shallow traps are saturated. The contribution of the deep traps to the phosphorescence at room temperature is insignificant. Little data are available on the variation of the intensity of radioluminescence with time. The present work is intended to help fill that gap.

Miller and Bube (1970) found that the emission intensity increased from a finite value at the commencement of x-irradiation until a maximum (at 5×10^4 rads) was reached, and then decreased towards an asymptotic value at a high dose ($\sim 10^6$ rads). The decrease in emission intensity at high dose cannot be attributed to the creation of centres which absorb the emissions.

Klick et al. (1967) measured the initial luminescence intensity and its variation with time in LiF and in LiF:Mg and found that the initial luminescence of the LiF:Mg is 2.3 times that of LiF; the luminescence of both materials increased identically with x-ray dose. The increase was explained as being due to an increase in F centres, which were assumed to be luminescent centres. Since the number of F centres created is independent of the number of Mg^{+2} ions, the increase in luminescence is therefore independent of the presence of Mg. This explanation contradicts the model for LiF proposed and confirmed by Christy and Mayhugh (1972). In this model, radioluminescence depends only on the absorbed dose rate in the phosphor and is time independent. Moreover, according to the "tracks interaction model" that predicts supralinearity in thermoluminescence, supralinearity is to be expected in phorphorescence and radioluminescence. Supralinearity should occur when the distance between two tracks (of α or of γ) in the crystal is comparable to the distance between two emitting centres, that is, when the absorbed dose in the phosphor is about 10^6 rads for α and 10^4 rads for γ.

Another point of interest is whether the emission spectrum from radioluminescence is different from the spectra from the thermoluminescence or phosphoresence processes. Gorbics et al. (1969) measured

radioluminescent light in LiF phosphors using x-rays at various temperatures in order to measure quenching. They found similarity between the emission spectra from the radioluminescence, phosphorescence and thermoluminescence processes, which suggests that the emitting centres involved in all processes are the same. Miller and Bube (1970) and Klick et al. (1967) showed that the x-ray induced emission at room temperature and thermo-stimulated luminescence have the same spectral emission.

3.2 Experimental Details

The general experimental procedure is described elsewhere (Mourad and Phillips, 1981). The exposure time of the phosphor varied between 1 min and 10 h and the exposure from 50 to 3×10^4 rads. For each observation the sample was placed on the α foil source and the sample and foil then placed on the reader pan, which was at room temperature. Using the external position of the heating cycle of a manual Harshaw reader (Model 2000 A), the luminescent intensity was measured during the exposure of the chip; after the removal of the α source, phosphorescence was measured as a function of time. LiF produces substantial light emissions during and after α irradiation. The reader was flushed with nitrogen at a flow-rate of 4 L/min during which thermoluminescence was measured, and with air duringwhich radioluminescence and phosphorescence were measured. During measurement of radioluminescence, it is necessary to control the atmosphere in the reader, specifically, to avoid any change in the oxygen and nitrogen concentrations. Such control is necessary because of the difference in light emission of the two gases when irradiated, and the difference in their light absorption. Oxygen absorbs light efficiently at wavelengths <200 nm while nitrogen slightly absorbs light in the range 150 to 500 nm.

Moreover nitrogen is much more fluorescent than oxygen when irradiated. Table 1 shows four representative readings for different relative concentrations of oxygen and nitrogen. It is clear from the values given in Table 1 that the background depends strongly on the type of gas in the reader. The reader was therefore continuously flushed with air under which conditions the background was 0.5 ± 0.1 nC/s when the α source was on the pan, and $(8 \pm 4)\ 10^{-4}$ nC/s when the α source was absent.

3.3 Results

The measurements reported here were made on TLD 100 and 700 chips, 0.015" and 0.035" thick, exposed to α radiation for up to 10 hours. The exposure of the chip was calculated at 50 ± 5 rads for 1 min exposure or equivalently to a total absorbed dose of 40 ± 4 erg/1 min exposure.

The results of the measurements are presented in Figs. 1 and 2 for 0.015" and 0.035" annealed chips irradiated for 10 minutes. No difference was found in the luminescence intensity of TLD 100 and 700. Figs. 1a and 1b show the radioluminescence, fluorescence and phosphorescence vs time relationships (after background subtraction) for 0.015" and 0.035" chips respectively. Figures 2a and 2b depict the phosphorescence decay after background subtraction. Each point is an average of 5 readings of the same chip. About 20 chips were used. Measurements using different chips were the same within experimental limits. The light intensity increased slowly with time of irradiation (<20% over 10 minutes of irradiation). Measurements of luminescence on chips irradiated up to 10 hours were conducted as well and the net increase in light intensity during the 10 hours did not exceed 25%. Using equation (1) and

Table 1

Reader Current Measurement (in nC/s) Under Various Concentrations of Oxygen and Nitrogen in the Reader

Concentration % / Case	O_2 / N_2	0 / 100	20 / 80	50 / 50	100 / 0
Bare α source placed on the pan		288	91	70	24
α source placed on the pan and covered with holed paper (size of the hole about the size of a chip)		133.8	11.0	9.0	4.5
α source placed on the pan covered with paper		2.45	2.45	2.45	2.45

Table 2

Ratio of Light Intensity for Annealed Chips: Light Intensity for Unannealed Chips for LiF:Mg

Experiment #	Radioluminescence	Phosphorescence	Thermoluminescence
1	1.14	1.13	1.10
2	1.27	1.27	1.20
3	1.26	1.28	1.27
4	1.28	1.24	1.16
5	1.17	1.08	1.02
6	1.12	1.10	1.05

Table 3

Integrated Light Emissions (nC) for LiF:Mg Chips

Process	0.015" chip	0.035" chip
Fluorescence + radioluminescence	420 ± 50	660 ± 70
Phosphorescence	40 ± 4	58 ± 6
Thermoluminescence	320 ± 35	385 ± 40

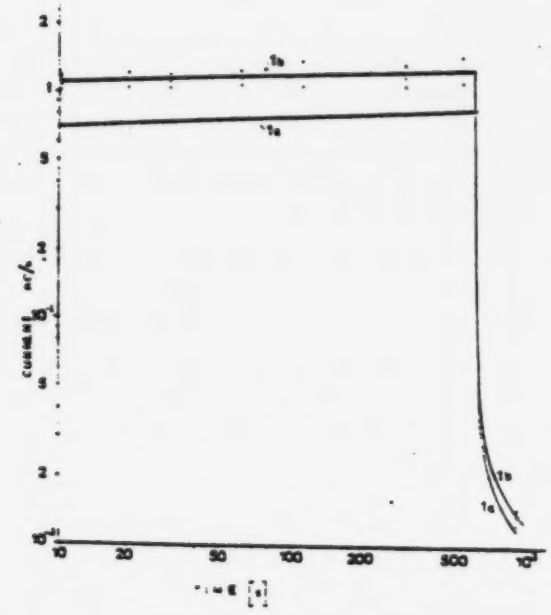

FIGURE 1. Fluorescence, Radioluminescence and Phosphorescence from 0.015" (Fig. 1a) and 0.035" (Fig. 1b) LiF:Mg Chips Irradiated for 10 min. Five readings were made for each chip.

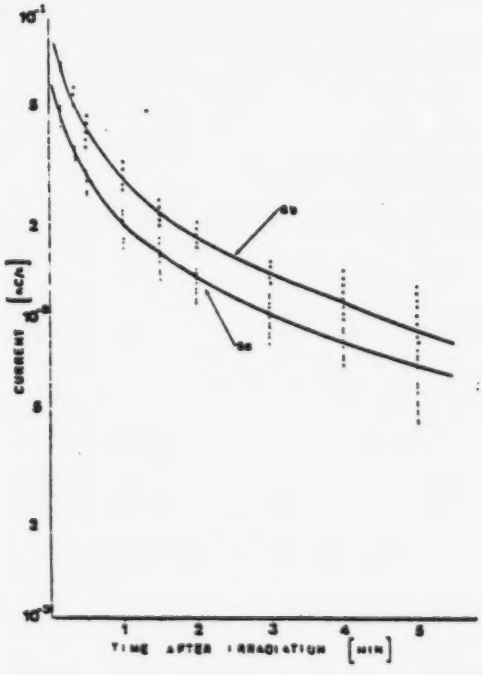

FIGURE 2. The Decay of Phosphorescence from 0.015" (Fig. 2a) and 0.035" (Fig. 2b) LiF:Mg Chips Irradiated for 10 min. Five readings were made for each chip.

values of R_S and τ from Mourad and Phillips (1981), it is found that for traps -1b to 3 the observed increment is equal to the predicted increase due to phosphorescence alone.

The procedure outlined above was followed for unannealed chips. Emitted light from all processes (radioluminescence, phosphorescence and thermoluminescence) was found to decrease when the chip is reused without annnealing; the annealing process improves the intrinsic efficiency. Ratios of light intensity from annealed and unannealed chips are shown in Table 2.

The integrated areas under the radioluminescence + fluorescence + phosphorescence curve (Fig. 1) and under the phosphorescence curve (Fig. 2) may be compared to the charge measured when the regular readout cycle is applied to the irradiated dosimeter. Table 3 summarizes the measured and calculated values (in nC) for the various light emission processes for the 0.015" and 0.035" chips.

3.4 Summary and Conclusions

The results of the experiments may be summarized and interpreted as follows:

1. Chips of thickness 0.035" show a higher sensitivity than the 0.015" chips, specifically, about a 50% increase in radioluminescence and phosphorescence, and about a 20% increase in thermoluminescence. The increase is not due to geometrical configuration (which was calculated to be negligible). It may be due to different concentrations of impurities in the two batches of chips.

2. Radioluminescence was found to be constant during irradiation for total exposures up to 3×10^4 rads. The slight increase in the luminescence during the irradiation time matches the increase in the phosphorescence process.

3. Annealed chips show a higher sensitivity than unannealed chips in thermoluminescence as well as in phosphorescence and in radioluminescence. The net increase in radioluminescence and phosphorescence sensitivity is higher than in thermoluminescence.

4. Gorbics et al. (1969) have determined that the radioluminescence output for a given dose at room temperature is about 6 times the thermoluminescent light output of the glow curve of LiF 100 exposed to x and γ radiation. In the present work, using α radiation, a factor of 1.7 $\pm$ 0.3 is found.

5. As was expected, supralinearity in radioluminescence was not observed up to exposures of 3×10^4 rads of α.

CHAPTER 4

DESIGN CONSIDERATIONS FOR AN ENERGY DISCRIMINATORY THERMOLUMINESCENT DOSIMETER TO MEASURE SEPARATELY RADON DAUGHTERS AND THORON DAUGHTERS

4.1 Introduction

Thermoluminescent dosimetry (TLD) has been used to monitor radiation exposures to individual uranium miners (McCurdy et al., 1969; Pai, Jokura and Phillips, 1981; Jacobi et al., 1981), the cumulative exposure to airborne radon daughters being expressed in terms of working level months. Heretofore, no differentiation has been made between the concentrations of radon daughters and thoron daughters. (In some Canadian uranium mines, the thoron daughter working level is significant (Pai, Jokura and Phillips, in press; Pai and Phillips, 1977). The possibility of designing an energy discriminatory thermoluminescent dosimeter capable of separately reporting radon daughters and thoron daughters is examined here.

4.2 Design of an Energy Discriminatory TL System

Although the CEA track etch dosimeter is energy discriminatory (Pai, Jokura and Phillips, 1981; Phillips, Pai and Stocker, 1978), there are significant differences between the detection properties of track etch film and those of TL phosphors. The track etch film responds only to α particles, which constitutes a major advantage over a TL phosphor. Further, the high track etch counting efficiency at 3 MeV under the proper etching conditions (90 minutes at 60°C in 2.5 N NaOH solution) simplifies the differentiation between RaA, RaC' and ThC'. In contrast, the TL

response to α, β and γ radiation makes the analysis complicated; this response is the most important disadvantage of the TL system. Table 1 summarizes the α, β and γ energies for the decay of radon and thoron daughters.

In most TL phosphors, an increase in the linear energy transfer (LET), results in a decrease in response per rad of absorbed dose (Fig. 1) (Tochilin et al., 1968). The TL response per rad of absorbed dose is different for α, β and γ exposures. In general, the alpha response per rad of absorbed dose is less than that of beta exposure and can be explained in terms of saturation effects in a narrow channel along the alpha tracks in which most of the delta electrons are deposited (Zimmerman, 1972).

Figure 2 shows the construction of the CEA dosimeter head. Three collimators are used to discriminate between the radon and thoron daughters. On top of the collimator, absorbers of three different thicknesses are placed such that one channel registers ThC' alone, the second channel registers both ThC' and RaC', and the third channel registers ThC', RaC' and RaA (ThC). After passing through 2 cm of air gap, the residual mean α energy reaching the absorber is as shown in Table 2. By appropriate choice of the thickness of the absorbers so that the final residual energy is degraded to the desired level, differentiation between RaA, RaC' and ThC' is possible.

4.3 Efficiency of the Energy Discriminatory TL System

One of the advantages of the energy discriminatory system is that the efficiency can be obtained theoretically as well as experimentally. The efficiency of the TL system, ε, can be defined as the TL reading in nano-

TABLE 1

Summary of the α, β and γ Energies from the Decay of Radon and Thoron Daughters

Type of radiation		Energy, MeV
α	RaA, ThC	6.0
	RaC'	7.7
	ThC'	8.8
β		0.3-3.3
γ		0.2-2.6

TABLE 2

Mean α Energies after Passing through a 2 cm Air Gap

	α energy (MeV)	After passing through a 2 cm air gap, residual mean α energy (MeV)
RaA	6.0	4.2
RaC'	7.7	6.2
ThC'	8.8	7.4

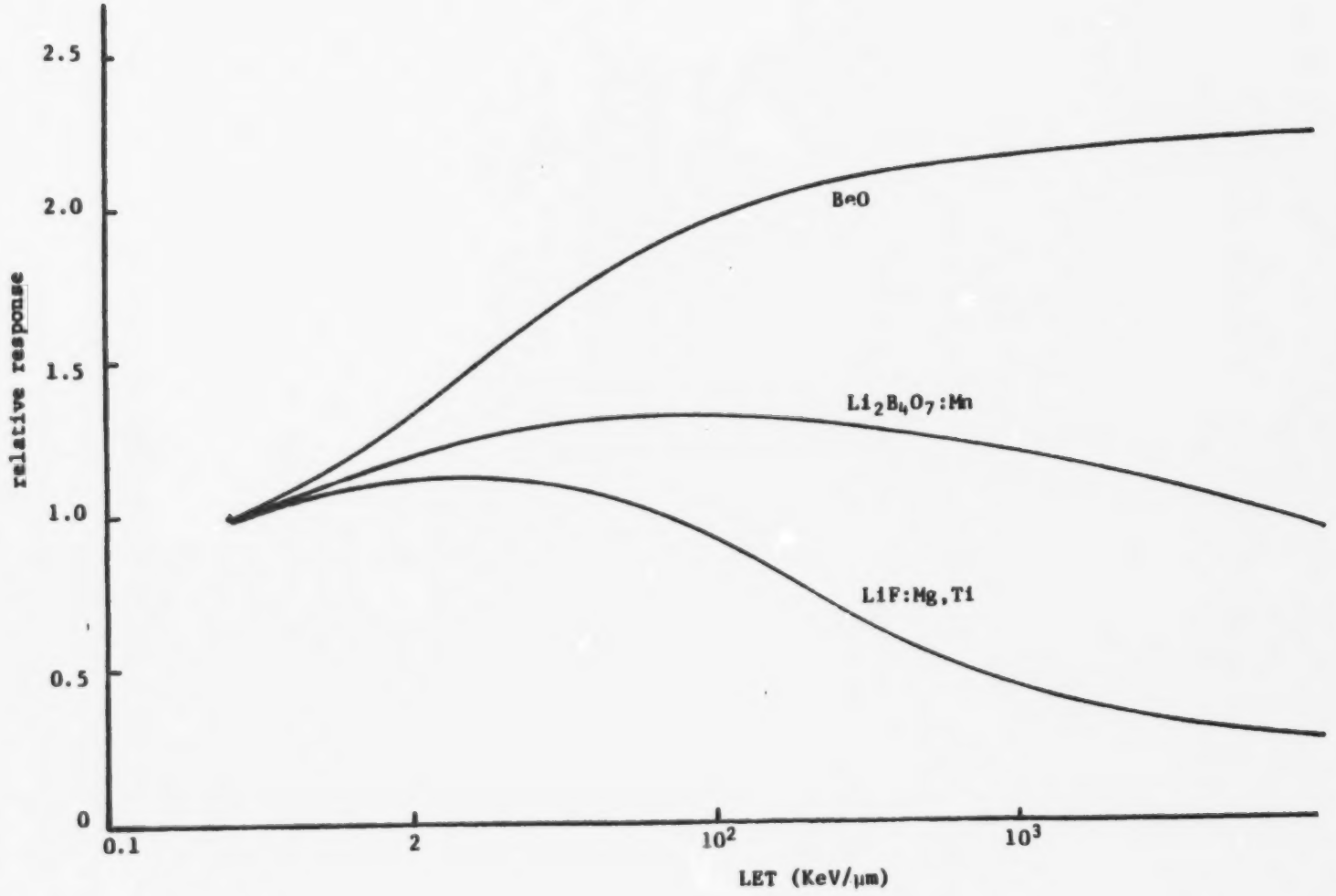

Fig. 1. Relative response (normalized for the response to gamma radiation) of three low Z TLD phosphors as a function of LET (after Tochilin et al., 1968).

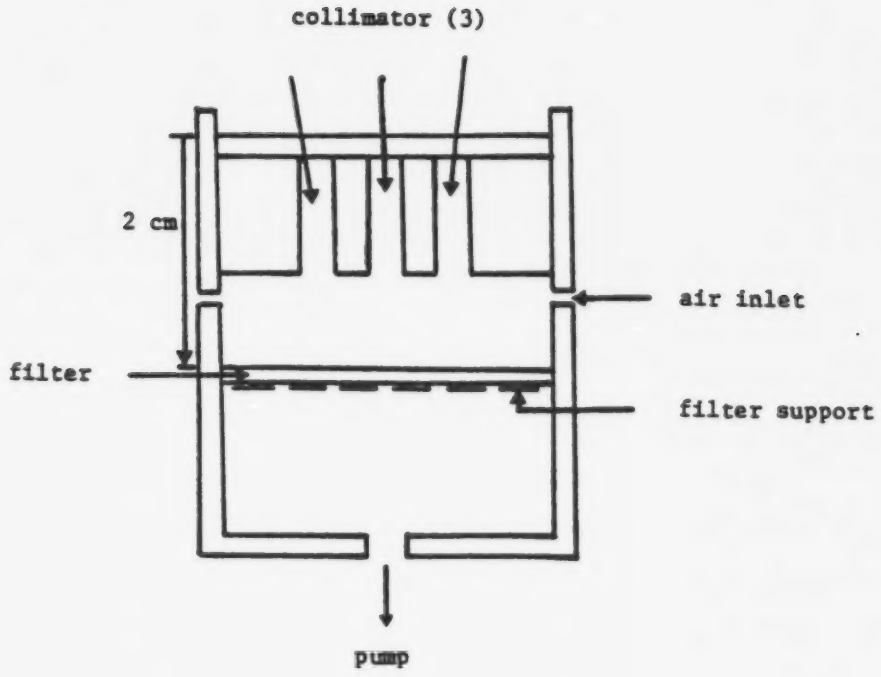

Figure 2. Schematic diagram of CEA dosimeter head.

coulomb obtained per atom of the particular radon daughter (or thoron daughter) deposited on the filter paper. It can be calculated as the product of the geometric efficiency, ε_G, and the intrinsic efficiency, ε_I. (For example, the geometric efficiency of the CEA head design has been calculated as 1.5×10^{-3} (Chapuis et al., 1972).)

The intrinsic efficiency is defined as the TL reading in nanocoulomb per alpha particle incident on the TLD. The efficiency depends on the TL material and is generally a function of alpha energy, E, the incident angle, θ, the pre-annealing conditions and the readout procedure. The efficiency can be expressed as:

$$\varepsilon_I = \int \phi(E)\, \bar{\varepsilon}_I(E)\, dE$$

where $\int \phi(E)dE$ = normalized alpha energy spectrum

$\bar{\varepsilon}_I(E)$ = intrinsic efficiency per alpha energy averaged over the range of possible incident angles

In the presence of the collimator, $\varepsilon_I(E,\theta) \sim \varepsilon_I(E)$. Therefore the total efficiency, ε, can be expressed as:

$$\varepsilon = \varepsilon_G \times \int \phi(E)\, \varepsilon_I(E)\, dE$$

The actual efficiency depends also on the collimator geometry and on the aerosol plate-out in the dosimeter head.

It is essential to choose the TL phosphor such that the intrinsic efficiency, ε_I, is not a function of alpha energy, for the following reasons:

a) knowledge of the alpha energy spectrum is then not needed, thereby simplifying the analysis.

b) In TL material which is thick relative to the range of the α-particles, the particle energy degrades from the incident α energy to rest energy. If the intrinsic efficiency is a function of α energy, the efficiency will vary along the α-track.

c) The principle of additivity of RaA, RaC' and ThC' in the TL reading cannot be used if ε_I is a function of α energy.

Finally, the total efficiency, ε, is simply the product of ε_G and ε_I, which is the same for RaA, RaC' and ThC'. Figure 3 shows the relative α response per incident α particle as a function of α particle energy (Zimmerman, 1972). For natural fluorite, CaF_2:Mn, and Norwegian quartz, the α response per incident α particle is nearly constant, rising only slowly with increasing energy. $CaSO_4$:Mn, on the other hand, shows a stronger dependence of α energy on the response.

4.4 TL Readout Procedure

The positioning of TL chips within the dosimeter is shown in Figure 4. Absorbers of different thicknesses are placed such that chip 1 registers ThC', chip 3 RaC' and ThC' and chip 4 RaA, RaC' and ThC'. Chip 2 is the β + γ compensation chip. The following assumptions are made:

a) the principle of additivity of β, γ and α exposures is valid, that is, there is no effect of β and γ exposure on the α sensitivity.

b) Neither β nor γ radiation attenuates appreciably in the absorbers or the TL material; thus only one β and γ compensation chip is required.

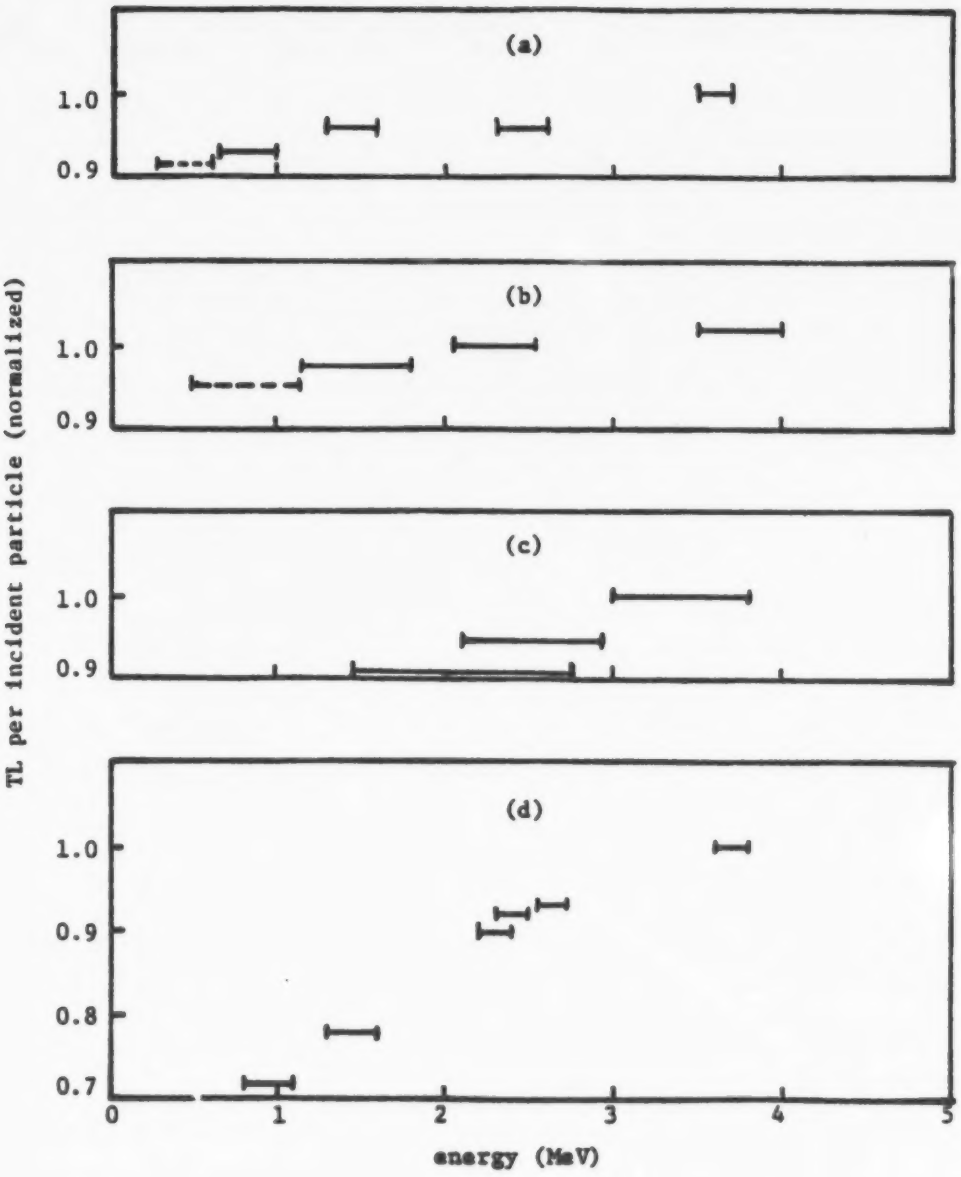

Fig. 3. TL induced per incident α-particle as a function of α-particle energy for (a) natural fluorite (MBLE type S), (b) CaF_2:Mn, (c) Norwegian quartz, and (d) $CaSO_4$:Mn. The width of the bars gives the average energy lost in traversing the sample. The dashed lines indicate points for which the accuracy is uncertain because of uncertainty in the calculation of stopping power at low energy (Zimmerman, 1972).

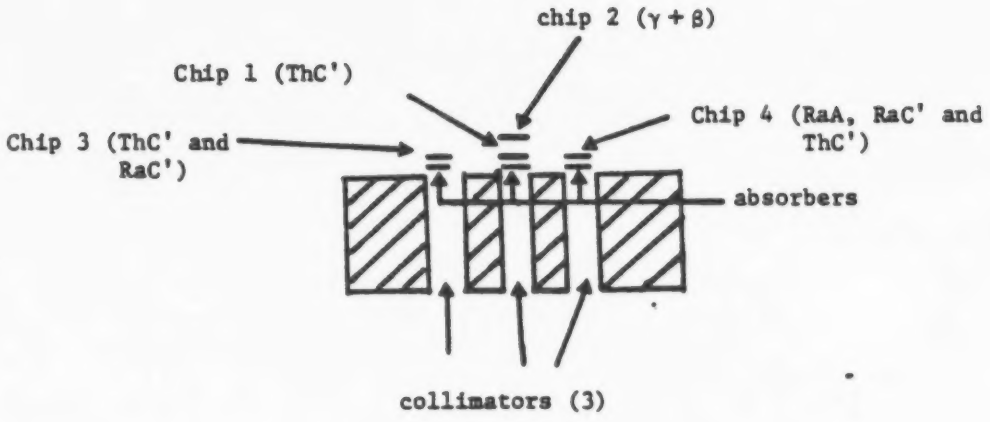

Figure 4. The positioning of TL chips within the dosimeter.

c) The principle of additivity of RaA, RaC' and ThC' exposures is valid, that is, the intrinsic efficiency of the TL material is not a function of the α energy.

The number of atoms of ThC', RaC' and RaA on the filter can then be obtained from the equations:

$$\text{ThC':} \qquad N_T = \frac{T_1 - T_2}{\epsilon}$$

$$\text{RaC':} \qquad N_C = \frac{T_3 - T_1}{\epsilon}$$

$$\text{RaA + ThC:} \qquad N_A = \frac{T_4 - T_3}{\epsilon}$$

$$\text{RaA:} \qquad N_A' = N_A - 0.5\, N_T$$

where T = TL reading of the respective chip in nanocoulomb.

The working levels for radon daughters and thoron daughters are defined by the equations:

$$WL_R = \frac{6 \times N_A' + 7.68 \times N_C}{1.3 \times 10^5\ V}$$

$$WL_T = \frac{6 \times 0.5\, N_T + 8.78 \times N_T}{1.3 \times 10^5\ V}$$

where WL_R = radon daughter working level

WL_T = thoron daughter working level

V = total volume pumped through the dosimeter filter paper (litres).

4.5 Uncertainty Analysis and Conclusions

In order to determine the uncertainty in the working level due to uncertainty in the TL reading and the TL efficiency, ε, an analysis is made through the following equation

$$N = \frac{x - y}{\varepsilon}$$

where N = number of atoms of the particular radon daughter (or thoron daughter) on the filter

x, y = TL reading for the respective chip in nanocoulomb.

The uncertainty in N is obtained from the equation:

$$\frac{dN}{N} = \frac{dx}{x}\left(\frac{x}{x - y}\right) - \frac{dy}{y}\left(\frac{y}{x - y}\right) - \frac{d\varepsilon}{\varepsilon}$$

Thus the uncertainty in N depends on the uncertainty in x, y and ε. The uncertainty depends greatly on the $\left(\frac{x}{x - y}\right)$, $\left(\frac{y}{x - y}\right)$ ratios which relate to the β/α ratios.

For a typical mine atmosphere, the activity ratio of RaA/RaB/RaC/ThB/ThC may be taken as 50/35/20/1/0.3.

The corresponding α/β ratios for ThC', RaC' and RaA can be estimated as:

ThC': $\frac{\alpha_T}{\beta} \sim 0.007$

RaC': $\frac{\alpha_C}{\beta} \sim 0.2$

RaA: $\frac{\alpha_A}{\beta} \sim 0.08$

where β = total β from radon and thoron daughters.

The uncertainty in N can be estimated if the following assumptions are made:

a) the maximum uncertainty in the TL reading and the TL efficiency is about 10%.

b) the β response is assumed to be one third of the α response.

c) the γ response is insignificant.

The maximum uncertainties for the radon and thoron daughters are estimated to be:

ThC': $\frac{x}{x-y} \sim 48$ $\frac{y}{x-y} \sim 48$

$\frac{dN}{N} \times 100\% \sim 970\%$

RaC': $\frac{x}{x-y} \sim 2.6$ $\frac{y}{x-y} \sim 1.7$

$\frac{dN}{N} \times 100\% \sim 50\%$

RaA + ThC: $\frac{x}{x-y} \sim 4$ $\frac{y}{x-y} \sim 4$

$\frac{dN}{N} \times 100\% \sim 90\%$

The maximum uncertainties for the radon daughter and thoron daughter working levels are predicted by:

$$\frac{dWL_T}{WL_T} \times 100\% \sim 970\%$$

$$\frac{dWL_R}{WL_R} \times 100\% \sim 60\%$$

The uncertainty in the thoron daughter working level is very high as a result of the high β/α_T ratio. A TL dosimeter based upon the proposed

design cannot therefore be used to discriminate radon daughters from thoron daughters.

For a pure radon daughter atmosphere, the maximum uncertainty in the radon daughter working level is about 50% if the uncertainties in the TL reading and the efficiency are assumed to be 10%. The proposed design can thus be used for monitoring the radon daughter working level provided that the uncertainties in the TL efficiency and in the TL readings are kept below 10%. (It has been suggested that the tolerable uncertainty in measuring the maximum permissible dose is in the range $\pm$25-50% (Becker, 1972).)

CHAPTER 5

THE EFFECT OF HUMIDITY ON THERMOLUMINESCENT MATERIALS

Conditions under which thermoluminescent dosimeters have been used in uranium mines often involve high humidity. Ideally, the dosimetric properties of the TL phosphors should be insensitive to the humidity conditions. It is thus important to study the effect of humidity on thermoluminescent material both during and after the alpha exposure. Figure 1 shows the effect of humidity on the fading of some common TL materials (Burgkhardt et al., 1976). It can be seen that at 25°C, CaF_2:Dy, LiF, $CuSO_4$:Dy do not show significant effects of humidity on fading. However for $Li_2B_4O_7$:Mn there is a large effect. This humidity effect can be explained in terms of the solubility of the TL material in water since by surface dissolution some of the information stored in the TL material can be lost. Table 1 shows the solubility of the common TL materials in water (Weast, 1978). Based on the solubility data, $Li_2B_4O_7$ should not be used in a uranium mine environment because of its high solubility. CaF_2 and Al_2O_3 on the other hand, show no humidity effect. Both LiF and $CaSO_4$ show slight humidity effects.

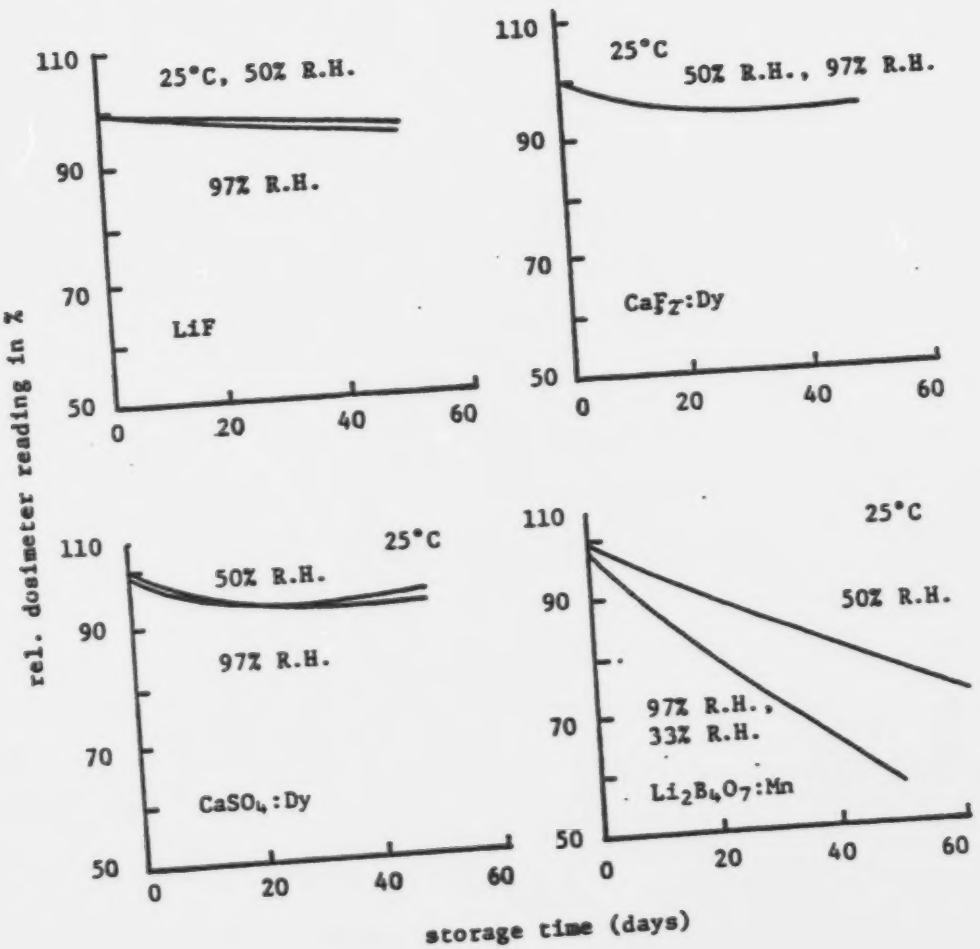

Fig. 1. Fading of TL at various relative humidities of different dosimeters (25°C). Post-irradiation annealing used for CaF_2:Dy was 100°C/25 min and for other dosimeters 100°C/10 min. (After Burgkhart et al., 1976).

TABLE 1

Solubility of TL Material in Water*

TL Phosphor	Solubility in grams per 100 mL of	
	Cold water	Hot water
$Li_2B_4O_7$	very soluble	--
$CaSO_4$ (anhydrite)	0.298	0.1619 (100°C)
LiF	0.27	--
CaF_2	0.0016	0.0017 (26°C)
Al_2O_3	0.000098	insoluble

* Weast, 1978.

CHAPTER 6

WORKING LEVEL MEASUREMENT OF RADON DAUGHTERS AND THORON DAUGHTERS BY PERSONAL DOSIMETRY AND CONTINUOUS MONITORING

6.1 Introduction

The health hazard resulting from the α-emissions of radon daughters is normally considered to be more important than that arising from thoron daughters. However, because of the high thorium concentration in some Canadian uranium mines (Pai and Phillips, 1977), the thoron daughter working level may be relatively high. Using energy discriminatory track etch dosimeters at Elliot Lake, Ontario, Phillips and Pai (1978) and Pai, Jokura and Phillips (1981) found that the working level for thoron daughters was about 50 to 100% that for radon daughters. Coté and Townsend (1981), using the Kusnetz method and α-spectroscopy, also found that thoron daughter working levels were about half the radon daughter working levels in an Elliot Lake uranium mine. The health hazards of radon and thoron daughters have been discussed by a number of workers (e.g., Duggan, 1973, Jacobi, 1972).

6.2 Dosimeter and Monitoring Developments

Several grab sampling methods may be used to determine the working level for mixed atmospheres of radon and thoron daughters. Coté and Townsend (1981) modified the Kusnetz method to account for the thoron daughter working level. They also suggested the use of 3 channel α-spectroscopy and the total β-method. Ogden (1974, 1977) developed a method based on α-activity of the filter samples for measuring the mixed radon and thoron daughter working levels.

Alternatively, integrating dosimeters may be used. The CEA track etch dosimeter has been modified (Pai and Phillips, 1977) to read ThC' as well as RaA and RaC' by the addition of a third channel with absorber to slow the 8.8 MeV alphas to 3 MeV as in the other two channels. On the other hand, a thermoluminescent dosimeter, responding to the total activity, is unable to differentiate between the radon daughters and thoron daughters. The significance of thoron daughters with respect to these dosimeter types can be seen from dosimeter data (Pai, Jokura and Phillips, 1981) for an Elliot Lake, Ontario uranium mine containing a mixed atmosphere of thoron daughters and radon daughters (Table 1). That in the track etch dosimeter the sum of the working level from radon daughters and the working level from thoron daughters ($WL_{Rn} + WL_{Tn}$) deviates from the working level recorded by the thermoluminescent dosimeter, WL_{TLD}, is in part due to the poor performance of the pumps (reflected in the laboratory data shown in Table 2), in part due to the statistics of sample comparison for those comparisons involving different carriers (miners), in part due to the uncertainty associated with reading LiF thermoluminescent chips which were exposed in a mixed radon daughter and thoron daughter atmosphere but calibrated in a radon daughter atmosphere (in both cases using only a simple gamma background subtraction), and in part due to the response characteristics in mixed atmospheres of radon daughters and thoron daughters that are described in the present work.

Radon daughter working levels themselves may be measured by a continuous working level monitor. For such a monitor, Kawaji, Pai and Phillips (1981) derived theoretical conversion factors for radon daughters so that the total α, total β, and total $\alpha + \beta$ counts can be converted

Table 1

Mine Test Results - One Month Test

Area/Carrier	Track Etch Dosimeter							Thermoluminescent Dosimeter					
	Total Flow (L)	N_A	N_C	N_T	$\frac{N_A}{N_C}$	WL_{Rn}	WL_{Tn}	Total Flow (L)	$\alpha+\beta+\gamma$	γ	WL_{TLD}	$WL_{Rn}+WL_{Tn}$	Δ
Jumbo crew/(1)	399	1731	2581	972	0.48	0.45	0.21	771	9.553	0.482	0.52	0.66	9%
(2)	299	990	1695	719	0.37	0.37	0.20	415	6.826	0.461	0.63	0.57	5%
S7-8 operator/(4)	560	1162	1612	903	0.44	0.19	0.13	321	2.307	0.369	0.18	0.32	44%
J.D.T. operator/(5)	409	866	1051	655	0.51	0.18	0.13	573	5.743	0.774	0.36	0.31	16%
C.C.-205/(6)	401	1353	1874	701	0.53	0.33	0.15	88	3.435	0.627	0.25	0.48	48%
(7)	564	1383	2019	857	0.47	0.25	0.13	413	4.342	0.695	0.43	0.38	13%
Crushing operator(8)	391	2676	8516	2965	0.14	1.22	0.63	-	-	-	-	-	-
	432	2730	8186	3168	0.14	1.07	0.62	-	-	-	-	-	-
Conveyor/(9)	448	1026	1446	661	0.53	0.23	0.13	-	-	-	-	-	-
	504	1481	1984	864	0.48	0.28	0.14	-	-	-	-	-	-
Technician/(10)	323	942	1582	603	0.40	0.30	0.16	652	5.105	0.495	0.34	0.49	33%
	388	1421	1904	660	0.57	0.36	0.14	-	-	-	-	-	-
Stationary/(11)	240	1269	1666	729	0.54	0.50	0.26	418	4.073	0.490	0.39	0.76	49%
Average (except crushing operator)					0.48	0.32	0.16				0.41		
Kusnetz grab sampling average						0.38	0.28						

Legend

N_A, N_C, N_T) track numbers in respective channels of dosimeter. (Note that diameters of A (RaA), and C (RaC') channels are identical; diameter of T (ThC') is less. The data reported are normalized to the A and C channel diameter.)

N_A' N_A corrected for the 6.04 and 6.08 MeV alphas of ThC (Bi-212). Correction is applied by subtracting one half of true ThC' tracks from RaA tracks. (The exact correction, calculated from branching ratios, is (25 + 10)/64.)

WL_{Rn} WL from radon daughters) track etch

WL_{Tn} WL from thoron daughters)

WL_{TLD} WL from calibration of TLD readout vs WL-litres; calibration on radon daughters only in laboratory chamber; exposure in mine to both radon daughters and thoron daughters) TLD

$$\Delta = \frac{(WL_{Rn} + WL_{Tn}) - WL_{TLD}}{(WL_{Rn} + WL_{Tn})} \times 100\%$$

The Working Levels are calculated as follows:

$$WL_{Rn} = \frac{6 \times N_A' + 7.68 \times N_C}{1.3 \times 10^5 \, c_R V} \quad ; \qquad WL_{Tn} = \frac{6 \times 0.5 \, N_T + 8.78 \times N_T}{1.3 \times 10^5 \, c_T V}$$

where V = total volume pumped through the dosimeter filter paper (litres)

$c_{R,T}$ = overall efficiency of registering and counting tracks of the appropriate alpha particles in detector

N_A' = total number of RaA tracks [corrected for 6.04 and 6.08 MeV alphas from ThC (Bi-212) as described above]

N_C = total number of RaC' tracks

N_T = total number of ThC' tracks

Table 2a

Summary of Pump Tests for Durability and Stability

Pump	Durability		Flowrate[1] stability (over 8 h)[2]		
	No. of pumps tested	No of pumps operating more than 10 h	(flowrate)$_i$ = $\frac{\text{initial} + \text{final}}{2}$	(flowrate)$_i$ = time average	$\frac{(\text{flowrate})_i - (\text{flowrate})_i}{(\text{flowrate})_i} \times 100\%$
CEA	25	17 (68%)	4.0	4.1	4.8%
H & H	12	12 (100%)	7.5	7.7	3.4%

[1] Flowrate in litres/h.

[2] Averaged over all dosimeters in class.

Table 2b

Summary of Pump Tests[1] for Attitude, Vibration and Impact

Pump	attitude[2]	vibration[3]	impact[4]
	$\frac{\text{max. fluctuation}}{(\text{flowrate})_{\text{operating position}}}$	$\frac{\text{max. fluctuation}}{(\text{flowrate})_{\text{operating position}}}$	$\frac{\text{max. fluctuation}}{(\text{flowrate})_{\text{operating position}}}$
CEA	3%	4-7%	2-3%
H & H	8-23%	5-28%	8-27%

[1] Ranges reported.

[2] Flowrate is measured after changing orientation with respect to the normal carrying position.

[3] Flowrate is measured after very rapid to and fro movements.

[4] Flowrate is measured after rapping dosimeter three times on wooden surface.

directly to working level. That work is extended here to a mixed radon daughter-thoron daughter system and used to interpret the response of both integrating dosimeters and continuous working level monitors for various weighted combinations of the radon daughter working level and the thoron daughter working level as a function of in-growth time, or age of the air.

6.3 Theoretical Procedure

The air concentrations of radon daughters or thoron daughters are given by the equation

$$\frac{dQ_i}{dt} = \lambda_{i-1} Q_{i-1} - \lambda_i Q_i \qquad (1)$$

where Q_i = atmospheric concentration of the ith member of the radon or thoron decay chain (atoms/L)

λ_i = decay constant (min^{-1})

i = 1 for radon (^{222}Rn), 2 for RaA (^{218}Po), 3 for RaB (^{214}Pb), 4 for RaC (^{214}Bi), 5 for thoron (^{220}Rn), 6 for ThB (^{212}Pb), 7 for ThC (^{212}Bi).

For constant radon or thoron concentration, equation (1) can be integrated directly to give Q_i at any in-growth time S.

$$Q_2 = \frac{\lambda_1 Q_1}{\lambda_2} (1 - e^{-\lambda_2 S})$$

$$Q_3 = \frac{\lambda_1 Q_1}{\lambda_3} (1 - e^{-\lambda_3 S}) + \frac{\lambda_1 Q_1}{\lambda_3 - \lambda_2} (e^{-\lambda_3 S} - e^{-\lambda_2 S})$$

$$Q_4 = \frac{\lambda_1 Q_1}{\lambda_4} (1 - e^{-\lambda_4 S}) + \frac{\lambda_1 Q_1}{\lambda_4 - \lambda_3} (e^{-\lambda_4 S} - e^{-\lambda_3 S})$$

$$+ \frac{\lambda_1\lambda_3 Q_1}{(\lambda_3 - \lambda_2)(\lambda_4 - \lambda_3)} (e^{-\lambda_3 S} - e^{-\lambda_4 S})$$

$$+ \frac{\lambda_1\lambda_3 Q_1}{(\lambda_3 - \lambda_2)(\lambda_4 - \lambda_2)} (e^{-\lambda_4 S} - e^{-\lambda_2 S})$$

$$Q_6 = \frac{\lambda_5 Q_5}{\lambda_6} (1 - e^{-\lambda_6 S})$$

$$Q_7 = \frac{\lambda_5 Q_5}{\lambda_7} (1 - e^{-\lambda_7 S}) + \frac{\lambda_5 Q_5}{\lambda_7 - \lambda_6} (e^{-\lambda_7 S} - e^{-\lambda_6 S}) \qquad (2)$$

The buildup and decay of radon or thoron daughters on a filter sample is given by the equation:

$$\frac{dN_i}{dt} = Q_i V + \lambda_{i-1} N_{i-1} - \lambda_i N_i \qquad (3)$$

where V = sampling rate (L/min)

N_i = number of atoms in ith member of radon or thoron decay chain on the filter

For steady state in the air and on the filter $\left(\frac{dN_i}{dt} = 0 \right)$, equation (3) reduces to:

$$\lambda_i N_i = Q_i V + \lambda_{i-1} N_{i-1} \qquad (4)$$

The steady state activities of the radon or thoron daughters on the filter are given by the equations:

$$D_2 = Q_2 V$$

$$D_3 = (Q_2 + Q_3) V$$

$$D_4 = (Q_2 + Q_3 + Q_4) V$$

$$D_6 = Q_6 V$$

$$D_7 = (Q_6 + Q_7) V \qquad (5)$$

The total α, β and α plus β activities at steady state are then described by the following equations:

Total α-activity,

$$\alpha_T = D_2 + D_4 + D_7$$
$$= (2Q_2 + Q_3 + Q_4 + Q_6 + Q_7)V \qquad (6\text{-}1)$$

Total β-activity,

$$\beta_T = D_3 + D_4 + D_6 + D_7$$
$$= (2Q_2 + 2Q_3 + Q_4 + 2Q_6 + Q_7)V \qquad (6\text{-}2)$$

Total α plus β activity,

$$\alpha_T + \beta_T = D_2 + D_3 + 2D_4 + D_6 + 2D_7$$
$$= (4Q_2 + 3Q_3 + 2Q_4 + 3Q_6 + 2Q_7)V \qquad (6\text{-}3)$$

The radon daughter and thoron daughter working levels are defined as follows:

$$WL_{Rn} = \frac{13.68 \times Q_2 + 7.68 \times (Q_3 + Q_4)}{130{,}000} \qquad (7\text{-}1)$$

$$WL_{Tn} = \frac{7.89 \times (Q_6 + Q_7)}{130{,}000} \qquad (7\text{-}2)$$

Definition of the total working level WL_T for a mixture of radon daughters and thoron daughters is open to argument. Ogden (1974, 1977) used the algebraic sum of WL_{Rn} and WL_{Tn} as the total working level. However, since the half-life of ThB is quite long (10.6 h), some of the ThB may escape from the respiratory system before alpha emission occurs. Hence the thoron daughter working level may be overestimated. In this paper, the total working level is defined as follows:

$$WL_T = WL_{Rn} + \omega WL_{Tn} \qquad (8)$$

where ω is the weighting factor for the thoron daughter working level.

A weighting factor $\omega = 0.1$ is consistent with the derived limits for radon daughters (designated employee 0.33 WL; other employee or member of the public 0.01 WL) and thoron daughters (designated employee 3.3 WL; other employee or member of the public 0.1 WL) suggested by the Department of Science and the Environment in Australia (1980). The effects of a variable weighting factor (0 to 1) are examined here.

The ratio of α-activity:WL_T is obtained by dividing equation (6-1) by equation (8):

$$\frac{\alpha_T}{WL_T} = \frac{(2Q_2 + Q_3 + Q_4 + Q_6 + Q_7)V\ 130{,}000}{[13.68 \times Q_2 + 7.68 \times (Q_3 + Q_4)] + \omega[7.89 \times (Q_6 + Q_7)]} \qquad (9\text{-}1)$$

$$\frac{\beta_T}{WL_T} = \frac{(2Q_2 + 2Q_3 + Q_4 + 2Q_6 + Q_7)V\ 130{,}000}{[13.68 \times Q_2 + 7.68 \times (Q_3 + Q_4)] + \omega[7.89 \times (Q_6 + Q_7)]} \qquad (9\text{-}2)$$

$$\frac{\alpha_T + \beta_T}{WL_T} = \frac{(4Q_2 + 3Q_3 + 2Q_4 + 3Q_6 + 2Q_7)V\ 130{,}000}{[13.68 \times Q_2 + 7.68 \times (Q_3 + Q_4)] + \omega[7.89 \times (Q_6 + Q_7)]} \qquad (9\text{-}3)$$

Substitution of Q_i from equation (2) into equations (9-1), (9-2), (9-3) respectively shows that $\alpha_T WL_T$, β_T/WL_T and $(\alpha_T + \beta_T)/WL_T$ depend on the ratio of radon:thoron concentration, R ($= \lambda_1 Q_1/\lambda_5 Q_5$), the in-growth time, S, and the weighting factor, ω, for the thoron daughter working level. The ratio of radon:thoron concentration, R, varies from 0.5 to 2 in a typical Canadian uranium mine. In recent measurements at Elliot Lake, it was found to be 0.64. Values of R ranging from 0.5 to 6 will be examined here.

6.4 Results and Discussion

The ratios of α_T/WL_T, β_T/WL_T and $(\alpha_T + \beta_T)/WL_T$ are calculated from equations (9-1), (9-2) and (9-3) respectively for various values of S at a fixed sampling rate of 1 L/min. Values of R from 0.5 to 6 and from 0 to 1 are used. The results are tabulated and presented in the Appendix.

Figure 1 (WL_T defined as $WL_{Rn} + WL_{Tn}$) shows the same trends as present in the work of Kawaji, Pai and Phillips (1981). α_T/WL_T, β_T/WL_T and $(\alpha_T + \beta_T)/WL_T$ show little change after 20 min of in-growth time. For in-growth times of less than 20 min, β_T/WL_T and $(\alpha_T + \beta_T)/WL_T$ change rapidly whereas α_T/WL_T remains relatively constant. Moreover, α_T/WL_T depends only slightly on the ratio of radon:thoron. However, as discussed earlier, the total working level defined as the algebraic sum of WL_{Rn} and WL_{Tn} probably overestimates the health hazard resulting from the thoron daughters. The three ratios plotted in Fig. 1 are therefore not directly applicable for the purposes of evaluating the health hazard.

Using weighted definitions of the total working level, it can be seen from Fig. 2 (WL_T defined as $WL_{Rn} + WL_{Tn}/3$), Fig. 3 (WL_T defined as $WL_{Rn} + 0.1\ WL_{Tn}$) and Fig. 4 (WL_T defined as WL_{Rn}), that β_T/WL_T and $(\alpha_T + \beta_T)/WL_T$ change constantly over the in-growth time, S, and are therefore unsuited for use in continuous monitoring methods in atmospheres of mixed radon daughters and thoron daughters. On the other hand, α_T/WL_T remains nearly constant for in-growth times of less than 40 minutes for the higher values of the radon:thoron gas ratio, R. After 40 minutes in-growth time, α_T/WL_T changes slowly. Further, α_T/WL_T depends on the radon:thoron gas ratio, R.

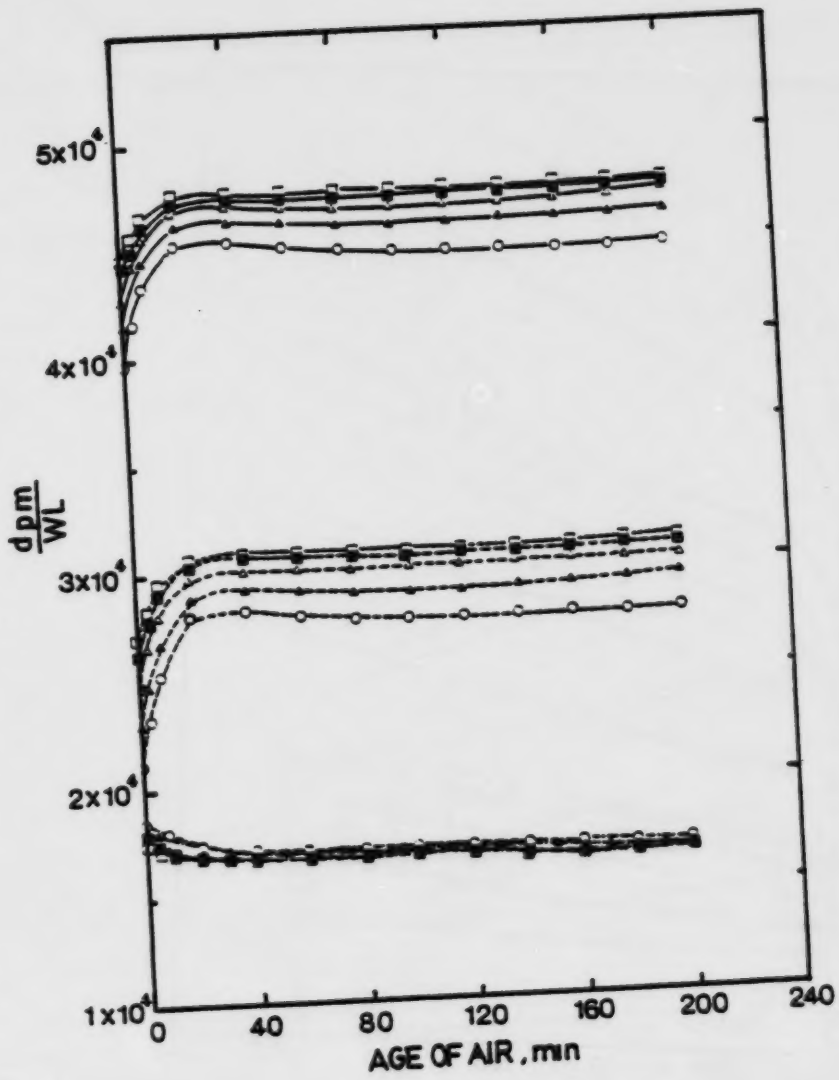

Fig. 1. Count to WL Ratio as a Function of the Age of the Air for a Mixed Atmosphere of Radon Daughters and Thoron Daughters: $WL_T = WL_{Rn} + WL_{Tn}$.

LEGEND

□ R = 0.5 ■ R = 0.64 — R = 1 ▲ R = 2 ○ R = 6 —— $\frac{\alpha_T + \gamma_T}{WL_T}$ ------ $\frac{\alpha_T}{WL_T}$ ·-·-·- $\frac{\gamma_T}{WL_T}$

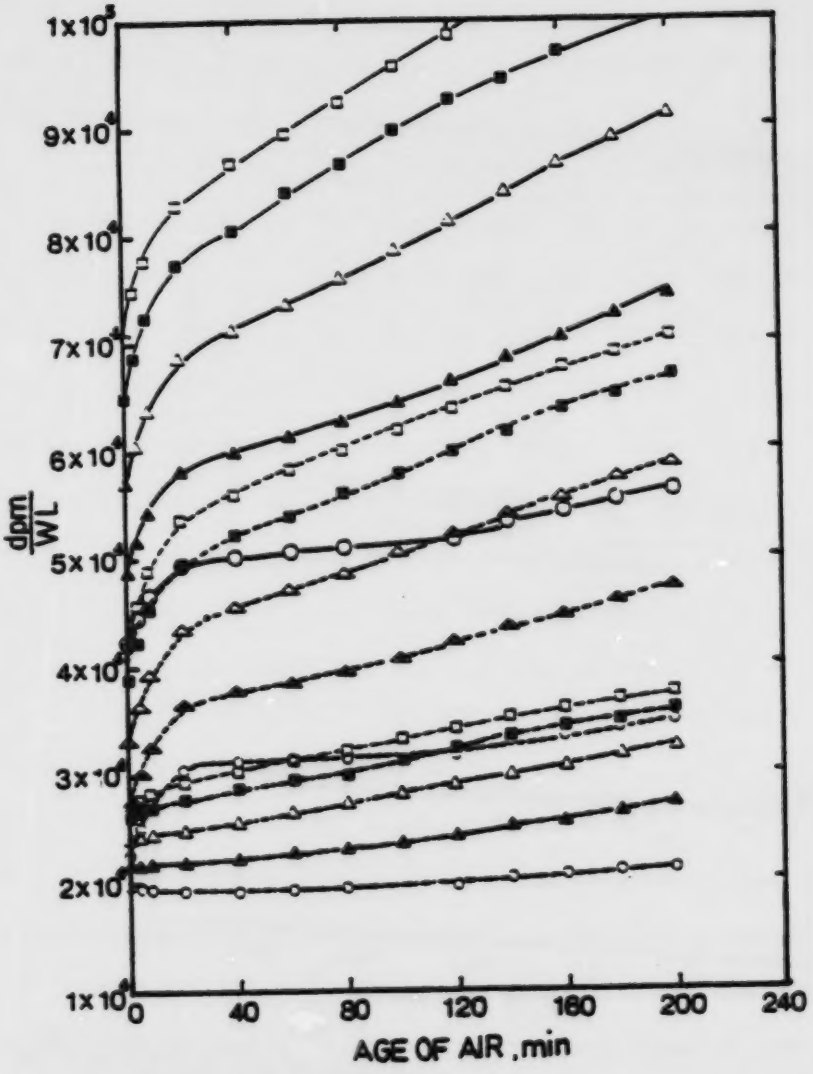

Fig. 2. Count to WL Ratio as a Function of the Age of the Air for a Mixed Atmosphere of Radon Daughters and Thoron Daughters: $WL_T = WL_{Rn} + WL_{Tn}/3$.

LEGEND

□ R = 0.5 ■ R = 0.6 — R = 1 ▲ R = 2 ○ R = 6 —— $\frac{\delta_T + \gamma_T}{WL_T}$ ------ $\frac{\delta_{Rn}}{WL_{Rn}}$ ..... $\frac{\gamma_{Tn}}{WL_T}$

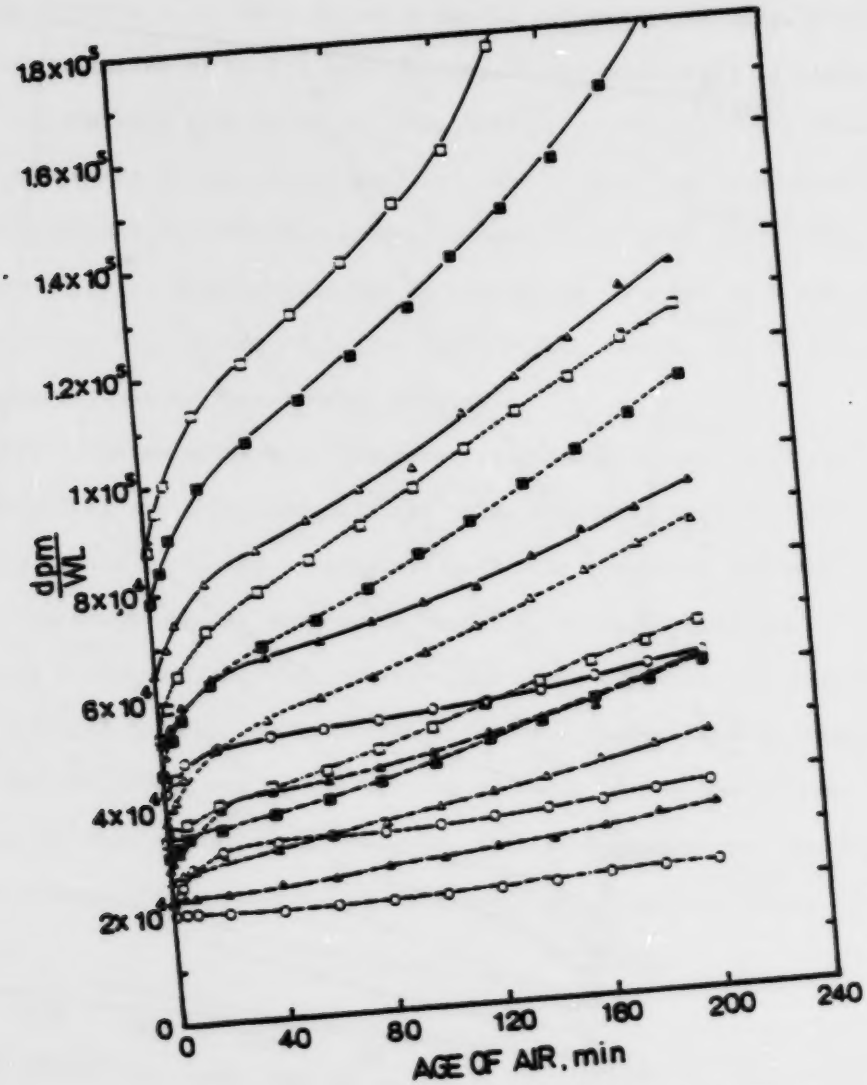

Fig. 3. Count to WL Ratio as a Function of the Age of the Air for a Mixed Atmosphere of Radon Daughters and Thoron Daughters: $WL_T = WL_{Rn} + 0.1\ WL_{Tn}$.

LEGEND

□ R = 0.5
■ R = 0.5
△ R = 1
▲ R = 2
○ R = 6
—— $\frac{\alpha_1 + \alpha_2}{WL_T}$
—— $\frac{\alpha_1}{WL_1}$
·-·-·- $\frac{\alpha_T}{WL_T}$

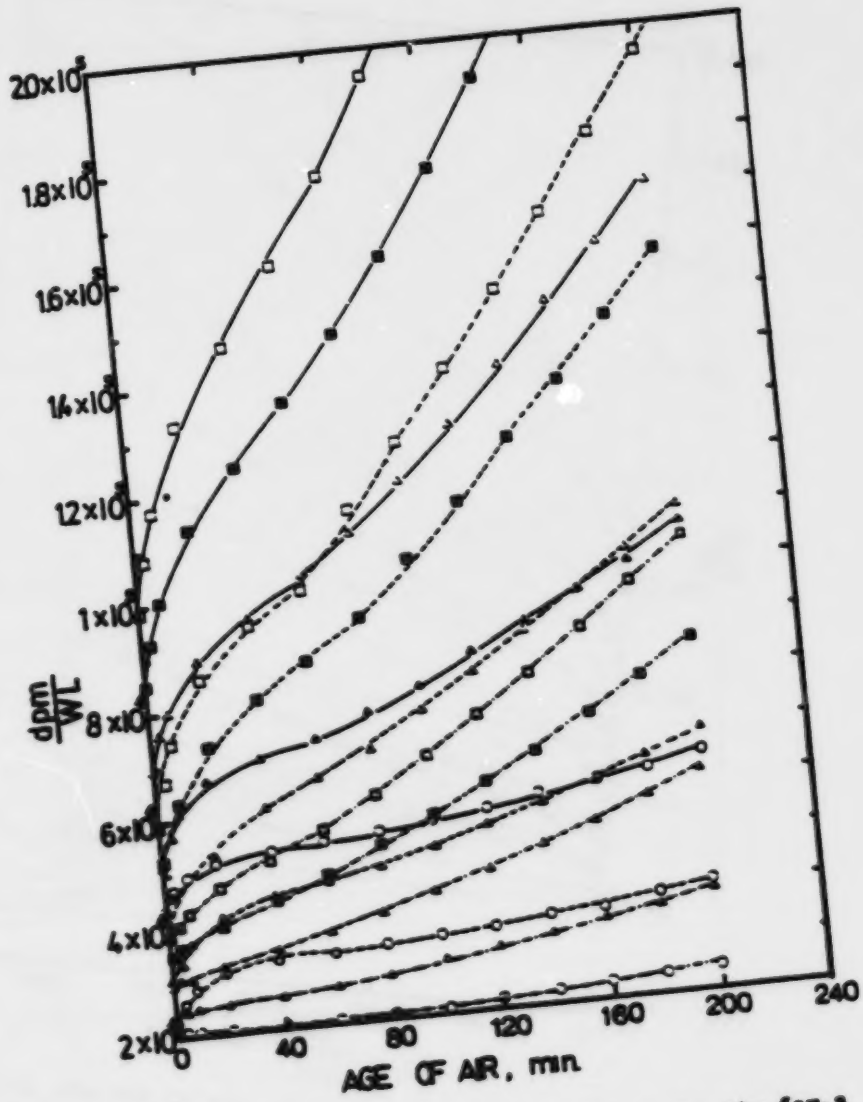

Fig. 4. Count to WL Ratio as a Function of the Age of the Air for a Mixed Atmosphere of Radon Daughters and Thoron Daughters: $WL_T = WL_{Rn}$.

Because of the large change in dpm/WL_T with change in radon: thoron concentration ratio, R (except in the case of the thoron daughter weighting factor $\omega = 1$, which is not a useful definition of total working level for evaluation of health hazard), continuous monitoring of alpha activity is the only mode which is conditionally acceptable for a direct reading continuous working level monitor. The conditional constraint is that R be constant or vary over a small range. Even under these conditions, the value of dpm/WL_T will not in general be constant with age of air (except for high values of R, for which α_T/WL_T remains fairly constant for in-growth times of less than 40 minutes).

For a thermoluminescent dosimeter responding to the total activity the implications are also that only the total α mode is conditionally acceptable, given $\omega = 1$ and constraints on R. In practice, however, existing thermoluminescent dosimeters record $\alpha_T + \beta_T$ although not necessarily with equal response to each (the gamma compensating chip is usually shielded from β), so that the calibration factor is more sensitive to age of the air and to the ratio R of radon:thoron gas concentrations. It must therefore be concluded that these dosimeters are not suitable for atmospheres containing both radon daughters and thoron daughters.

6.5 Conclusions

The continuous β-monitoring and α plus β monitoring modes are not suitable for use in continuous working level monitors operating in an atmosphere containing both radon daughters and thoron daughters. The continuous α-monitoring mode, however, can be used but only under severe

constraints with respect to the ratio of radon:thoron gas concentrations and the age of the air; even then, the α mode is least satisfactory for values of the thoron daughter weighting factor, ω, equal to values of health significance ($\sim$0.1 to 0.3).

Thermoluminescent dosimeters responding to total activity are not suitable for use in mixed atmospheres of radon daughters and thoron daughters. Strictly speaking, total alpha dosimeters based upon other measuring principles are also not suitable for use in mixed atmospheres. For both continuous monitoring and integrating dosimetry, methods other than those based on total activity should be used.

Appendix

The detailed data for Figures 1-4 are listed in Tables 1-4 below. These data show exact calibration factors (dpm/WL) for the α_T, β_T and $\alpha_T + \beta_T$ methods for various values of age of the air and the radon to thoron gas ratio and for different definitions of the total working level of mixture of radon and thoron daughter weighting factor, ω.

Table 1

Calculated Activity to WL Ratios for Various Ventilation Conditions (V = 1 L/min). WL_T is defined as $WL_{Rn} + WL_{Tn}$

Radon Thoron, R	Age of Air (min)	$\frac{a_T}{WL_T}$ (dpm/WL)	$\frac{\delta_T}{WL_T}$ (dpm/WL)	$\frac{a_T + \delta_T}{WL_T}$ (dpm/WL)
0.5	1	17563	27052	44615
	2	17484	27557	45042
	3	17413	28002	45415
	4	17350	28392	45742
	5	17293	28734	46027
	6	17242	29032	46274
	7	17197	29292	46488
	8	17156	29518	46674
	9	17119	29715	46835
	10	17087	29887	46973
	15	16965	30457	47423
	20	16890	30733	47623
	30	16804	30915	47719
	40	16757	30929	47685
	50	16726	30904	47630
	60	16703	30880	47583
	70	16685	30864	47550
	80	16671	30859	47530
	90	16658	30863	47521
	100	16647	30874	47521
	110	16638	30889	47527
	120	16629	30907	47536
	130	16621	30927	47548
	140	16614	30948	47562
	150	16608	30968	47576
	160	16602	30987	47591
	170	16597	31008	47605
	180	16592	31026	47618
	190	16587	31044	47631
	200	16583	31060	47643
	500	16530	31244	47774
	1000	16511	31294	47806
0.64	1	17111	26230	43961
	2	17624	26809	44433
	3	17546	27304	44850
	4	17475	27740	45215
	5	17412	28122	45535
	6	17356	28458	45814
	7	17304	28751	46056
	8	17259	29007	46266
	9	17218	29231	46449
	10	17181	29428	46606
	15	17043	30078	47121
	20	16957	30397	47353
	30	16859	30611	47470
	40	16805	30630	47435
	50	16770	30605	47376
	60	16745	30580	47324
	70	16724	30564	47289
	80	16708	30561	47269
	90	16694	30569	47262
	100	16681	30584	47264
	110	16670	30606	47276
	120	16660	30631	47291
	130	16651	30657	47309
	140	16643	30686	47329
	150	16636	30714	47350
	160	16629	30741	47371
	170	16623	30768	47391
	180	16617	30794	47411

Table 1 (continued)

Radon Thoron, R	Age of Air (min)	$\frac{a_T}{WL_T}$ (dpm/WL)	$\frac{\delta_T}{WL_T}$ (dpm/WL)	$\frac{a_T + \delta_T}{WL_T}$ (dpm/WL)
0.64	190	16612	30818	47430
	200	16607	30841	47448
	500	16543	31125	47669
	1000	16520	31216	47737
1	1	17972	24830	42803
	2	17874	25476	43350
	3	17784	26050	43835
	4	17703	26561	44264
	5	17629	27012	44642
	6	17563	27410	44973
	7	17503	27760	45263
	8	17449	28068	45516
	9	17400	28337	45737
	10	17356	28572	45928
	15	17190	29368	46558
	20	17085	29761	46847
	30	16964	30027	46993
	40	16900	30050	46951
	50	16857	30018	46875
	60	16827	29984	46810
	70	16803	29963	46765
	80	16783	29958	46740
	90	16766	29966	46732
	100	16751	29986	46738
	110	16738	30015	46753
	120	16726	30048	46773
	130	16715	30083	46801
	140	16706	30125	46831
	150	16697	30165	46862
	160	16688	30205	46894
	170	16681	30245	46926
	180	16674	30283	46957
	190	16667	30320	46987
	200	16661	30355	47015
	500	16576	30844	47420
	1000	16543	31026	47569
2	1	18320	22946	41266
	2	18209	23685	41895
	3	18107	24351	42459
	4	18013	24949	42962
	5	17928	25481	43410
	6	17851	25955	43806
	7	17780	26374	44154
	8	17716	26744	44460
	9	17657	27070	44728
	10	17604	27357	44962
	15	17403	28335	45739
	20	17274	28823	46097
	30	17126	29147	46273
	40	17045	29160	46205
	50	16994	29098	46092
	60	16958	29033	45991
	70	16930	28985	45915
	80	16907	28959	45866
	90	16888	28952	45840
	100	16871	28962	45833
	110	16856	28985	45841
	120	16843	29018	45861
	130	16831	29058	45889
	140	16819	29103	45922
	150	16809	29151	45960
	160	16799	29201	46000
	170	16790	29252	46042
	180	16781	29302	46083

Table 1 (continued)

Radon Thoron, R	Age of Air (min)	$\frac{a_T}{UL_T}$ (dpm/WL)	$\frac{\beta_T}{UL_T}$ (dpm/WL)	$\frac{a_T+\beta_T}{UL_T}$ (dpm/WL)
2	190	16773	29352	46125
	200	16766	29400	46166
	500	16649	30201	46851
	1000	16397	30563	47160
6	1	18658	21113	39771
	2	18340	21923	40462
	3	18429	22660	41089
	4	18327	23327	41653
	5	18232	23926	42159
	6	17146	24464	42609
	7	18066	24942	43009
	8	17994	25368	43361
	9	17927	25744	43672
	10	17867	26077	43943
	15	17633	27220	44853
	20	17482	27791	45273
	30	17308	28150	45457
	40	17214	28125	45339
	50	17136	28004	45140
	60	17117	27874	44991
	70	17088	27762	44851
	80	17066	27677	44743
	90	17049	27616	44664
	100	17033	27578	44611
	110	17020	27538	44578
	120	17008	27554	44563
	130	16998	27563	44561
	140	16988	27581	44569
	150	16979	27606	44586
	160	16971	27637	44608
	170	16963	27672	44635
	180	16956	27711	44667
	190	16949	27751	44700
	200	16942	27792	44734
	500	16819	28726	45544
	1000	16742	29323	46065

Table 2

Calculated Activity to UL Ratios for Various Ventilation Conditions (V = 1 L/min). UL_T is defined as $UL_{Rn} + UL_{Tn}/3$.

Radon Thoron, R	Age of Air (min)	$\frac{a_T}{UL_T}$ (dpm/WL)	$\frac{\beta_T}{UL_T}$ (dpm/WL)	$\frac{a_T+\beta_T}{UL_T}$ (dpm/WL)
0.5	1	27682	42887	70269
	2	27846	43890	71736
	3	28015	45052	73067
	4	28170	46100	74270
	5	28312	47043	75355
	6	28442	47890	76332
	7	28561	48650	77210
	8	28670	49330	78000
	9	28771	49940	78712
	10	28864	50487	79352
	15	29247	52505	81752
	20	29543	53757	83300
	30	30041	55268	85309
	40	30517	56328	86842
	50	31004	57287	88291

Table 2 (continued)

Radon Thoron, R	Age of Air (min)	$\frac{a_T}{UL_T}$ (dpm/WL)	$\frac{\beta_T}{UL_T}$ (dpm/WL)	$\frac{a_T+\beta_T}{UL_T}$ (dpm/WL)
0.5	60	31507	58249	89756
	70	32021	59232	91253
	80	32539	60234	92773
	90	33055	61242	94298
	100	33564	62247	95811
	110	34062	63238	97300
	120	34543	64206	98751
	130	35011	65145	100156
	140	35459	66050	101509
	150	35887	66918	102805
	160	36296	67747	104043
	170	36684	68537	105221
	180	37053	69288	106341
	190	37403	70000	107403
	200	37734	70674	108408
	300	42719	80743	123462
	1000	44863	85029	129892
0.64	1	26200	38833	65034
	2	25390	40084	66434
	3	26487	41219	67706
	4	26614	42245	68859
	5	26729	43171	69901
	6	26837	44003	70841
	7	26935	44751	71687
	8	27025	45422	72448
	9	27110	46024	73134
	10	27188	46564	73752
	15	27511	48552	76063
	20	27768	49776	77544
	30	28213	51226	79439
	40	28650	52219	80869
	50	29107	53119	82226
	60	29583	54027	83611
	70	30076	54964	85040
	80	30577	55929	86506
	90	31080	56913	87993
	100	31581	57902	89482
	110	32074	58886	90960
	120	32557	59856	92413
	130	33026	60805	93832
	140	33480	61728	95209
	150	33918	62620	96537
	160	34338	63478	97815
	170	34740	64300	99040
	180	35123	65087	100210
	190	35490	65838	101327
	200	35838	66553	102391
	300	41321	77725	119038
	1000	43804	82776	126582
1	1	24007	33168	57175
	2	24092	34338	58430
	3	24170	35405	59576
	4	24243	36374	60617
	5	24310	37250	61560
	6	24373	38039	62412
	7	24431	38749	63179
	8	24485	39386	63871
	9	24535	39957	64493
	10	24583	40470	65053
	15	24787	42347	67133
	20	24940	43478	68418
	30	25187	44734	70041
	40	25431	45578	71207
	50	26005	46307	72312
	60	28406	47053	73439

Table 2 (continued)

Radon Thoron, R	Age of Air (min)	$\frac{a_T}{UL_T}$ (dpm/WL)	$\frac{\beta_T}{UL_T}$ (dpm/WL)	$\frac{a_T+\beta_T}{UL_T}$ (dpm/WL)
1	70	26828	47840	74668
	80	27285	48668	75933
	90	27711	49529	77240
	100	28161	50412	78573
	110	28611	51306	79917
	120	29058	52203	81261
	130	29498	53094	82592
	140	29930	53972	83902
	150	30350	54834	85184
	160	30759	55673	86432
	170	31154	56489	87644
	180	31537	57278	88815
	190	31905	58040	89945
	200	32259	58774	91033
	500	38318	71302	109620
	1000	41427	77699	119126
2	1	21678	27151	48829
	2	21678	28197	49876
	3	21679	29155	50834
	4	21680	30026	51706
	5	21681	30815	52496
	6	21683	31527	53210
	7	21685	32167	53852
	8	21688	32741	54429
	9	21692	33255	54947
	10	21696	33715	55411
	15	21726	35374	57100
	20	21773	36331	58104
	30	21913	37293	59206
	40	22102	37809	59911
	50	22329	38232	60561
	60	22585	38669	61254
	70	22864	39148	62014
	80	23164	39675	62839
	90	23475	40245	63720
	100	23796	40849	64646
	110	24124	41481	65605
	120	24454	42132	66587
	130	24787	42795	67582
	140	25119	43464	68582
	150	25447	44133	69581
	160	25772	44799	70572
	170	26092	45458	71550
	180	26406	46108	72513
	190	26713	46745	73458
	200	27012	47369	74381
	500	32897	59671	92568
	1000	38604	67406	106010
6	1	19872	22487	42359
	2	19796	23409	43206
	3	19726	24255	43981
	4	19660	25024	44685
	5	19600	25721	45321
	6	19544	26349	45894
	7	19494	26913	46406
	8	19447	27417	46864
	9	19405	27866	47272
	10	19367	28266	47633
	15	19225	29677	48902
	20	19144	30433	49577
	30	19088	31041	50127
	40	19103	31211	50314
	50	19161	31276	50438
	60	19246	31341	50587
	70	19350	31437	50787

Table 2 (continued)

Radon Thoron, R	Age of Air (min)	$\frac{a_T}{UL_T}$ (dpm/WL)	$\frac{\beta_T}{UL_T}$ (dpm/WL)	$\frac{a_T+\beta_T}{UL_T}$ (dpm/WL)
6	80	19468	31571	51039
	90	19596	31743	51339
	100	19733	31949	51682
	110	19876	32184	52060
	120	20025	32442	52467
	130	20177	32718	52896
	140	20333	33010	53343
	150	20490	33313	53803
	160	20648	33624	54272
	170	20806	33941	54746
	180	20964	34260	55224
	190	21121	34581	55702
	200	21277	34903	56179
	500	24926	42574	67500
	1000	27988	49020	77009

Table 3

Calculated Activity to WL Ratios for Various Ventilation Conditions (V = 1 L/min)
WL_T is defined as $WL_{Rn} + 0.1\ WL_{Tn}$

Radon Thoron, R	Age of Air (min)	$\frac{a_T}{UL_T}$ (dpm/WL)	$\frac{\beta_T}{UL_T}$ (dpm/WL)	$\frac{a_T+\beta_T}{UL_T}$ (dpm/WL)
0.5	1	34631	53342	87973
	2	35134	55377	90511
	3	35602	57253	92855
	4	36036	58973	95010
	5	36439	60547	96985
	6	36811	61981	98792
	7	37155	63288	100443
	8	37473	64478	101949
	9	37768	65557	103325
	10	38043	66541	104583
	15	39171	70322	109493
	20	40042	72862	112904
	30	41477	76307	117783
	40	42825	79063	121888
	50	44216	81697	125912
	60	45677	84444	130121
	70	47208	87323	134531
	80	48796	90327	139123
	90	50429	93431	143860
	100	52092	96608	148700
	110	53772	99831	153603
	120	55457	103074	158531
	130	57137	106314	163452
	140	58803	109533	168336
	150	60447	112713	173160
	160	62062	115841	177904
	170	63645	118908	182552
	180	65190	121904	187094
	190	66697	124823	191520
	200	68162	127663	195825
	500	93890	181241	277131
	1000	112431	213093	325524
0.64	1	31483	46662	78145
	2	31873	48486	80359
	3	32237	50167	82404
	4	32576	51709	84285

Table 1 (continued)

Radon Thoron, R	Age of Air (min)	$\frac{\alpha_T}{UL_T}$ (dpm/WL)	$\frac{\beta_T}{UL_T}$ (dpm/WL)	$\frac{\alpha_T + \beta_T}{UL_T}$ (dpm/WL)
0.64	5	32889	53120	86010
	6	33181	54406	87587
	7	33450	55577	89027
	8	33700	56641	90342
	9	33993	57607	91541
	10	34149	58486	92635
	15	35044	61846	96890
	20	35743	64073	99816
	30	36914	67023	103937
	40	38033	69320	107353
	50	39199	71538	110738
	60	40435	73844	114279
	70	41738	76277	118014
	80	43098	78833	121930
	90	44503	81493	125996
	100	45943	84235	130178
	110	47406	81034	134439
	120	48880	89868	138749
	130	50359	92717	143077
	140	51833	95565	147398
	150	53295	98394	151689
	160	54739	101193	155933
	170	56162	103951	160113
	180	57558	106660	164219
	190	58923	109314	168239
	200	60261	111908	172169
	500	86791	163290	250081
	1000	103826	196187	300014
1	1	27204	37384	64789
	2	27432	39099	66530
	3	27643	40495	68140
	4	27843	41776	69619
	5	28028	42946	70974
	6	28199	44012	72212
	7	28360	44980	73340
	8	28508	45858	74366
	9	28647	46654	75301
	10	28777	47374	76151
	15	29322	50095	79417
	20	29761	51840	81602
	30	30527	54029	84556
	40	31289	55636	86925
	50	32102	57164	89287
	60	32977	58782	91739
	70	33909	60468	94377
	80	34892	62283	97175
	90	35917	64197	100114
	100	36976	66192	103168
	110	38061	68251	106312
	120	39164	70358	109523
	130	40279	72498	112777
	140	41399	74656	116056
	150	42520	76820	119340
	160	43636	78980	122616
	170	44743	81127	125870
	180	45838	83253	129091
	190	46919	85353	132271
	200	47982	87420	135402
	500	70838	131815	202653
	1000	87491	164093	251584
2	1	23164	29012	52175
	2	23227	30212	53439
	3	23287	31317	54604
	4	23343	32329	55672
	5	23395	33251	56647

Table 1 (continued)

Radon Thoron, R	Age of Air (min)	$\frac{\alpha_T}{UL_T}$ (dpm/WL)	$\frac{\beta_T}{UL_T}$ (dpm/WL)	$\frac{\alpha_T + \beta_T}{UL_T}$ (dpm/WL)
2	6	23445	34088	57533
	7	23491	34846	58337
	8	23535	35529	59065
	9	23577	36146	59723
	10	23617	36700	60317
	15	23795	38743	62538
	20	23957	39975	63932
	30	24289	41337	65626
	40	24662	42189	66851
	50	25085	42951	68036
	60	25554	43751	69305
	70	26064	44625	70689
	80	26610	45579	72189
	90	27187	46608	73795
	100	27788	47703	75491
	110	28411	48853	77264
	120	29050	50049	79099
	130	29702	51280	80981
	140	30362	52537	82899
	150	31029	53813	84842
	160	31698	55101	86799
	170	32369	56394	88763
	180	33037	57688	90725
	190	33703	58977	92680
	200	34363	60259	94622
	500	49959	90622	140581
	1000	63320	116603	179923
6	1	20335	23011	43346
	2	20278	23978	44256
	3	20224	24867	45091
	4	20174	25678	45853
	5	20128	26415	46543
	6	20086	27079	47166
	7	20048	27678	47726
	8	20013	28215	48228
	9	19982	28694	48676
	10	19953	29122	49076
	15	19852	30643	50498
	20	19803	31480	51283
	30	19798	32199	51997
	40	19866	32438	52323
	50	19979	32610	52589
	60	20122	32768	52890
	70	20290	32964	53253
	80	20476	33207	53683
	90	20678	33496	54173
	100	20892	33826	54718
	110	21117	34192	55309
	120	21350	34589	55939
	130	21591	35011	56602
	140	21837	35453	57290
	150	22088	35911	57999
	160	22341	36383	58724
	170	22597	36863	59460
	180	22854	37350	60204
	190	23112	37842	60953
	200	23369	38335	61705
	500	29986	51215	81201
	1000	38392	64089	100680

Table 4

Calculated Activity to WL Ratios for Various Ventilation Conditions (V = 1 L/min)
WL_T is defined as WL_{Rn}

Radon Thoron, R	Age of Air (min)	$\frac{a_T}{WL_T}$ (dpm/WL)	$\frac{\delta_T}{WL_T}$ (dpm/WL)	$\frac{a_T+\delta_T}{WL_T}$ (dpm/WL)
0.5	1	38823	59799	98622
	2	39573	62373	101946
	3	40277	64770	105047
	4	40935	66990	107926
	5	41550	69040	110590
	6	42123	70926	113048
	7	42655	72657	115313
	8	43151	74246	117397
	9	43613	75702	119316
	10	44044	77039	121083
	15	45838	82290	128127
	20	47237	85954	133190
	30	49562	91182	140744
	40	51774	95561	147335
	50	54094	99949	154043
	60	56583	104605	161188
	70	59250	109599	168850
	80	62091	114937	177028
	90	65091	120595	185686
	100	68234	126545	194779
	110	71505	132753	204258
	120	74886	139184	214070
	130	78361	145804	224165
	140	81914	152583	234498
	150	85532	159490	245022
	160	89201	166497	255698
	170	92908	173581	266489
	180	96643	180718	277361
	190	100395	187890	288285
	200	104156	195079	299235
	500	205522	388453	593978
	1000	317133	601072	918205
0.64	1	34460	51073	85533
	2	35019	53271	88290
	3	35544	55313	90857
	4	36036	57201	93237
	5	36494	58942	95436
	6	36922	60540	97462
	7	37319	62005	99325
	8	37690	63346	101036
	9	38036	64573	102608
	10	38358	65695	104054
	15	39703	70069	109773
	20	40761	73066	113827
	30	42536	77231	119767
	40	44242	80637	124879
	50	46042	84024	130065
	60	47977	87618	135595
	70	50056	91479	141535
	80	52271	95613	147884
	90	54612	100003	154616
	100	57065	104627	161693
	110	59619	109457	169076
	120	62259	114465	176724
	130	64973	119624	184597
	140	67749	124909	192657
	150	70574	130296	200870
	160	73440	135764	209203
	170	76336	141292	217628
	180	79253	146884	226117
	190	82185	152463	234648

Table 4 (continued)

Radon Thoron, R	Age of Air (min)	$\frac{a_T}{WL_T}$ (dpm/WL)	$\frac{\delta_T}{WL_T}$ (dpm/WL)	$\frac{a_T+\delta_T}{WL_T}$ (dpm/WL)
0.64	200	85123	158077	243200
	500	164315	309142	473457
	1000	251511	475249	726759
1	1	28851	39859	68710
	2	29165	41568	70733
	3	29460	43153	72613
	4	29736	44615	74351
	5	29994	45958	75952
	6	30235	47187	77422
	7	30459	48309	78768
	8	30668	49332	80000
	9	30864	50264	81128
	10	31047	51111	82158
	15	31817	54357	86173
	20	32434	56498	88933
	30	33302	59295	92797
	40	34358	61649	96007
	50	35688	63550	99238
	60	36914	65777	102690
	70	38234	68181	106415
	80	39645	70768	110413
	90	41139	73529	114668
	100	42706	76447	119153
	110	44337	79505	123842
	120	46024	82683	128707
	130	47760	85963	133723
	140	49535	89327	138862
	150	51343	92761	144104
	160	53176	96249	149425
	170	55029	99778	154807
	180	56896	103336	160232
	190	58771	106915	165686
	200	60652	110503	171154
	500	111333	207168	318501
	1000	167139	313476	480615
2	1	23865	29890	53754
	2	23961	31166	55127
	3	24051	32345	56396
	4	24138	33428	57564
	5	24216	34417	58633
	6	24291	35318	59609
	7	24361	36136	60496
	8	24426	36873	61302
	9	24489	37544	62033
	10	24548	38148	62696
	15	24807	40391	65198
	20	25033	41770	66804
	30	25472	43351	68824
	40	25950	44393	70344
	50	26486	45350	71836
	60	27079	46362	73441
	70	27726	47471	75197
	80	28423	48684	77106
	90	29163	49996	79158
	100	29941	51399	81340
	110	30753	52881	83634
	120	31594	54432	86025
	130	32460	56042	88501
	140	33346	57699	91043
	150	34248	59396	93644
	160	35164	61123	96288
	170	36089	62876	98966
	180	37022	64646	101668
	190	37960	66427	104388

Table 4 (continued)

Radon Thoron, R	Age of Air (min)	$\frac{a_T}{UL_T}$ (dpm/UL)	$\frac{\beta_T}{UL_T}$ (dpm/UL)	$\frac{a_T + \beta_T}{UL_T}$ (dpm/UL)
2	200	38899	68214	107114
	500	64329	116524	180763
	1000	92142	169678	261820
6	1	20341	23243	43784
	2	20491	24231	44722
	3	20445	25139	45585
	4	20403	25969	46372
	5	20364	26723	47807
	6	20328	27405	47733
	7	20295	28020	48315
	8	20266	28571	48837
	9	20239	29064	49304
	10	20216	29505	47921
	15	20134	31080	51214
	20	20099	31952	52051
	30	20119	32722	52841
	40	20212	33023	53235
	50	20351	33217	53568
	60	20523	33420	53942
	70	20721	33664	54385
	80	20941	33961	54901
	90	21179	34307	55486
	100	21431	34699	56131
	110	21697	35132	56829
	120	21974	35599	57572
	130	22259	36094	58354
	140	22552	36614	59167
	150	22852	37153	60005
	160	23156	37708	60864
	170	23463	38275	61739
	180	23773	38852	62625
	190	24085	39345	63520
	200	24398	40022	64422
	500	32843	56094	88937
	1000	42144	73812	115956

CHAPTER 7

AN OPTIMIZED SCHEME FOR MEASUREMENT OF THE CONCENTRATIONS OF THE DECAY PRODUCTS OF RADON AND THORON

7.1 Introduction

Thorium may be present in uranium ores at a mass concentration up to almost half that of uranium. The ratios of U_3O_8 to ThO_2 in the Canadian mines at Elliot Lake, Bancroft and Agnew Lake are reported to be 2.5:1, 2.5:1 and 2.4:4 respectively (Pai and Phillips, 1977). From a series of measurements employing energy discriminatory track etch dosimetry at Elliot Lake, Phillips et al. (1978) found the working level for thoron daughters to be about one half that for radon daughters. Duggan (1973) recommends that for a complete assessment of the alpha radiation hazard associated with thoron and its daughters, the concentration of both should be meausred. For this purpose, however, he considers the measurement of thoron daughter concentration alone to be acceptable in circumstances in which there are no sharp thoron gradients, which is true for uranium mines.

Busigin and Phillips (1980) optimized the modified Tsivoglou method for radon daughters to include the commonly neglected uncertainties associated with fluctuations in flowrate and concentration. Their work is extended here to a mixed system of radon daughters and thoron daughters. An optimization search through a wide range of counting schemes was conducted for sampling times of 5, 10, 15, 30 and 60 min. Results which required counting beyond a normal 8 h working shift were rejected on practical grounds.

7.2 Analysis Technique

The modified Tsivoglou method for the measurement of radon daughters (Thomas, 1970, 1972) is based on counting the alpha activity

of filtered air samples over optimized time intervals after sampling. For the measurement of both radon daughter and thoron daughter concentrations, RaA, RaB, RaC, ThB and ThC need to be taken into consideration. Because of the extremely short half-life of RaC' (164 μs) its parent RaC can be considered to be a simultaneous alpha and beta emitter. Similarly, because of the very short half-life of ThA (0.15 s), ThB can be considered to be formed directly from thoron. ThC' (half-life 0.3 μs), like RaC', can be taken into account by assuming its parent ThB to be a simultaneous alpha and beta emitter. The time-weighted averages of RaA, RaB, RaC, ThB and ThC concentrations during sampling, $\bar{C}_1$, $\bar{C}_2$, $\bar{C}_3$, $\bar{C}_4$, $\bar{C}_5$, respectively, are assumed to vary randomly, following a normal distribution, during the course of sampling with standard deviations ΔC_1, ΔC_2, ΔC_3, ΔC_4 and ΔC_5, respectively. The concentrations cannot vary independently, yet they do not vary identically. At the end of sampling for a time T (min) the expected number of atoms of each species on the filter is $\bar{N}_1$, $\bar{N}_1$, $\bar{N}_2$, $\bar{N}_3$ and $\bar{N}_4$. The time-weighted average of the sampling flowrate is $\bar{V}$ litres per minute with an associated standard deviation ΔV. From the decay constants of the five species, λ_1, λ_2, λ_3, λ_4 and λ_5, respectively, the following five equations give the expected number of atoms at the end of sampling:

$$\bar{N}_1 = \frac{\bar{V}\bar{C}_1}{\lambda_1}(1 - e^{-\lambda_1 T}) \tag{1}$$

$$\bar{N}_2 = \frac{\bar{V}\bar{C}_1}{\lambda_2}(1 - \exp^{-\lambda_2 T})\left[1 + \frac{\lambda_2(e^{-\lambda_2 T} - e^{-\lambda_1 T})}{(\lambda_2 - \lambda_1)(1 - e^{-\lambda_2 T})}\right] + \frac{\bar{V}\bar{C}_2}{\lambda_2}(1 - e^{-\lambda_2 T}) \tag{2}$$

$$\bar{N}_3 = \frac{\bar{V}\bar{C}_1}{\lambda_3}(1 - e^{\lambda_3 T})\left[1 + \frac{\lambda_3(e^{-\lambda_3 T} - e^{-\lambda_2 T})}{(\lambda_3 - \lambda_2)(1 - e^{-\lambda_3 T})}\right.$$

$$+\frac{\lambda_2\lambda_3(e^{-\lambda_2 T}-e^{-\lambda_3 T})}{(\lambda_3-\lambda_2)(\lambda_2-\lambda_1)(1-e^{-\lambda_3 T})}+\frac{\lambda_2\lambda_3(e^{-\lambda_3 T}-e^{-\lambda_1 T})}{(\lambda_3-\lambda_1)(\lambda_2-\lambda_1)(1-e^{-\lambda_3 T})}\Big]$$

$$+\frac{\bar{V}\bar{C}_2}{\lambda_3}(1-e^{-\lambda_3 T})\Big[1+\frac{\lambda_3(e^{-\lambda_3 T}-e^{-\lambda_2 T})}{(\lambda_3-\lambda_2)(1-e^{-\lambda_3 T})}\Big]+\frac{\bar{V}\bar{C}_3}{\lambda_3}(1-e^{-\lambda_3 T}) \tag{3}$$

$$\bar{N}_4 = \frac{\bar{V}\bar{C}_4}{\lambda_4}(1-e^{-\lambda_4 T}) \tag{4}$$

$$\bar{N}_5 = \frac{\bar{V}\bar{C}_4}{\lambda_5}(1-e^{-\lambda_5 T})\Big[1+\frac{\lambda_5(e^{-\lambda_5 T}-e^{-\lambda_4 T})}{(\lambda_5-\lambda_4)(1-e^{-\lambda_5 T})}\Big]+\frac{\bar{V}\bar{C}_5}{\lambda_5}(1-e^{-\lambda_5 T}) \tag{5}$$

These equations can be expressed as:

$$\bar{N}_i = \sum_{j=1}^{5} a_{ij}\,\bar{V}\bar{C}_j \quad \text{for} \quad i = 1, 2, 3, 4, 5 \tag{6}$$

where $a_{ij} = 0$, for $j > i$

and for $i = 4,5$ as $j = 1,2,3$

or

$$\begin{bmatrix}\bar{N}_1\\ \bar{N}_2\\ \bar{N}_3\\ \bar{N}_4\\ \bar{N}_5\end{bmatrix} = \begin{bmatrix}a_{11} & 0 & 0 & 0 & 0\\ a_{21} & a_{22} & 0 & 0 & 0\\ a_{31} & a_{32} & a_{33} & 0 & 0\\ 0 & 0 & 0 & a_{44} & 0\\ 0 & 0 & 0 & a_{54} & a_{55}\end{bmatrix}\begin{bmatrix}\bar{V}\bar{C}_1\\ \bar{V}\bar{C}_2\\ \bar{V}\bar{C}_3\\ \bar{V}\bar{C}_4\\ \bar{V}\bar{C}_5\end{bmatrix} \tag{7}$$

The expected number of alpha disintegrations obtained in an interval t_1 to t_2 minutes after sampling is

$$\bar{I}(t_1,t_2) = \Big[\bar{N}_1+\frac{\lambda_2\lambda_3\bar{N}_1}{(\lambda_3-\lambda_1)(\lambda_2-\lambda_1)}\Big](e^{-\lambda_1 t_1}-e^{-\lambda_1 t_2})$$

$$+\left[\frac{\lambda_1\lambda_3\bar{N}_1}{(\lambda_1-\lambda_2)(\lambda_3-\lambda_2)}+\frac{\lambda_3\bar{N}_2}{(\lambda_3-\lambda_2)}\right](e^{-\lambda_2 t_1}-e^{-\lambda_2 t_2})$$

$$+\left[\frac{\lambda_1\lambda_2\bar{N}_1}{(\lambda_1-\lambda_3)(\lambda_2-\lambda_3)}+\frac{\lambda_2\bar{N}_2}{(\lambda_2-\lambda_3)}+\bar{N}_3\right](e^{-\lambda_3 t_1}-e^{-\lambda_3 t_2})$$

$$+\frac{\lambda_5\bar{N}_4}{\lambda_5-\lambda_4}(e^{-\lambda_4 t_1}-e^{-\lambda_4 t_2})+\left[\frac{\lambda_4\bar{N}_4}{\lambda_4-\lambda_5}+\bar{N}_5\right](e^{-\lambda_5 t_1}-e^{-\lambda_5 t_2}) \quad (8)$$

If $\bar{I}_1$, $\bar{I}_2$, $\bar{I}_3$, $\bar{I}_4$ and $\bar{I}_5$ are defined as the expected number of alpha disintegrations in the five independent counting intervals (t_1,t_2), (t_3,t_4), (t_5,t_6), (t_7,t_8) and (t_9,t_{10}) respectively then

$$\bar{I}_k = \sum_{i=1}^{5} b_{ki}\,\bar{N}_i \quad (9)$$

The coefficients b_{ki} can be calculated from equation (8) and similar equations for I_2, I_3, I_4 and I_5.

The set of equations contained in equation (9) can be solved for $\bar{N}_i$ as:

$$\bar{N}_i = \sum_{k=1}^{5} d_{ik}\,\bar{I}_k \quad (9a)$$

From the relationship between the $\bar{N}_i$'s (equation (9a)) and the airborne concentrations $\bar{C}_j$'s (equation (6)) the final solution can be expressed as

$$\bar{V}\,\bar{C}_j = \sum_{k=1}^{5} e_{jk}\,\bar{I}_k \quad (10)\ (10)$$

Equation (10) gives the airborne concentrations of radon and thoron daughters firectly from the number of alpha disintegrations on the filter obtained in five successive time intervals after the end of sampling.

To determine optimal intervals the following calculations for uncertainties were carried out. The standard deviations of the number of atoms present on the filter at the end of sampling for RaA, RaB, RaC, ThB and ThC were estimated by standard statistical procedures:

$$(\Delta N_1)^2 = a_{11}^2[(\bar{V}\Delta C_1)^2 + (\bar{C}_1\Delta V)^2] + \bar{V}\bar{C}_1 T - \bar{N}_1 \quad (11)$$

$$(\Delta N_2)^2 = a_{21}^2[(\bar{V}\Delta C_1)^2 + (\bar{C}_1\Delta V)^2] + a_{22}^2[(\bar{V}\Delta C_2)^2 + (\bar{C}_2\Delta V)^2] + 2\bar{V}\bar{C}_1 T + \bar{V}\bar{C}_2 T - 2\bar{N}_1 - \bar{N}_2 \quad (12)$$

$$(\Delta N_3)^2 = a_{31}^2[(\bar{V}\Delta C_1)^2 + (\bar{C}_1\Delta V)^2] + a_{32}^2[(\bar{V}\Delta C_2)^2 + (\bar{C}_2\Delta V)^2] + a_{33}^2[(\bar{V}\Delta C_3)^2 + (\bar{C}_3\Delta V)^2] + 2\bar{V}\bar{C}_1 T + 2\bar{V}\bar{C}_2 T + \bar{V}\bar{C}_3 T - 2\bar{N}_1 - 2\bar{N}_2 - \bar{N}_3 \quad (13)$$

$$(\Delta N_4)^2 = a_{44}^2[(\bar{V}\Delta C_4)^2 + (\bar{C}_4\Delta V)^2] + \bar{V}\bar{C}_4 T - \bar{N}_4 \quad (14)$$

$$(\Delta N_5)^2 = a_{54}^2[(\bar{V}\Delta C_4)^2 + (\bar{C}_4\Delta V)^2] + a_{55}^2[(\bar{V}\Delta C_5)^2 + (\bar{C}_5\Delta V)^2] + 2\bar{V}\bar{C}_4 T + \bar{V}\bar{C}_5 T - 2\bar{N}_4 - \bar{N}_5 \quad (15)$$

It should be noted that it was assumed that the concentrations C_1 to C_5 and the flowrate V can be treated as independent random variables. While this is not completely rigorous, since these variables do have some degree of interdependency, it has been shown (Busigin and Phillips, 1980) that it is nonetheless a reasonable approximation.

The first terms in the above five equations represent the uncertainties due to flow rate and concentration fluctuations while the last terms represent the uncertainty due to the randomness of radioactive decay.

The standard deviations of $\bar{I}_1$, $\bar{I}_2$, $\bar{I}_3$, $\bar{I}_4$ and $\bar{I}_5$, ΔI_1, ΔI_2, ΔI_3, ΔI_4 and ΔI_5, respectively depend upon ΔN_1, ΔN_2, ΔN_3, ΔN_4 and ΔN_5. They

also depend upon the counting statistics and the counting efficiency E (cpm/dpm) of the alpha counter employed in the measurement. The effect of counting statistics is usually of the same order as the other contributions to uncertainty. Hence the following equation can be used to calculate the values of the ΔI_k's:

$$(\Delta I_k)^2 = \sum_{i=1}^{5} (b_{ki}\ \Delta N_i) + \frac{\bar{I}_k}{E} \qquad (16)$$

The standard deviations in concentration measurements (S_j's) are then

$$S_j^2 = \sum_{k=1}^{5} (e_{jk}\ \Delta I_k)^2/\bar{V}^2 \qquad (17)$$

The relative standard deviation RS_j is defined as

$$R\,S_j = \frac{S_j}{\bar{C}_j} \qquad (18)$$

In order to find optimal counting intervals, a performance index was defined equivalent to the relative standard deviation for ThC measurement (RS_5), since it was found that in most practical uranium mine measurements, the highest relative uncertainty in concentration among the various radionuclides would be that of ThC. A similar optimization criterion was used by previous workers in optimization of the modified Tsivoglou method (for radon daughters alone) with respect to RaA measurement (Busigin and Phillips, 1980; Thomas, 1970, 1972).

Some limits were defined to constrain the counting time so as to obtain a practical optimum rather than a global optimum. It was assumed that, following sampling, two minutes were required for transferring a filter into a counting instrument. Also each counting interval was to begin and end at some multiple of 1 minute after the end of sampling with

at least one minute required between adjacent counting intervals for recording of data. The first three counting intervals (corresponding to radon daughters) were limited to a total of 60 min following sampling while the last two intervals (corresponding to thoron daughters) were fixed in the following ways:

In Case I, the limit was fixed such that the fifth counting interval began exactly 24 h after the beginning of sampling (thus implying the resumption of work at exactly the same time next day), allowing one hour for counting in this last interval. The fourth interval in this case had to be within 3 1/2 h after the beginning of sampling so as to allow noon samples to be counted during the same shift.

In Case II, the total counting time (CT) was limited to 5 1/2 h after the beginning of sampling in order that sampling and counting could be completed within the same working shift.

All possible permutations of time intervals within the above mentioned constraints were evaluated. The time intervals corresponding to the minimum value of the performance index (RS_5) within the defined limits were then recorded as the optimal intervals for five different sampling times.

The results of these calculations expressed as relative standard deviations of concentration measurements of the various daughters and of the radon and thoron daughter working levels, are plotted against the relative standard deviations in concentration $\frac{\Delta C_j}{C_j}$ and the relative standard deviations in flow rate $\frac{\Delta V}{V}$ using realistic levels of uncertainty. The solutions corresponding to the optimized intervals are presented in the form of equation (10) later.

These calculations may be extended to radon and thoron daughter working levels by use of the following equations:

$$\overline{\text{Rn WL}} = \frac{1.03\ \bar{C}_1 + 5.07\ \bar{C}_2 + 3.73\ \bar{C}_3}{1000} \qquad (19)$$

$$\overline{\text{Tn WL}} = \frac{123.19\ \bar{C}_4 + 12.67\ \bar{C}_5}{1000} \qquad (20)$$

In the above definitions 1 WL is assumed to correspond to the quantity of short lived radon or thoron daughters per litre of air which in decaying to Pb-210 in the case of radon daughters and Pb-208 in the case of thoron daughters will yield 1.3×10^5 MeV of alpha energy. This definition for thoron WL differs slightly from that used by Rock (1975) since Rock considered the potential alpha energy yield of Pb-212 (ThB) only and did not include a contribution from any other short lived thoron daughters.

Relative standard deviations for radon and thoron daughter working levels, RSRWL and RSTWL respectively, may be calculated from

$$\text{RSRWL} = \frac{[(1.03\ S_1)^2 + (5.07\ S_2)^2 + (3.73\ S_3)^2]^{1/2}}{\text{RnWL} \times 1000} \qquad (21)$$

$$\text{RSTWL} = \frac{[(123.19\ S_4)^2 + (12.67\ S_5)^2]^{1/2}}{\text{TnWL} \times 1000} \qquad (22)$$

For the purpose of calculations, the concentrations of RaA, RaB, RaC, ThB and ThC were taken to be 100, 60, 40, 2 and 1 in pCi L^{-1} respectively, since these are representative of a typical situation in many uranium mines. The flow rate was taken to be 3 L per min for all calculations, but in order to demonstrate higher accuracy with a higher

flow rate two other values, 5 Lpm and 10 Lpm were used for a sampling time (ST) of 10 min. The counting efficiency was taken as 40%.

7.3 Results

The imposed time limits within which optimization was performed are shown in summary form in Table 1.

The relative standard deviation in flow rate was taken as 0.00 and 0.03. The effect of flow rate on measurement precision is given for Table 2. RSD flow refers to the relative standard deviation in flow, ΔV, and RSD concentration is the ΔC defined earlier.

The results for cases I and II are given in Table 3 and Table 4, respectively. Only RS1 and RS5, RSRWL and RSTWL are tabulated since RS1 represents the worst precision amongst radon daughters and RS5 is much greater than RS4 for thoron daughters; RSRWL and RSTWL give a measure of the accuracy with which working levels for radon and thoron daughters can be estimated from concentration measurements.

7.4 Discussion and Conclusions

Because of the interdependence of several variables, selection of the optimization criterion raises certain problems. The criterion of a combined minimum statistical uncertainty in concentration was found to result in extremely good measurement precision for one set of daughters but extremely poor precision for the other set. Optimization was therefore made with respect to ThC alone, since the ThC measurement always ended up with the worst statistical uncertainty of all the daughters of radon and thoron. Recalculation of optimal counting intervals using this criterion resulted in a large decrease in the relative standard deviation

Table 1

Limits on Counting Intervals Used in Calculation

Case No.	Starting from the end of sampling		Starting from the beginning of sampling			General comments
	t_1 (min)	t_5 (min)	ST + t_8 (min)	ST + t_9 (min)	ST + t_{10} (min)	
I	2	60	210 or less	1440	t_9 + 60	More accurate; sampling and counting takes 25 hours
II	2	60	not fixed	not fixed	330	Less accurate; sampling and counting takes 5½ hours

Table 2

Effect of Flow Rate on Measurement Precision

ST = 10 min
Optimum intervals: (2,4), (5,20), (30,60), (140,200), (1430, 1490)
RSD flow = 0.00 (0.03)
RSD concentration = 0.03

Flow rate (Lpm)	RS1	RS2	RS3	RS4	RS5	RSRWL	RSTWL
3	0.17	0.06	0.08	0.05	1.69	0.05	0.09
	(0.24)	(0.09)	(0.12)	(0.06)	(2.32)	(0.07)	(0.12)
5	0.16	0.06	0.08	0.04	1.59	0.05	0.09
	(0.23)	(0.09)	(0.12)	(0.05)	(2.25)	(0.07)	(0.12)
10	0.15	0.06	0.08	0.04	1.52	0.05	0.08
	(0.22)	(0.09)	(0.11)	(0.05)	(2.20)	(0.07)	(0.12)

RS refers to 'relative standard deviation' and is defined in equation (18) as RS_j for j = 1,2,3,4,5 for RaA, RaB, RaC, ThB and ThC, respectively. RSRWL and RSTWL are defined in equations (21) and (22) respectively. RSD flow refers to the relative standard deviation in flowrate. RSD concentration refers to the relative standard deviation in concentration.

Table 3

Results of Calculations for Case I

Case I: RSD flow = 0.00 (0.03)
Flow rate = 3 Lpm
RnWL = 0.56
TnWL = 0.26
Total counting time >24 h
(RSD flow refers to the relative standard deviation in flow rate)

ST (min)	Parameter	RSD Concentration*				
		0.00	0.015	0.03	0.045	0.06
5	RS1	0.09 (0.14)	0.10 (0.15)	0.14 (0.18)	0.18 (0.21)	0.23 (0.25)
	RS5	1.22 (1.99)	1.43 (2.13)	1.92 (2.48)	2.53 (2.98)	3.20 (3.56)
	RSRWL	0.03 (0.05)	0.03 (0.06)	0.05 (0.07)	0.07 (0.08)	0.09 (0.10)
	RSTWL	0.08 (0.11)	0.09 (0.12)	0.11 (0.14)	0.14 (0.16)	0.17 (0.19)
10	RS1	0.09 (0.19)	0.12 (0.20)	0.17 (0.24)	0.23 (0.28)	0.29 (0.34)
	RS5	0.88 (1.82)	1.14 (1.96)	1.69 (2.32)	2.33 (2.83)	3.02 (3.41)
	RSRWL	0.02 (0.06)	0.03 (0.06)	0.05 (0.07)	0.07 (0.09)	0.09 (0.11)
	RSTWL	0.06 (0.10)	0.07 (0.11)	0.09 (0.12)	0.13 (0.15)	0.16 (0.18)
15	RS1	0.10 (0.25)	0.14 (0.27)	0.21 (0.31)	0.29 (0.37)	0.38 (0.44)
	RS5	0.73 (1.86)	1.05 (2.00)	1.67 (2.39)	2.37 (2.92)	3.09 (3.53)
	RSRWL	0.02 (0.06)	0.03 (0.07)	0.06 (0.08)	0.08 (0.10)	0.10 (0.12)
	RSTWL	0.05 (0.10)	0.06 (0.11)	0.09 (0.13)	0.13 (0.15)	0.16 (0.19)

Table 3 (cont'd)

ST (min)	Parameter	RSD Concentration*				
		0.00	0.015	0.03	0.045	0.06
30	RS1	0.14 (0.45)	0.21 (0.47)	0.34 (0.54)	0.48 (0.65)	0.63 (0.76)
	RS5	0.58 (2.07)	1.01 (2.23)	1.77 (2.66)	2.57 (3.25)	3.39 (3.92)
	RSRWL	0.03 (0.10)	0.05 (0.11)	0.08 (0.12)	0.11 (0.15)	0.14 (0.17)
	RSTWL	0.03 (0.11)	0.05 (0.11)	0.09 (0.14)	0.13 (0.17)	0.18 (0.20)
60	RS1	0.19 (0.79)	0.32 (0.83)	0.56 (0.95)	0.82 (1.12)	1.08 (1.32)
	RS5	0.59 (3.17)	1.38 (3.41)	2.58 (4.05)	3.81 (4.92)	5.05 (5.94)
	RSRWL	0.04 (0.17)	0.07 (0.18)	0.12 (0.20)	0.18 (0.24)	0.23 (0.28)
	RSTWL	0.03 (0.16)	0.07 (0.17)	0.13 (0.20)	0.19 (0.25)	0.25 (0.30)

Optimum intervals for counting are the following:

ST:5 min; (2,4), (5,20), (30,60), (140,200), (1435,1495)
10 min; (2,4), (5,20), (30,60), (140,200), (1430,1490)
15 min; (2,4), (5,20), (30,60), (135,195), (1425,1485)
30 min; (2,4), (5,20), (30,60), (125,180), (1410,1470)
60 min; (2,4), (5,20), (30,60), (95,150), (1380,1440)

Equation (10) for the optimum sampling time of 10 min assumes the following form:

$$C_1V = 0.15863\ I_1 - 0.03689\ I_2 + 0.01176\ I_3 - 0.00437\ I_4 + 0.00915\ I_5$$

$$C_2V = -0.01063\ I_1 - 0.00257\ I_2 + 0.00710\ I_3 - 0.00846\ I_4 + 0.02276\ I_5$$

$$C_3V = -0.00968\ I_1 + 0.00916\ I_2 - 0.00273\ I_3 - 0.00588\ I_4 + 0.02087\ I_5$$

$$C_4V = 0.00335\ I_5$$

$$C_5V = -0.00227\ I_1 + 0.00171\ I_2 - 0.00217\ I_3 + 0.00791\ I_4 - 0.02516\ I_5$$

* All concentrations are in pCi/L.

Table 4

Results of Calculations for Case II

Case II: RSD flow = 0.00 (0.03)
Flow rate = 3 Lpm
RnWL = 0.56
TnWL = 0.26
Total counting time <5½ h

ST (min)	Parameter	RSD Concentration*				
		0.00	0.015	0.03	0.045	0.06
5	RS1	0.09 (0.15)	0.10 (0.15)	0.14 (0.18)	0.18 (0.21)	0.23 (0.25)
	RS5	1.47 (2.62)	1.79 (2.80)	2.51 (3.31)	3.38 (4.01)	4.32 (4.83)
	RSRWL	0.03 (0.06)	0.04 (0.06)	0.05 (0.07)	0.07 (0.09)	0.10 (0.11)
	RSTWL	0.09 (0.15)	0.10 (0.16)	0.14 (0.19)	0.19 (0.22)	0.24 (0.27)
10	RS1	0.09 (0.19)	0.12 (0.20)	0.17 (0.24)	0.23 (0.28)	0.30 (0.34)
	RS5	1.08 (2.48)	1.48 (2.68)	2.29 (3.20)	3.22 (3.91)	4.18 (4.74)
	RSRWL	0.02 (0.06)	0.03 (0.06)	0.05 (0.08)	0.08 (0.09)	0.10 (0.11)
	RSTWL	0.06 (0.14)	0.08 (0.15)	0.13 (0.18)	0.18 (0.22)	0.23 (0.26)
15	RS1	0.10 (0.25)	0.14 (0.27)	0.21 (0.31)	0.29 (0.37)	0.38 (0.44)
	RS5	0.92 (2.54)	1.39 (2.75)	2.28 (3.29)	3.27 (4.04)	4.28 (4.89)
	RSRWL	0.02 (0.07)	0.04 (0.07)	0.06 (0.09)	0.08 (0.10)	0.11 (0.12)
	RSTWL	0.05 (0.14)	0.08 (0.15)	0.13 (0.18)	0.18 (0.22)	0.24 (0.27)

Table 4 (cont'd)

ST (min)	Parameter	RSD Concentration*				
		0.0	0.015	0.03	0.045	0.06
30	RS1	0.14 (0.45)	0.21 (0.48)	0.34 (0.56)	0.49 (0.65)	0.64 (0.77)
	RS5	0.74 (2.57)	1.29 (2.78)	2.24 (3.33)	3.26 (4.09)	4.29 (4.95)
	RSRWL	0.03 (0.10)	0.05 (0.11)	0.08 (0.12)	0.11 (0.15)	0.15 (0.17)
	RSTWL	0.04 (0.14)	0.07 (0.15)	0.13 (0.18)	0.18 (0.23)	0.24 (0.28)
60	RS1	0.19 (0.78)	0.32 (0.82)	0.55 (0.94)	0.80 (1.10)	1.06 (1.30)
	RS5	0.69 (3.10)	1.44 (2.75)	2.63 (4.01)	3.86 (4.91)	5.12 (5.95)
	RSRWL	0.04 (0.17)	0.07 (0.18)	0.12 (0.20)	0.17 (0.24)	0.23 (0.28)
	RSTWL	0.04 (0.17)	0.08 (0.19)	0.15 (0.22)	0.22 (0.27)	0.29 (0.33)

Optimum intervals for counting are the following:

ST:5 min; (2,4), (5,20), (30,60), (140,200), (275,325)
10 min; (2,4), (5,20), (30,60), (140,200), (270,320)
15 min; (2,4), (5,20), (30,60), (135,195), (270,315)
30 min; (2,4), (5,20), (30,60), (135,195), (260,300)
60 min; (2,4), (5,20), (30,60), (125,185), (230,270)

Equation (10) for the optimum sampling time of 10 min are the following in this case:

$$C_1V = 0.15894\ I_1 - 0.03712\ I_2 + 0.01205\ I_3 - 0.00563\ I_4 + 0.00465\ I_5$$

$$C_2V = -0.00988\ I_1 - 0.00313\ I_2 + 0.00783\ I_3 - 0.01158\ I_4 + 0.01158\ I_5$$

$$C_3V = -0.00898\ I_1 + 0.00864\ I_2 - 0.00206\ I_3 - 0.00875\ I_4 + 0.01062\ I_5$$

$$C_4V = 0.00011\ I_1 - 0.00008\ I_2 + 0.00011\ I_3 - 0.00046\ I_4 + 0.00171\ I_5$$

$$C_5V = -0.00311\ I_1 + 0.00233\ I_2 - 0.00298\ I_3 + 0.01136\ I_4 - 0.01281\ I_5$$

* All concentrations are in pCi/L.

of ThC measurement, RS5, with very little increase in the uncertainty of measurement of the other radionuclides. The constraints which were placed on the length of counting intervals (Table 1) and the counting time insured that the solution was optimized over a practical domain.

The results seem to suggest that the first three optimal counting intervals were fixed throughout the calculations. In fact, the selection of these intervals was freely optimized over the range 2 to 60 minutes each iteration. The resulting optimal intervals differed from each other by only a minute or two; fixing them all at the same values each time did not seem to alter the results by more than a small fraction of a percent. It was therefore decided to specify a common set of values for the first three counting intervals for all sampling and counting times.

The results of the calculations are plotted in Figs. 1 - 9. For no uncertainty in flow rate (Fig. 1) measurement of ThC is statistically most accurate for ST = 60 min for RSD concentration = 0.00, and most inaccurate for RSD concentration > 0.02 (which is closer to a practical situation). Relative to the even more practical situation in Fig. 5 for RSD flow = 0.03 measurement of ThC is most inaccurate for ST = 60 min. For a total counting time of 5 1/2 hr the overall minimum uncertainty of measurement is that corresponding to ST = 10 min. The measurement of radon daughters is, in almost all cases, most accurate for ST = 5 min, but due to the fact that this sampling time results in higher uncertainty in ThB and ThC concentration measurement (in comparison with ST = 10 min), the best overall choice of sampling time is 10 min.

For measurement of radon daughter-thoron daughter mixtures, Rock (1975) recommends that at least 50 litres of air be filtered to allow sufficient sensitivity for thoron daughter detection. For this purpose,

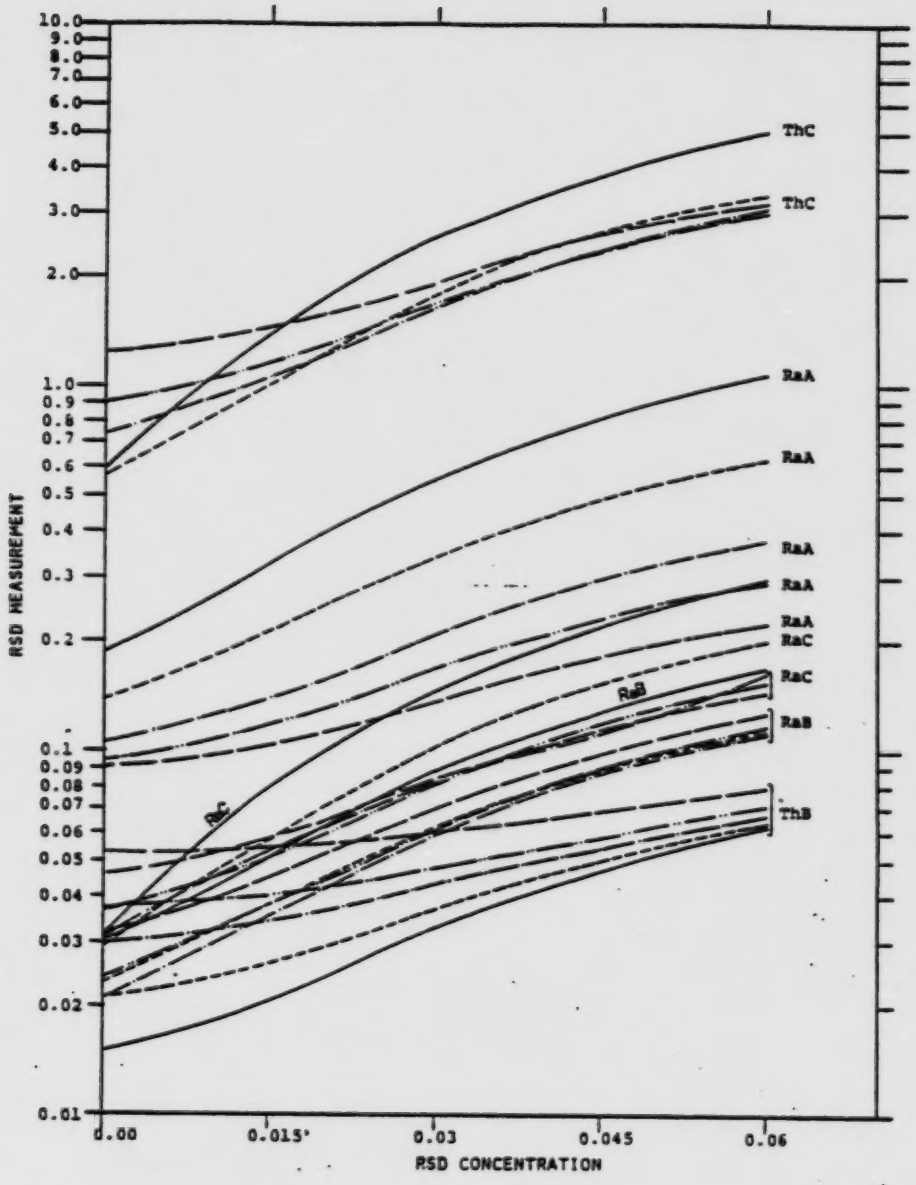

Fig. 1. Effect of concentration fluctuations on measurement precision for case I. (RSD flow = 0.00)

ST = 5 min (— — —); ST = 10 min (—··—); ST = 15 min (—·—); ST = 30 min (- - - - - -); ST = 60 min (————).

RSD flow and RSD concentration refer to the relative standard deviations in flowrate and concentration, respectively, whereas RSD measurement refers to the calculated relative standard deviation of measurement.

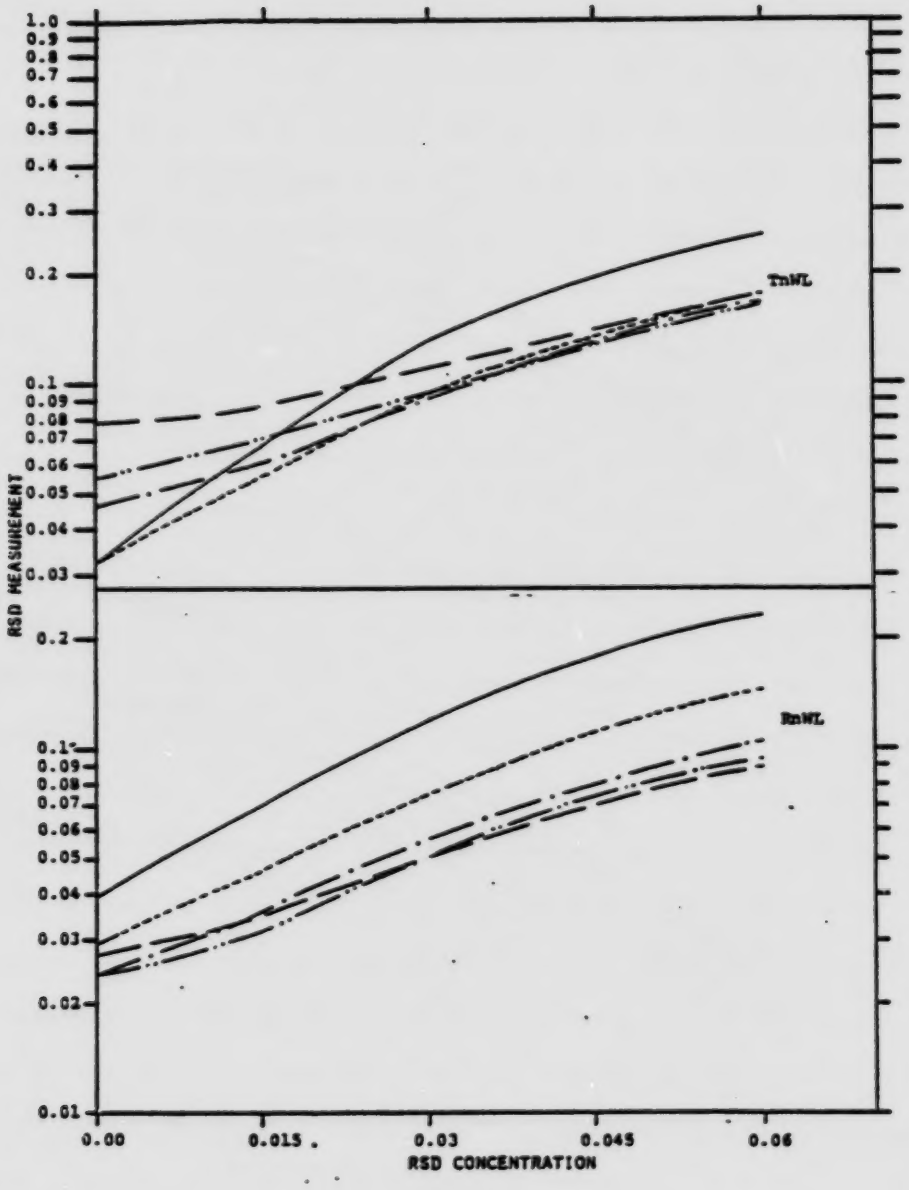

Fig. 2. Effect of concentration fluctuations on measurement precision on working level for case I. (RDS flow = 0.00).

ST = 5 min (— — —); ST = 10 min (— ·· —); ST = 15 min (— · —); ST = 30 min (- - - - - -); ST = 60 min (————).

RSD flow and RSD concentration refer to the relative standard deviations in flowrate and concentration, respectively, whereas RSD measurement refers to the calculated relative standard deviation of measurement.

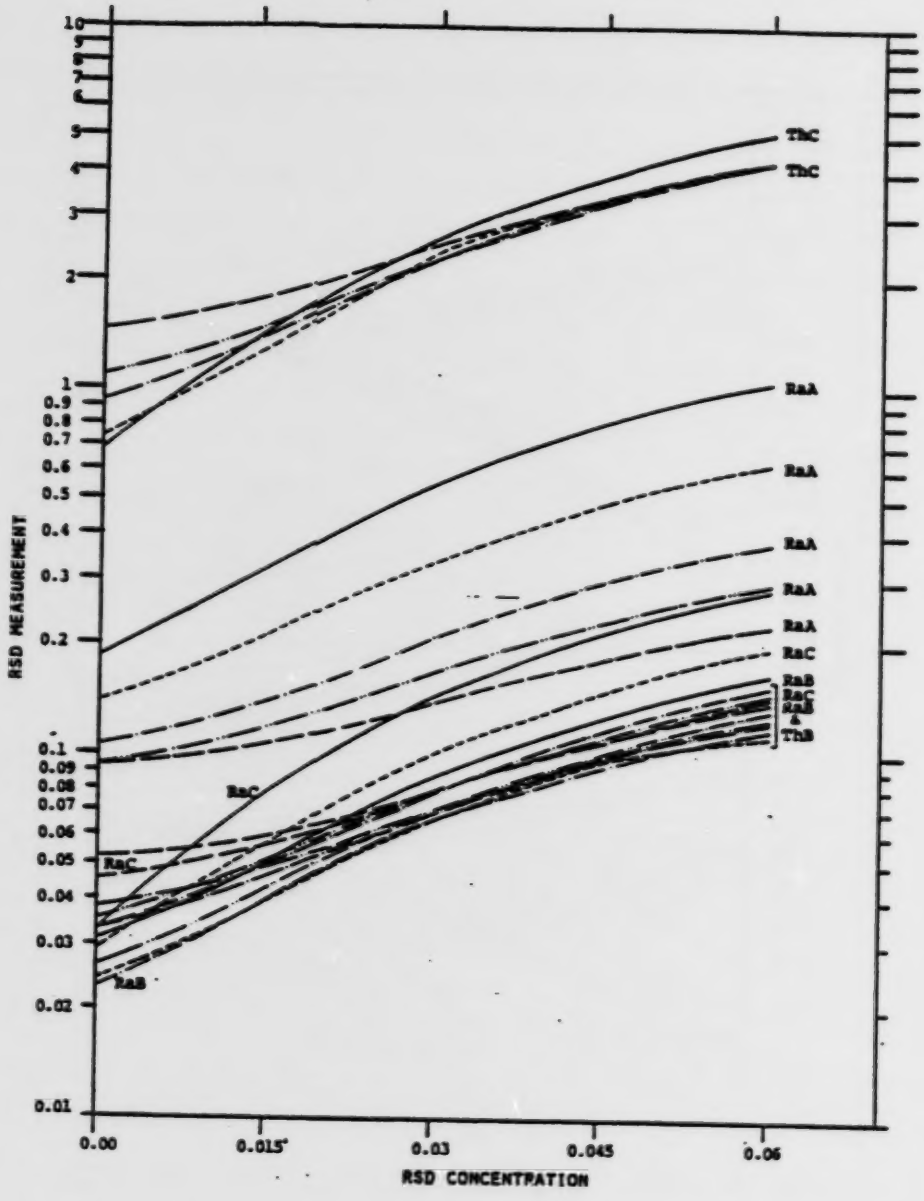

Fig. 3. Effect of concentration fluctuations on measurement precision for case II. (RSD flow = 0.00)

ST = 5 min (— — —); ST = 10 min (——··——); ST = 15 min (——·——); ST = 30 min (- - - - - -); ST = 60 min (————).

RSD flow and RSD concentration refer to the relative standard deviations in flowrate and concentration, respectively, whereas RSD measurement refers to the calculated relative standard deviation of measurement.

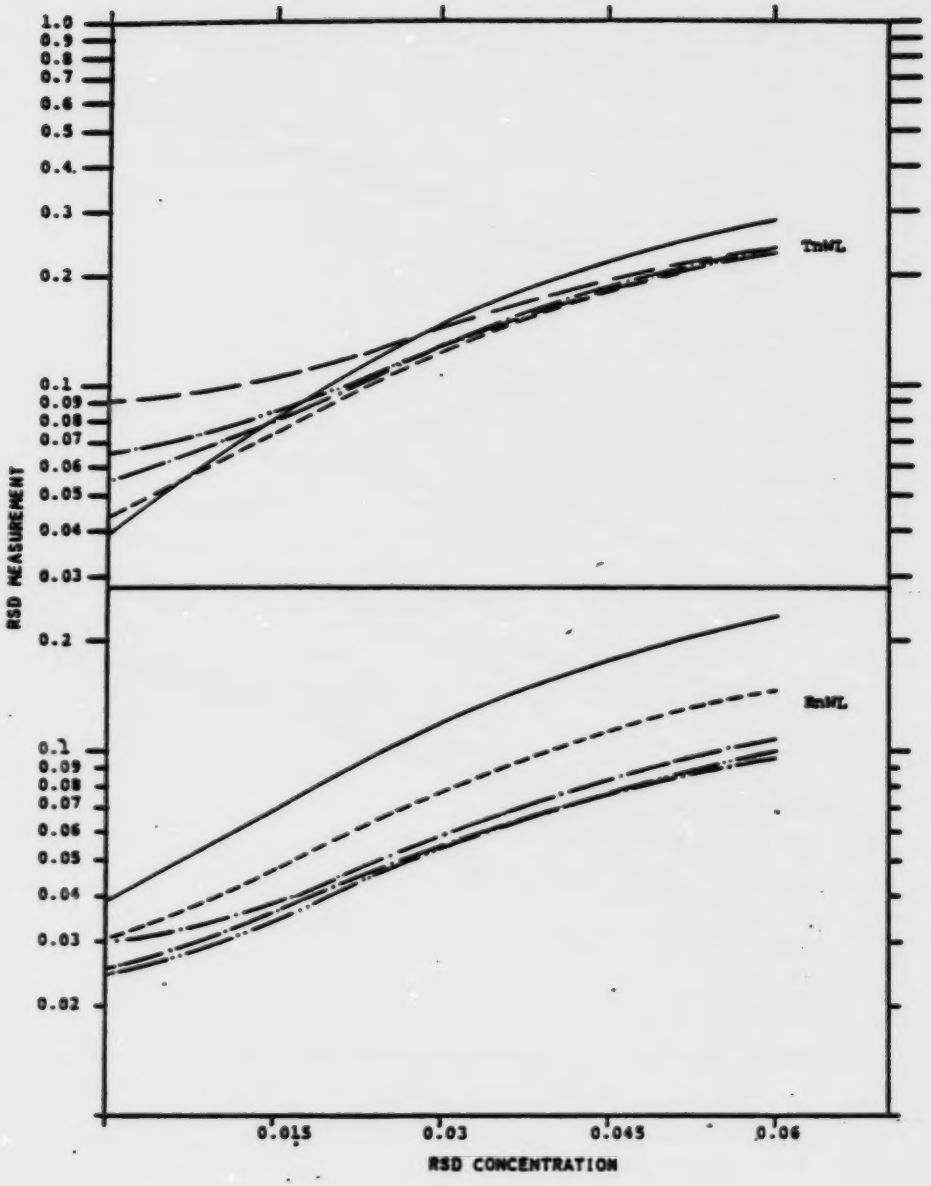

Fig. 4. Effect of concentration fluctuations on measurement precision of working level for case II. (RSD flow = 0.00)

ST = 5 min (——— ———); ST = 10 min (——·· ——); ST = 15 min (———· ———); ST = 30 min (- - - - - - -); ST = 60 min (————————).

RSD flow and RSD concentration refer to the relative standard deviations in flowrate and concentration, respectively, whereas RSD measurement refers to the calculated relative standard deviation of measurement.

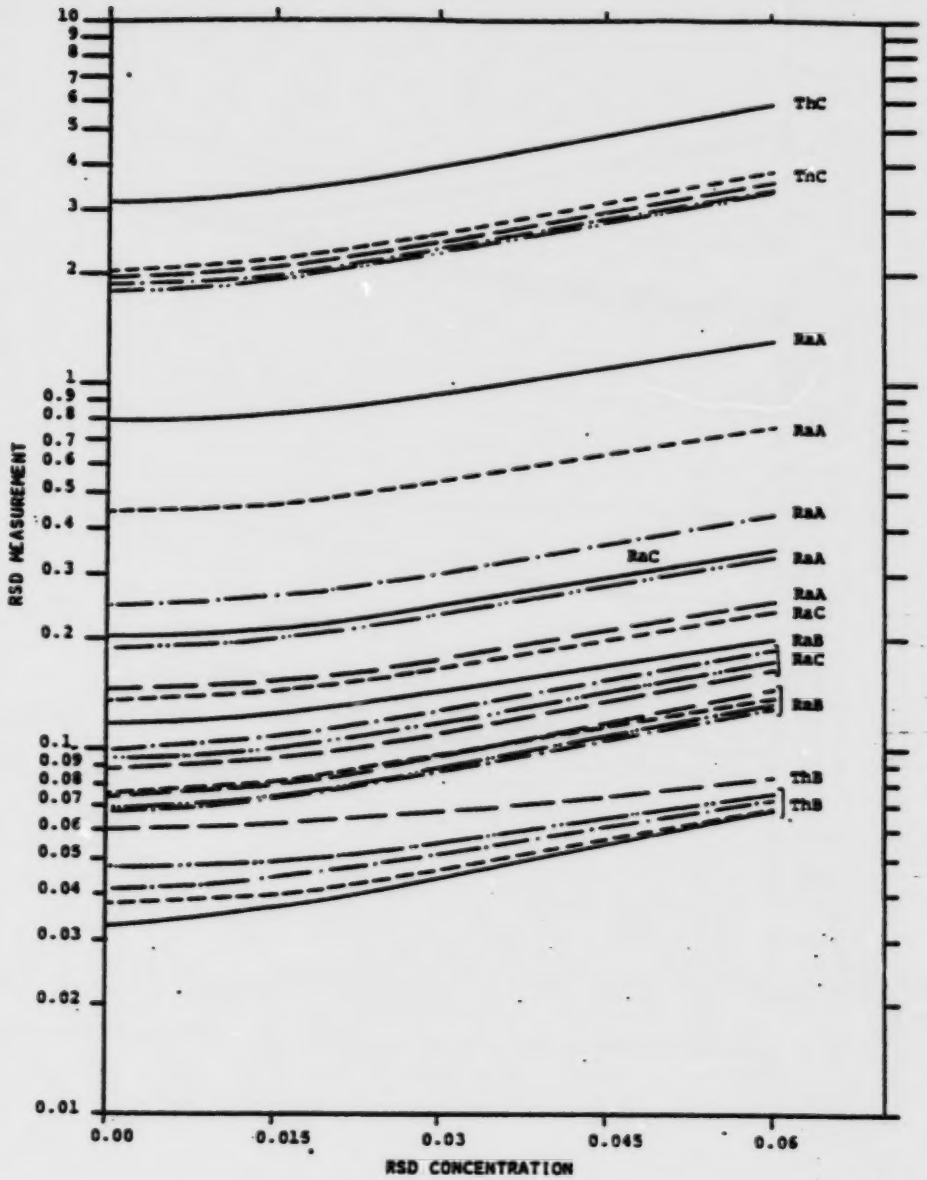

Fig. 5. Effect of concentration and flow fluctuations on measurement precision for case I. (RSD flow = 0.03).

ST = 5 min (——— ———); ST = 10 min (——·· ——); ST = 15 min (——·——); ST = 30 min (- - - - - - -); ST = 60 min (————————).

RSD flow and RSD concentration refer to the relative standard deviations in flowrate and concentration, respectively, whereas RSD measurement refers to the calculated relative standard deviation of measurement.

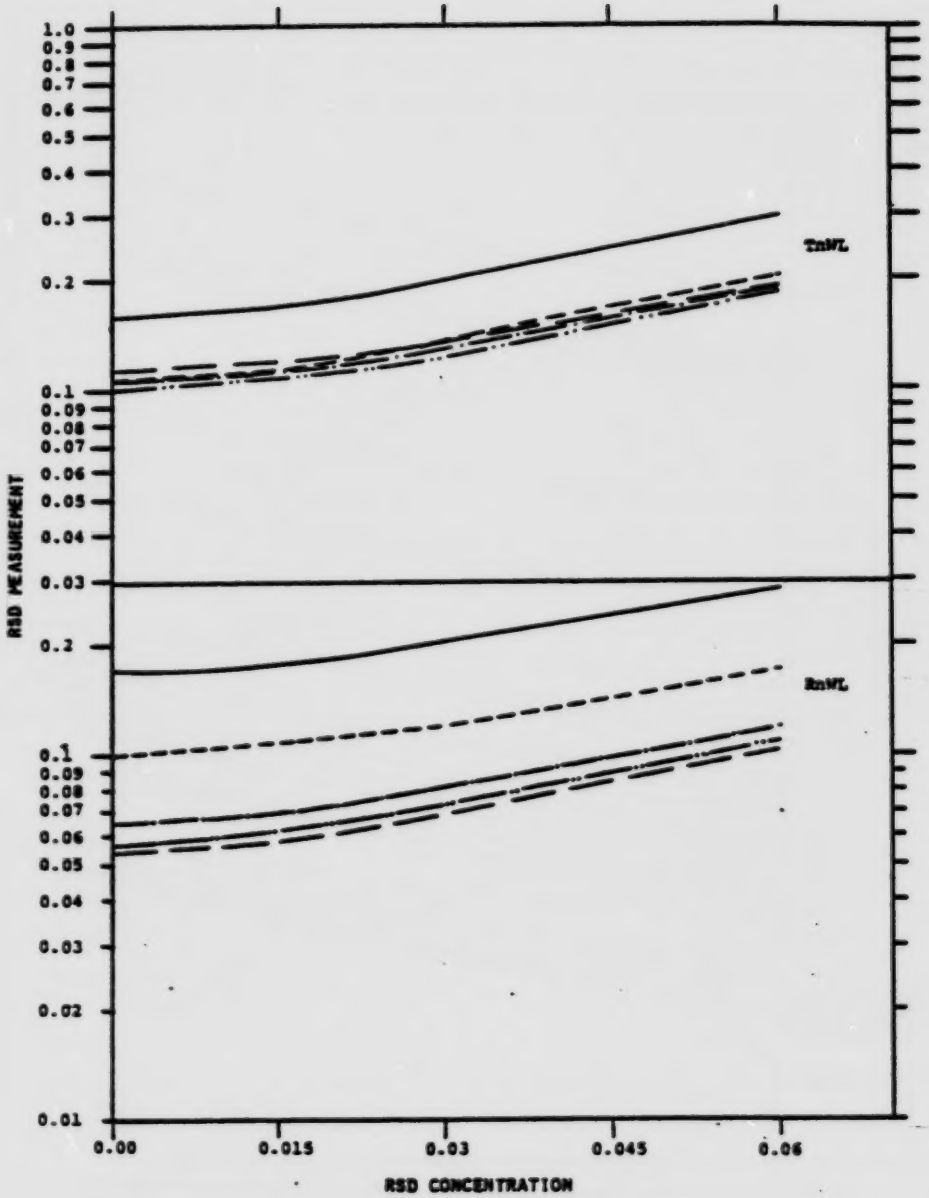

Fig. 6. Effect of concentration and flow fluctuations on measurement precision of working level for case I. (RSD flow = 0.03)

ST = 5 min (——— ———); ST = 10 min (——·· ——); ST = 15 min (——·—); ST = 30 min (- - - - - - -); ST = 60 min (————).

RSD flow and RSD concentration refer to the relative standard deviations in flowrate and concentration, respectively, whereas RSD measurement refers to the calculated relative standard deviation of measurement.

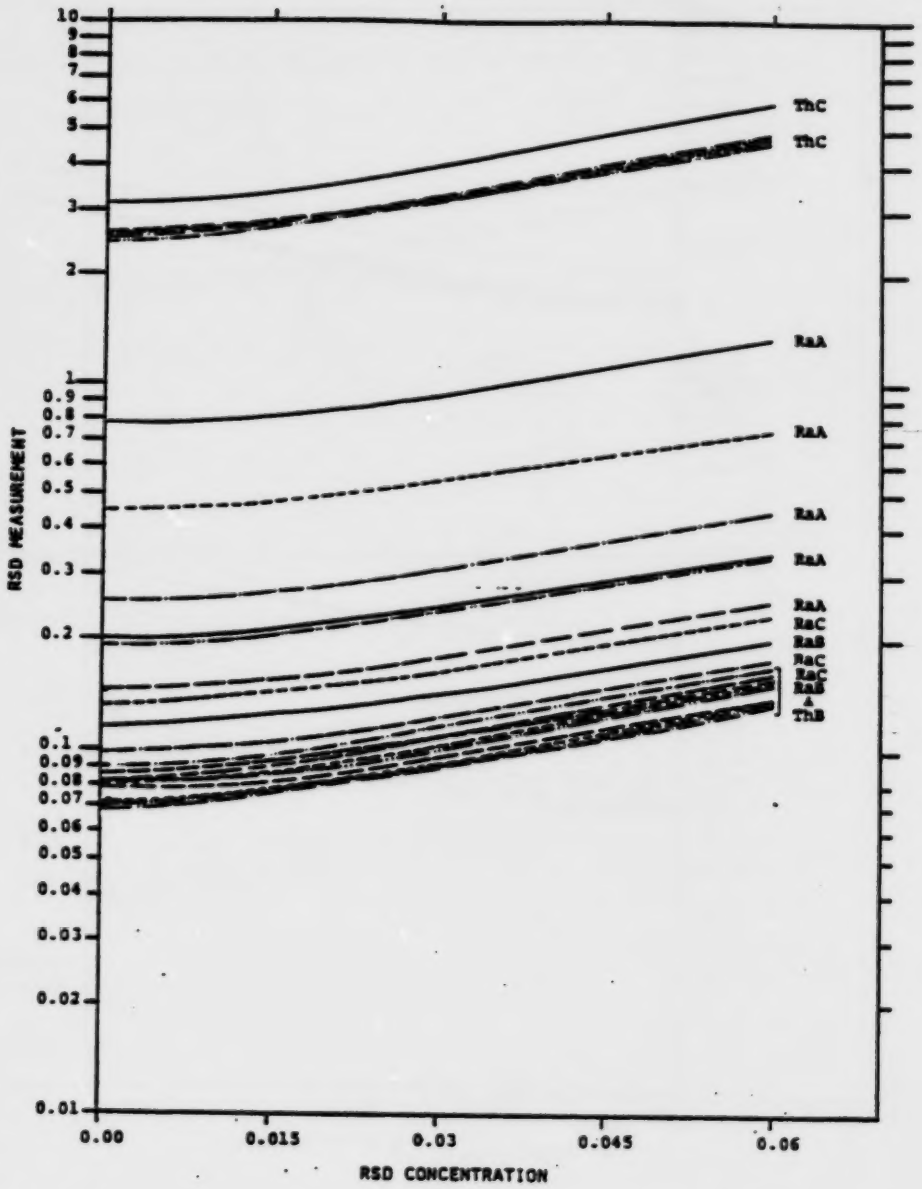

Fig. 7. Effect of concentration and flow fluctuations on measurement precision for case II. (RSD flow = 0.03)

ST = 5 min (——— ———); ST = 10 min (——·· ——); ST = 15 min (———·——); ST = 30 min (- - - - - - -); ST = 60 min (————).

RSD flow and RSD concentration refer to the relative standard deviations in flowrate and concentration, respectively, whereas RSD measurement refers to the calculated relative standard deviation of measurement.

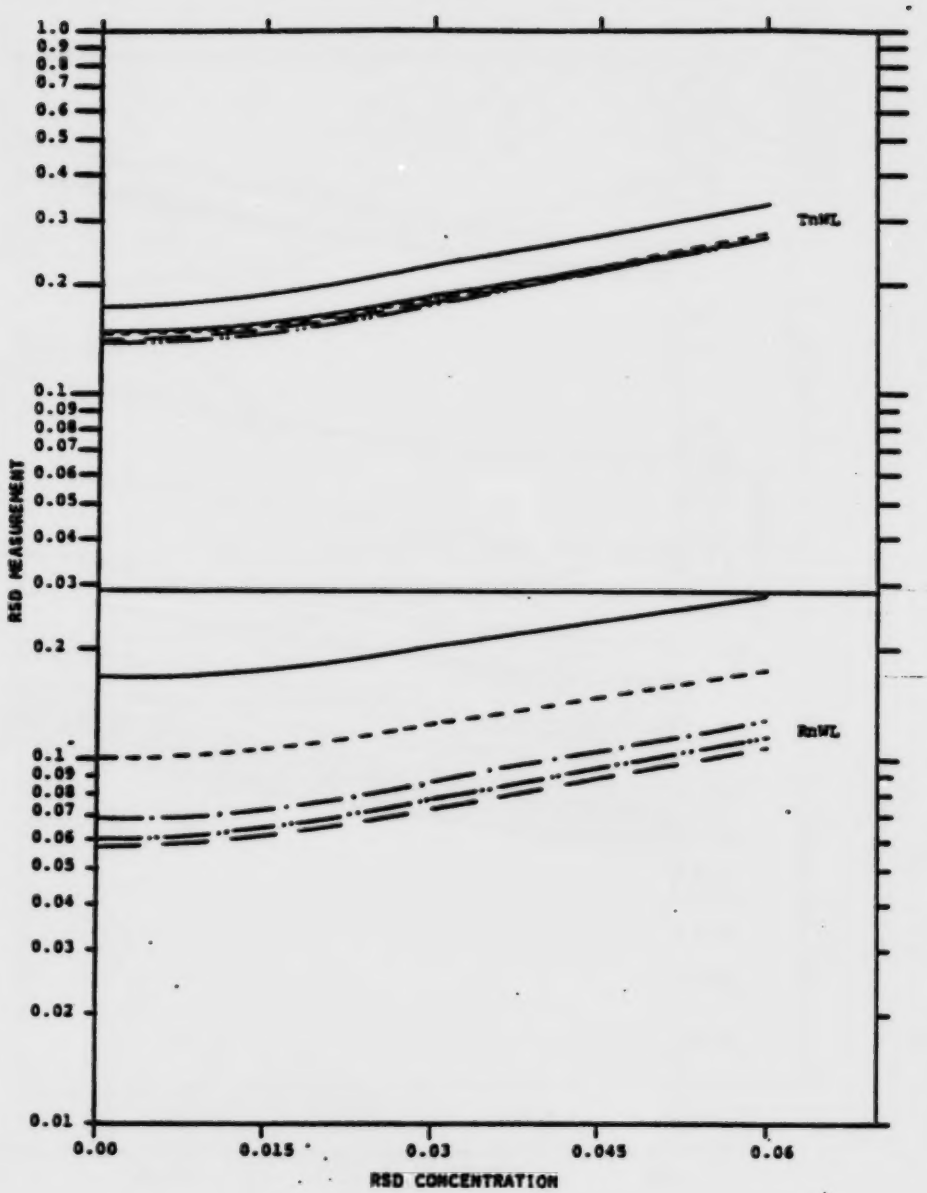

Fig. 8. Effect of concentration and flow fluctuations on measurement precision of working level for case II. (RSD flow = 0.03)

ST = 5 min (— — —); ST = 10 min (—··—); ST = 15 min (—·—); ST = 30 min (- - - - - -); ST = 60 min (————).

RSD flow and RSD concentration refer to the relative standard deviations in flowrate and concentration, respectively, whereas RSD measurement refers to the calculated relative standard deviation of measurement.

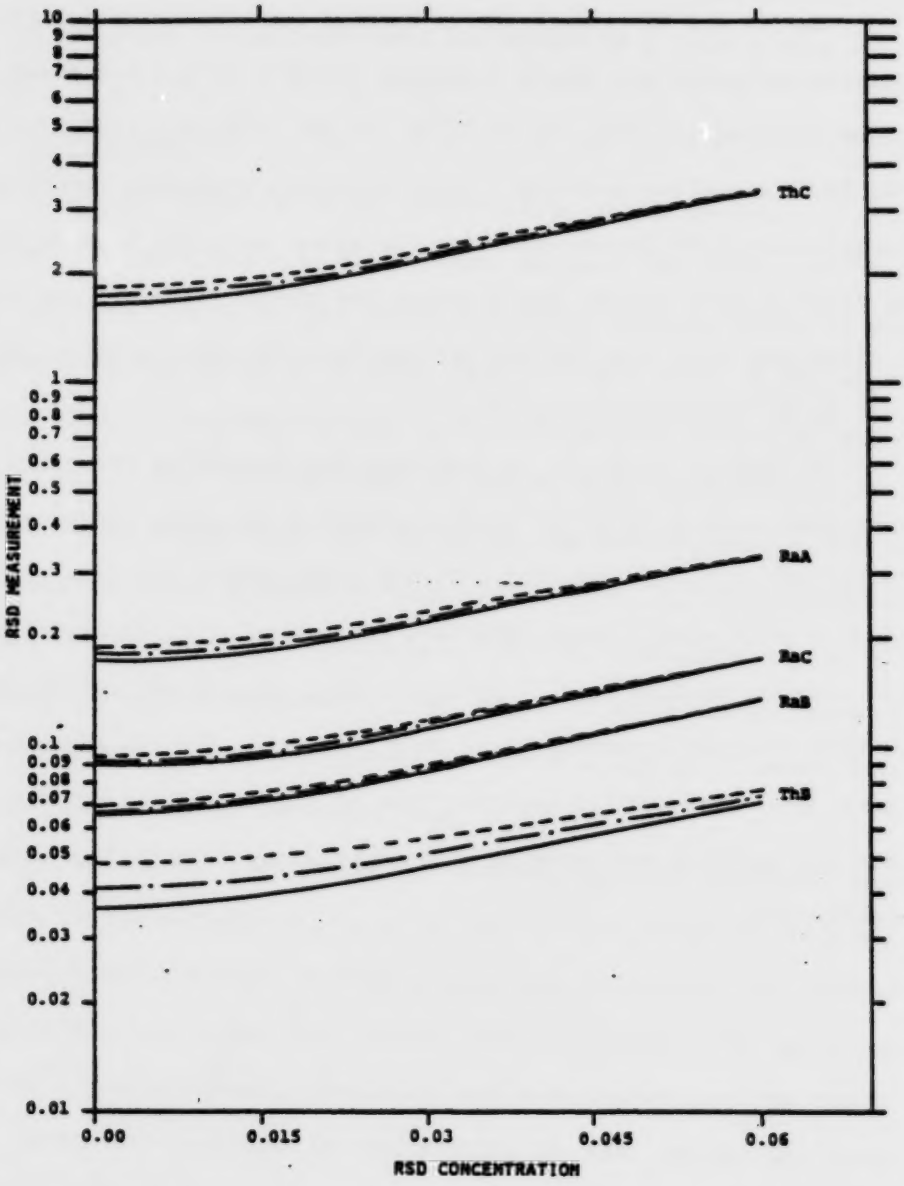

Fig. 9. Effect of varying flowrate on measurement precision for case I. (Sampling time = 10 min; RSD flow = 0.03)

Flowrate = 10 LPM (————); flowrate = 5 LPM (—·——·—); flowrate = 3 LPM (– – – – –).

RSD flow and RSD concentration refer to the relative standard deviations in flowrate and concentration, respectively, whereas RSD measurement refers to the calculated relative standard deviation of measurement.

a flow rate of 5 Lpm for a 10 min sampling would be appropriate. This is also supported by Fig. 9 which is plotted for RSD flow of 0.03.

Harley and Pasternack (1973) carried out similar calculations for environmental radon and thoron daughters for ST = 60 min and found their optimum counting intervals to be (2,5), (6,20), (21,30), (200,300) and (1440,2440) min after sampling. These intervals obviously correspond to a large uncertainty in concentration for radon daughters because of the long sampling time chosen, and likewise for thoron daughters for practical situations with fluctuations in flow rate and concentration, as confirmed by the present calculations.

In another study for optimum counting procedures for radon and thoron daughters, Cote et al. (1978) recommend the three counting intervals (11,26), 155,170) and (255,270) min (considering sampling time to be from 0 to 10 min). There intervals correspond to a 20% error in the radon daughter working level. In comparison, the present calculations with five counting intervals yield only 7-8% error for the radon daughter working level over a total counting time of either 320 min or 24 h, using 10 min for sampling and assuming a 3% uncertainty in both flow rate and concentration.

CHAPTER 8

OPTIMIZED COUNTING INTERVALS FOR CONCENTRATION MEASUREMENT OF THE DECAY PRODUCTS OF RADON AND THORON IN A URANIUM MINE

8.1 Introduction

The implications for dosimeter design of the presence of thorium in uranium mines at Elliot Lake, Bancroft and Agnew Lake, Ontario have been reported by Pai and Phillips (1977). Working levels of thoron daughters as high as those of radon daughters were found in dosimetric studies (Pai, Jokura and Phillips, 1981). Using the Kusnetz method, Bigu et al. (1980) concluded that the thoron daughter working level at Denison Mines, Elliot Lake, was on the average substantially higher (over 35%) than the radon daughter working level. Such high thoron daughter working levels contribute significantly to the total alpha radiation hazard. A complete assessment of the potential alpha energy release, therefore, must include measurement of thoron daughter concentrations as well as radon daughter concentrations.

The commonly used method for determining radon daughter concentrations is the modified Tsivoglou method (Thomas, 1970) in which air is sampled through a filter for five minutes and the filter then counted in the intervals 2-5, 6-20, 21-30 minutes after sampling. The integrated activity in these three intervals is then substituted in three theoretically determined equations for calculating the RaA, RaB and RaC concentrations. This method can easily be extended to include ThB and ThC with two additional appropriately chosen intervals and two more equations. Harley and Pasternack (1973) reported such calculations for a sampling time

of 60 minutes, with additional counting intervals of 200-300 minutes and 1440-2440 minutes after sampling for determining ThB and ThC. However, a serious source of error in the modified Tsivoglou method is the neglect of uncertainties associated with fluctuations in sampling flowrate and concentrations. This was taken into account by Busigin and Phillips (1980) in optimizing the modified Tsivoglou method for radon daughters. Busigin and Phillips showed that deviations of about 3% in flowrate or concentration, or both, could magnify the uncertainties associated with measurements to about 30% or more. Their optimized counting intervals are 2-5, 7-15, 25-30 minutes after sampling. Extending the concept of including flowrate and concentration deviations in the calculations, Khan, Busigin and Phillips (in press) optimized counting intervals for a mixture of radon daughters and thoron daughters for five different sampling times. Within a total counting period of less than 5 1/2 hours, their optimized intervals are 2-4, 5-20, 30-60, 140-200 and 270-300 minutes after sampling for ten minutes, which is their optimum sampling time.

The present work is an experimental comparison of the extended modified Tsivoglou method (Harley and Pasternack, 1973) and the optimized version of the same (Khan, Busigin and Phillips, in press). The measurements were carried out in Denison Mines, Elliot Lake, using Harley and Pasternack's counting intervals of 2-5, 6-20, 21-30, 200-300 and 1440-2440 minutes after 60 minutes of sampling and Khan, Busigin and Phillips' counting intervals of 2-4, 5-20, 30-60, 160-220, 270-320 minutes after sampling for ten minutes, with the fourth interval modified slightly for convenience.

8.2 Experimental Procedure

A mine area not subject to intense mining activity was chosen for the measurements in order to minimize concentration fluctuations due to mining operations. Two sets of measurements were obtained, each consisting of seven simultaneous samples for a 60 minute sampling time and seven simultaneous samples for a 10 minute sampling time. In obtaining a sample, air was drawn through 0.8 μm, 47 mm dia. Gelman glass fibre filters (loaded in open face magnetic filter holders) using three Dupont Model P-4000 pumps and four Bendix (BDX-44) pumps previously calibrated in the range of 2.5-3 L/min. The filters were counted using seven calibrated Trimet alpha counters (efficiencies ~ 42%) according to the specified counting intervals. In order to complete the measurements with a limited number of sampling pumps and alpha counters, the fourth optimum interval for ten minute samples had to be shifted from 140-220. This change had to be made in order to make possible same day measurements for both counting schemes, and did not alter significantly the theoretically determined relative standard deviations of the measurements, as can be seen from Table 1. (The definitions of the radon daughter working level, RnWL, and the thoron daughter working level, TnWL, are given in the next section.)

The pumps were calibrated above ground using a bubble flowmeter both before and after sampling and a linear average of the two flowrates taken to be the flowrate during sampling. It was assumed that all filters were sampling the same quality of air.

Table 1

Relative Standard Deviations (RSD) of Measurement for Optimum Counting Intervals (Khan, Busigin and Phillips, in press) and the Modified Counting Scheme (this work) for no Fluctuations in Flowrate or Concentration

RSD Measurement for:	RaA	RaB	RaC	ThB	ThC	RnWL	InWL
Khan, Busigin and Phillips (in press)	0.094	0.026	0.035	0.038	1.082	0.024	0.064
This work	0.094	0.027	0.038	0.041	1.159	0.025	0.069

Table 2

Equations for Calculation of Radon Daughter and Thoron Daughter Concentrations

For 60 minute samples and 40 hour counting (Harley and Pasternack, 1973):

$$C_{RaA}^{V} = 0.1150621181\ I_1 - 0.0561546896\ I_2 + 0.0535600794\ I_3 - 0.0022608313\ I_4 + 0.0010620597\ I_5$$

$$C_{RaB}^{V} = -0.0108636066\ I_1 + 0.0018996062\ I_2 + 0.0032237791\ I_3 - 0.0022095355\ I_4 + 0.0011544030\ I_5$$

$$C_{RaC}^{V} = -0.0043700733\ I_1 + 0.0083974896\ I_2 - 0.0122070810\ I_3 - 0.0010243723\ I_4 + 0.0006518130\ I_5$$

$$C_{ThB}^{V} = 0.0000553498\ I_5$$

For 10 minute samples and 5 1/2 hour counting (Khan, Busigin and Phillips, in press)

$$C_{RaA}^{V} = 0.1585995873\ I_1 - 0.0368631326\ I_2 + 0.0117030135\ I_3 - 0.0070240641\ I_4 + 0.0065554595\ I_5$$

$$C_{RaB}^{V} = -0.0105716687\ I_1 - 0.0026135006\ I_2 + 0.0071091861\ I_3 - 0.0144536185\ I_4 + 0.0154950087\ I_5$$

$$C_{RaC}^{V} = -0.0095080612\ I_1 + 0.0090318326\ I_2 - 0.0026023969\ I_3 - 0.0109176105\ I_4 + 0.0135772760\ I_5$$

$$C_{ThB}^{V} = 0.0000838203\ I_1 - 0\ 0000628888\ I_2 + 0.0000794121\ I_3 - 0.0005746054\ I_4 + 0.0018619709\ I_5$$

$$C_{ThC}^{V} = -0.0024296372\ I_1 + 0.0018228255\ I_2 - 0.0022774660\ I_3 + 0.0141778068\ I_4 - 0.0166438971\ I_5$$

8.3 Data Analysis

The equations used to calculate the concentrations are shown in Table 2.

The C's in Table 2 refer to the calculated concentrations of subscripted decay products of radon and thoron in pCi/L; V is the flowrate in L/min. The concentrations calculated by substituting the I's (the number of alpha disintegrations obtained in the five consecutive counting intervals) in the equations given in Table 2 are listed in Table 3.

Assuming 1 WL to correspond to the quantity of short-lived radon daughters or thoron daughters per litre of air which in decaying to Pb-210 in the case of radon daughters and to Pb-208 in the case of thoron daughters will yield 1.3×10^5 MeV of alpha energy, the radon and thoron daughter working levels were calculated from the average concentrations, $\bar{C}_{i,s}$, by:

$$\overline{RnWL} = \frac{1.03\ \bar{C}_{RaA} + 5.07\ \bar{C}_{RaB} + 3.73\ \bar{C}_{RaC}}{1000}$$

$$\overline{RnWL} = \frac{123.19\ \bar{C}_{ThB} + 12.67\ \bar{C}_{ThC}}{1000}$$

The relative standard deviations for concentrations were calculated as $S_i/\bar{C}_I$ for the ith decay product, where S_i is the standard deviation of the experimentally determined set of concentration measurements. For the radon and thoron daughter working levels, the relative standard deviations were calculated as

$$RsRnWL = \frac{[(1.03\ S_{RaA})^2 + (5.07\ S_{RaB})^2 + (3.73\ S_{RaC})^2]^{1/2}}{RnWL \times 1000}$$

$$RsTnWL = \frac{[(123.19\ S_{ThB})^2 + (12.67\ S_{ThC})^2]^{1/2}}{TnWL \times 1000}$$

Table 3

Calculated Concentrations (in $pCiL^{-1}$)

Sample No.	10 minute samples					60 minute samples				
	C_{RaA}	C_{RaB}	C_{RaC}	C_{ThB}	C_{ThC}	C_{RaA}	C_{RaB}	C_{RaC}	C_{ThB}	C_{ThC}
1	79.64	31.46	17.95	2.09	1.14	115.71	38.71	20.48	2.31	0.00
2	72.45	32.37	20.38	2.16	3.97	91.91	40.15	24.60	2.29	0.76
3	86.63	34.04	18.77	2.38	0.33	90.53	34.50	23.79	2.11	0.56
4	72.41	32.49	20.39	1.99	3.39	113.43	35.62	17.49	2.20	0.81
5	55.63	27.78	15.34	1.66	2.83	68.72	41.42	25.87	2.38	0.69
6	67.31	35.23	24.15	2.45	1.06	91.36	39.49	24.42	2.30	0.21
7	68.78	32.71	18.64	2.04	2.13	92.13	37.56	25.89	2.23	0.21
Mean	72.27	32.31	19.37	2.11	2.15	73.83	38.21	23.22	2.26	0.463
S.D.	8.98	2.37	2.71	0.26	1.38	33.38	2.48	3.11	0.09	0.257
% R.S.D.	12.42	7.32	13.99	12.38	64.30	45.18	6.48	13.40	3.96	55.6
1	94.22	39.01	19.42	2.18	0.30	34.48	39.07	29.69	2.27	2.36
2	79.05	36.52	19.39	2.11	1.93	63.09	33.33	20.83	2.03	2.96
3	38.57	38.52	17.67	2.22	1.68	54.02	44.35	27.30	2.31	1.14
4	101.51	41.61	20.20	2.46	0.00	61.54	34.78	23.97	2.23	2.79
5	79.90	31.29	14.50	1.91	0.40	63.40	44.99	29.07	2.58	1.61
6	90.10	36.37	17.57	2.09	1.46	66.66	41.39	33.71	2.70	2.51
7	68.02	29.95	14.25	1.85	0.26	82.02	40.58	29.96	2.63	2.28
Mean	85.84	36.18	17.57	2.12	0.82	60.75	39.79	27.79	2.42	2.29
S.D.	11.15	4.20	2.38	0.20	0.84	14.35	4.44	4.25	0.25	0.65
% R.S.D.	13.00	11.61	13.57	9.67	102.00	23.63	11.16	15.29	10.17	29.52

Table 4

Concentrations Expressed in Terms of Working Levels

Set No.	Sampling time (min)	$\overline{RnWL}$	$\overline{TnWL}$	%RnWL (%)	%TnWL (%)
1	10	0.31	0.29	5.9	12.6
	60	0.36	0.28	10.7	4.1
2	10	0.34	0.27	7.6	9.2
	60	0.37	0.33	8.44	9.66

The concentrations expressed in terms of working levels are listed in Table 4.

In order to compare the precision of the 60 minute sample (Harley and Pasternack, 1973) with the precision of the 10 minute sample (Khan, Busigin and Phillips, in press), an F-test was performed on normalized distributions. The conclusions are summarized in Table 5.

Theoretically obtained relative standard deviations for the two methods are plotted in Figs. 1-6 in order to demonstrate the effect of flowrate and concentration fluctuations on both 10 minute and 60 minute samples. The major contribution to overall errors of measurement comes from RaA and ThC. RaB, RaC and ThB do not differ significantly in measurement precision for the two methods, as is evident from Table 3.

8.4 Discussion

The overall precision of measurement is subject to the effect of various sources of errors, most of which have been described by Loysen (1969). The largest error is probably that due to the above ground calibration of pumps, which, according to Loysen's estimate, could be 4-11%. Also, the pumps were calibrated above ground using dry filters, whereas in actual measurements, the mine air was humid (~95% R.H.), and tended to make the filters moist, which could change the flowrate. Dust loading of the filters could also affect the flowrate since the 10 minute sample filters turned light grey and 60 minute sample filters dark grey after sampling. Counting errors seemed to be within $\pm 2\sigma$.

Results for the 10 minute sample could have had even better precision (a few percent) if the fourth counting interval had not been

Table 5

F-Test Comparison of 60 Minute Sample with 10 Minute Sample

Set No.	RaA	RaB	RaC	ThB	ThC
1	$\sigma^2_{60} > \sigma^2_{10}$ at 99% confidence	$\sigma^2_{60} = \sigma^2_{10}$ at 99% and 90% confidence	$\sigma^2_{60} = \sigma^2_{10}$ at 99% and 90% confidence	$\sigma^2_{10} > \sigma^2_{60}$ at 90% confidence	$\sigma^2_{10} = \sigma^2_{60}$ at 99% and 90% confidence
2	$\sigma^2_{60} > \sigma^2_{10}$ at 90% confidence	$\sigma^2_{60} = \sigma^2_{10}$ at 99% and 90% confidence	$\sigma^2_{60} = \sigma^2_{10}$ at 99% and 90% confidence	$\sigma^2_{60} = \sigma^2_{10}$ at 99% and 90% confidence	$\sigma^2_{10} > \sigma^2_{60}$ at 99% and 90% confidence
Conclusions	$\sigma^2_{60} > \sigma^2_{10}$ at 90% confidence	variances same at 90% confidence	variances same at 90% confidence	variances not significantly different	too much error involved, therefore no definite conclusion

Table 6

Theoretical Comparison of Relative Standard Deviations of the 60 Minute and 10 Minute Sampling Methods (ΔC's refer to fluctuations from measurement to measurement)

Parameter	Sampling time	ΔV = 0.00		ΔC = 0.00	ΔC = 0.05
		ΔC = 0.00	ΔC = 0.05	ΔV = 0.05	ΔV = 0.05
RaA	10 min[1]	9.5%	25%	30%	37%
	60 min[2]	24%	130%	175%	225%
ThC	10 min[1]	115%	325%	340%	470%
	60 min[2]	38%	295%	315%	430%
RnWL	10 min[1]	2.5%	8%	9%	12%
	60 min[2]	5.2%	28%	40%	50%
TnWL	10 min[1]	7%	17.5%	20%	26%
	60 min[2]	1.9%	15.5%	16%	22.5%

[1] Method of Khan, Busigin and Phillips (in press).
[2] Method of Harley and Pasternack (1973).

shifted for the sake of convenience. However, even with the modified intervals, the results are promising. One obvious advantage of using a shorter sampling time is better precision for RaA measurement because of its short half-life (3.05 minutes). Although a 10 minute sampling time improves the precision for ThC, the significance of the results is not much affected since ThC only represents 9% of the total alpha energy delivered by thoron daughters; 91% comes from ThB (Stranden, 1980).

The significant effect of fluctuations associated with flowrate and concentration on measurement precision as shown in Figs. 1-6 suggests that a shorter sampling period is also advisable from the point of view of minimizing these fluctuations. In a stable mine area, ΔC could be close to zero for a 10 minute sampling time and may not be more than 5% in a relatively active mine area. But for a 60 minute sampling time the fluctuations could be 5% even in a mine area of low mining activity and could be well above 5% for an active mine area, thereby rendering the measurement precision unacceptably poor as shown in Table 6.

For a practical case of 5% fluctuation in concentration and 5% fluctuation in flowrate, it is apparent from Table 6 that the 10 minute sampling - 5 1/2 hour counting method of Khan, Busigin and Phillips (in press), is superior to the 60 minute sampling - 40 hour counting method of Harley and Pasternack (1973) for the determination of radon daughter working levels in the presence of thoron daughters. For the determination of thoron daughter working levels in the presence of radon daughters, the two methods are comparable under the practical operating conditions of $\Delta C = \Delta V = 0.05$.

The relative standard deviation for RaA is extremely poor for the 60 minute sampling - 40 hour count method; and for ThC the relative standard

deviations for both methods are extremely poor (400-500%). In consequence, negative values for ThC concentrations may result from calculations of field data based on either method, particularly if ThC concentrations are low. In this work, both methods resulted in some negative values, which have been taken as zero in Table 3. Rounding off the coefficients of I_i,s in Table 2 results in an even greater number of negative ThC values.

It is generally considered better to have as large a sampling flowrate as possible. Although the precision would improve for a larger sampling flowrate for a short sampling time, calculations by Khan, Busigin and Phillips (in press) have shown that for a sampling time of ten minutes, considering a 3% deviation in flowrate, the precision is not affected much by using a 5 Lpm or 10 Lpm flowrate instead of the 3 Lpm flowrate (Fig. 7).

8.5 Conclusions

From the analysis of data obtained in mine experiments (as presented in Tables 1-6), it is apparent that the concentrations of radon daughters and thoron daughters can be obtained from 10 minute sampling and subsequent counting over 5 1/2 hours using the optimized intervals of Khan, Busigin and Phillips (in press) with an average better precision than from 60 minute sampling and subsequent counting over a period of greater than 40 hours (Harley and Pasternack, 1973). The precision of measurement for RaA is extremely poor for the 60 minute sample - 40 hour count; likewise, the precision of measurement of ThC for the 10 minute sample - 5 1/2 hour count is also very poor. However, RaA is a major

contributor to the radon daughter working level by virtue of its high concentration, whereas ThC is a minor contributor to the thoron daughter working level by virtue of its low concentration.

The effect of concentration and flowrate fluctuations is significant as shown in Figs. 1-6 and Table 6.

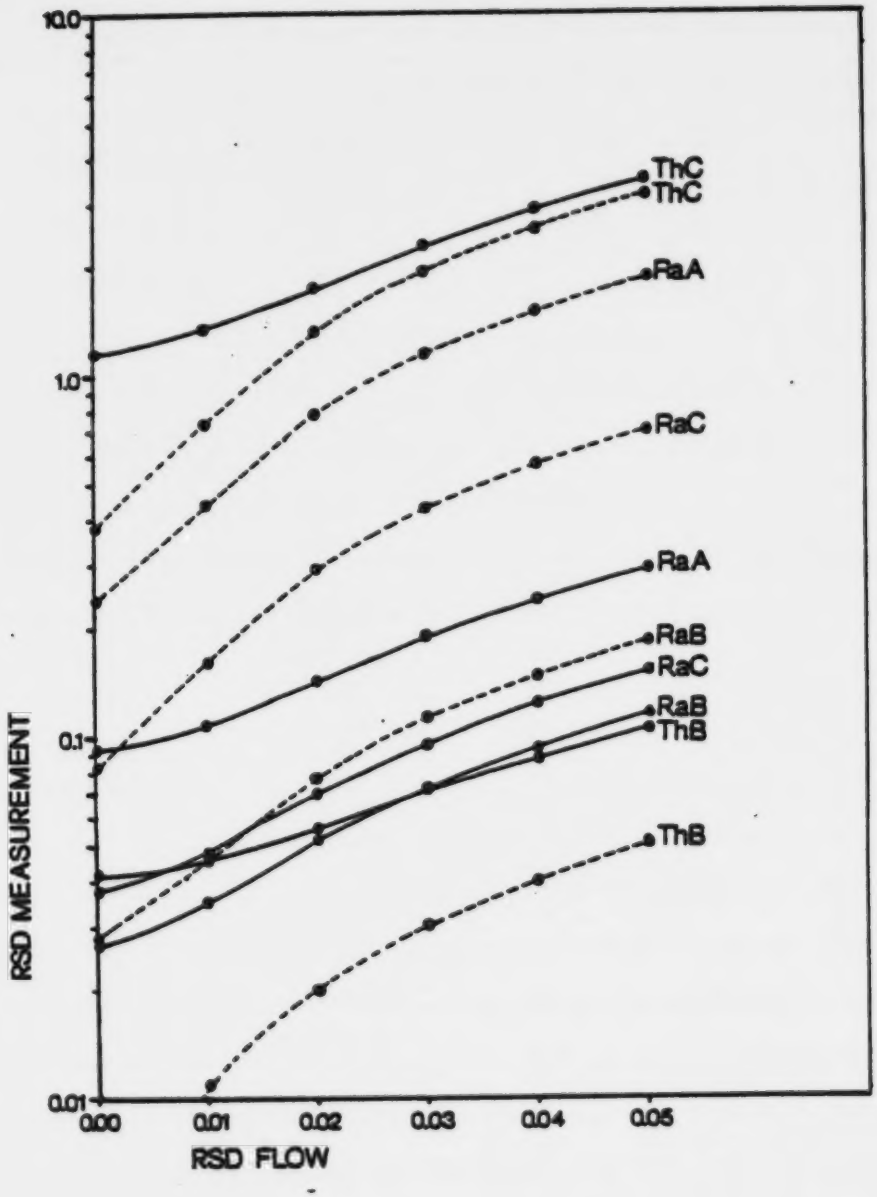

FIGURE 1. Calculated relative standard deviations of measurement (RSD measurement) of radon and thoron daughters vs flow fluctuations (RSD flow) for no fluctuation in concentration for Harley and Pasternack's method (-----) and Khan, Busigin and Phillips' method (———).

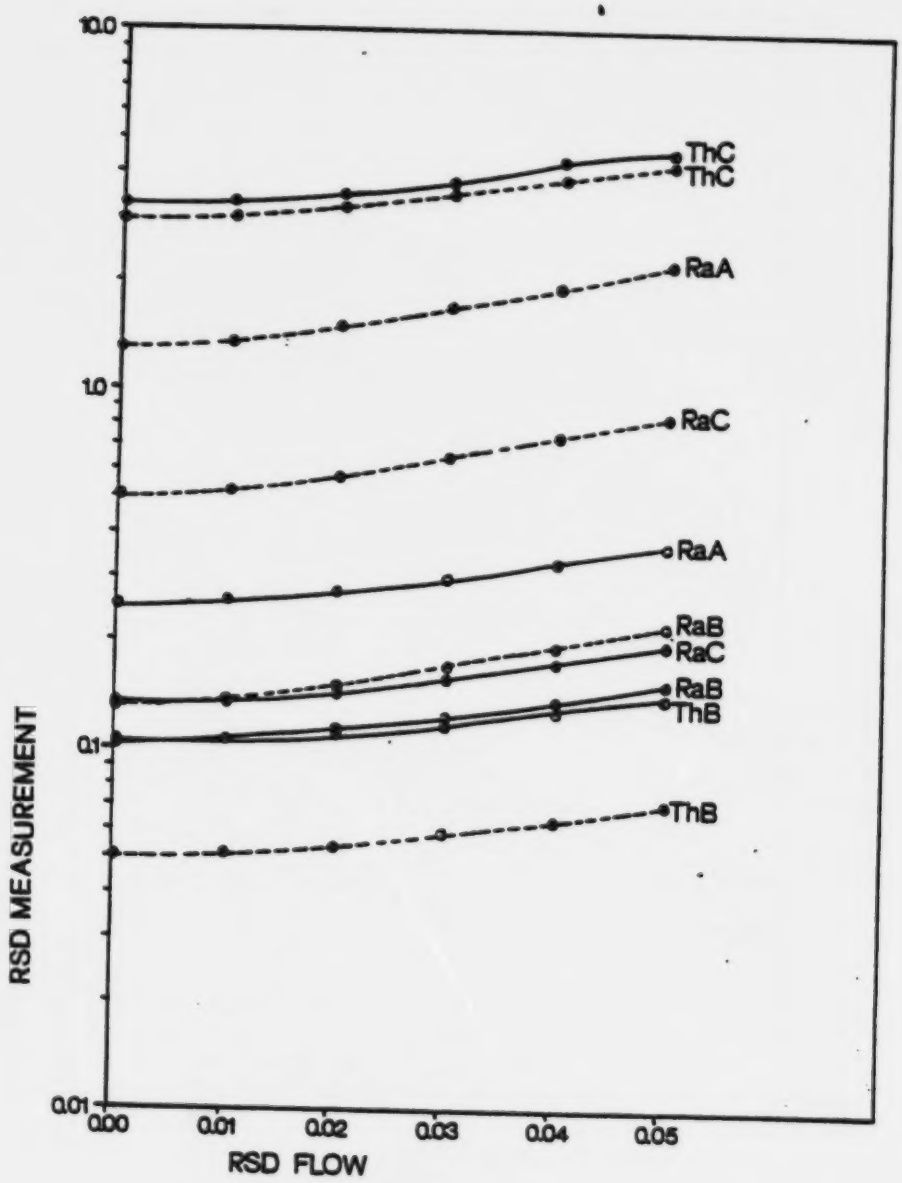

FIGURE 2. Calculated RSD measurement of radon and thoron daughters vs RSD flow for 5% fluctuation in concentration for Harley and Pasternack's method (-----) and Khan, Busigin and Phillips' method (———).

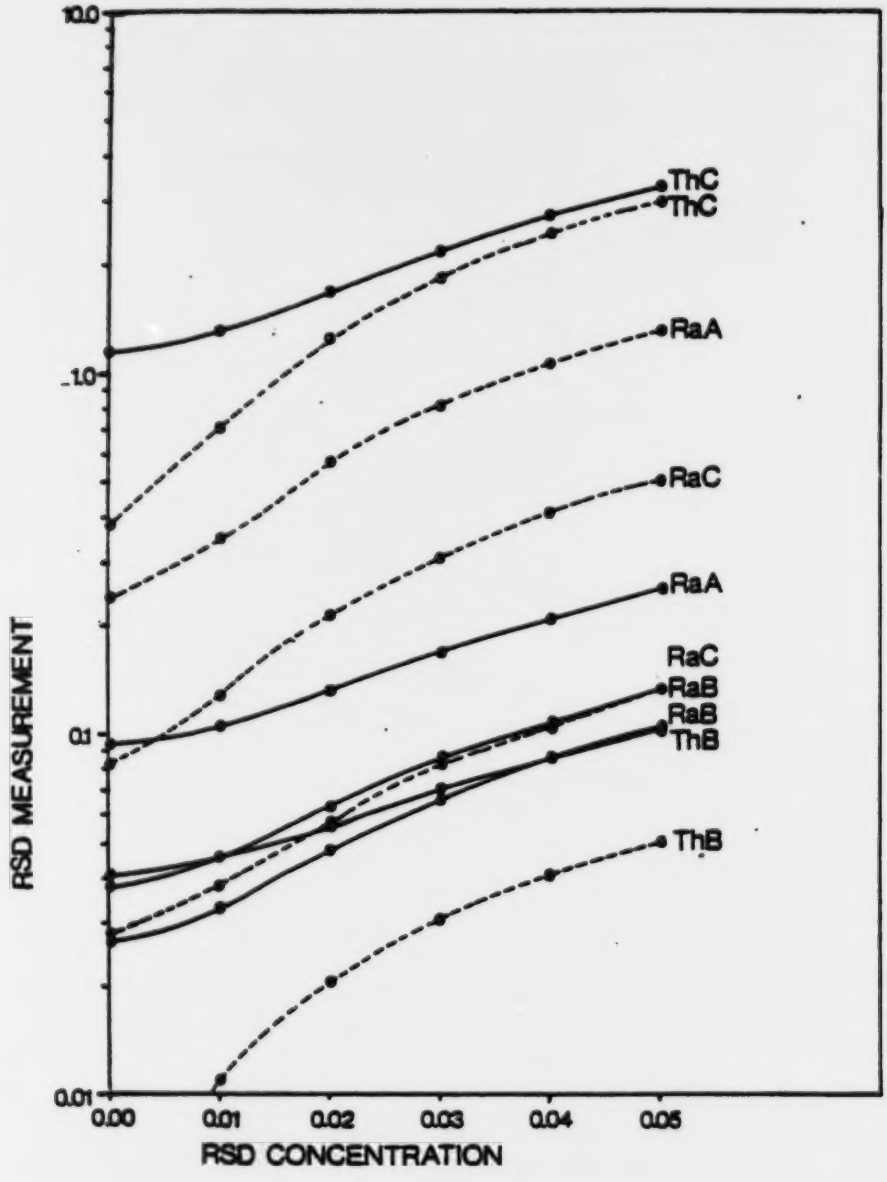

FIGURE 3. Calculated RSD measurement of radon and thoron daughters vs concentration fluctuations (RSD concentration) for no fluctuations in flow for Harley and Pasternack's method (-----) and Khan, Busigin and Phillips' method (———).

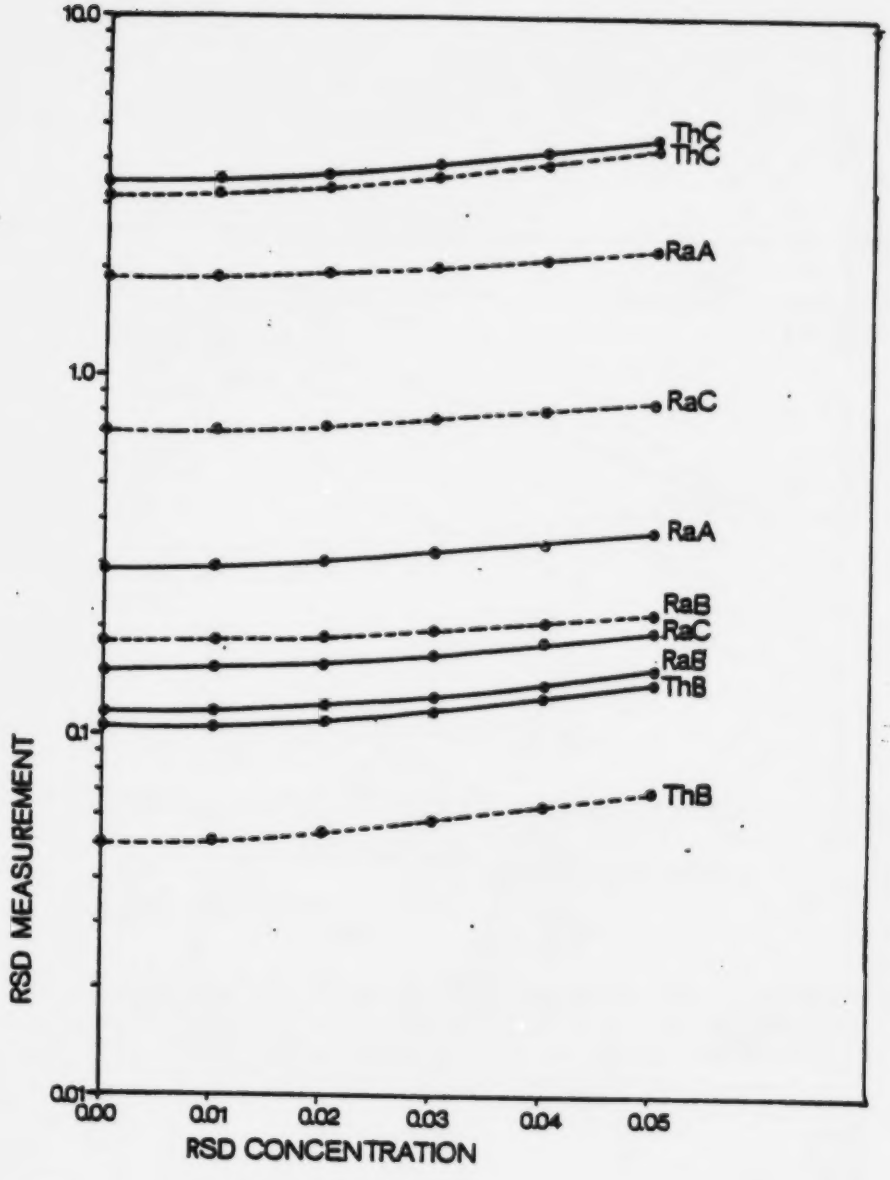

FIGURE 4. Calculated RSD measurement of radon and thoron daughters vs RSD concentration for 5% fluctuations in flow for Harley and Pasternack's method (-----) and Khan, Busigin and Phillips' method (———).

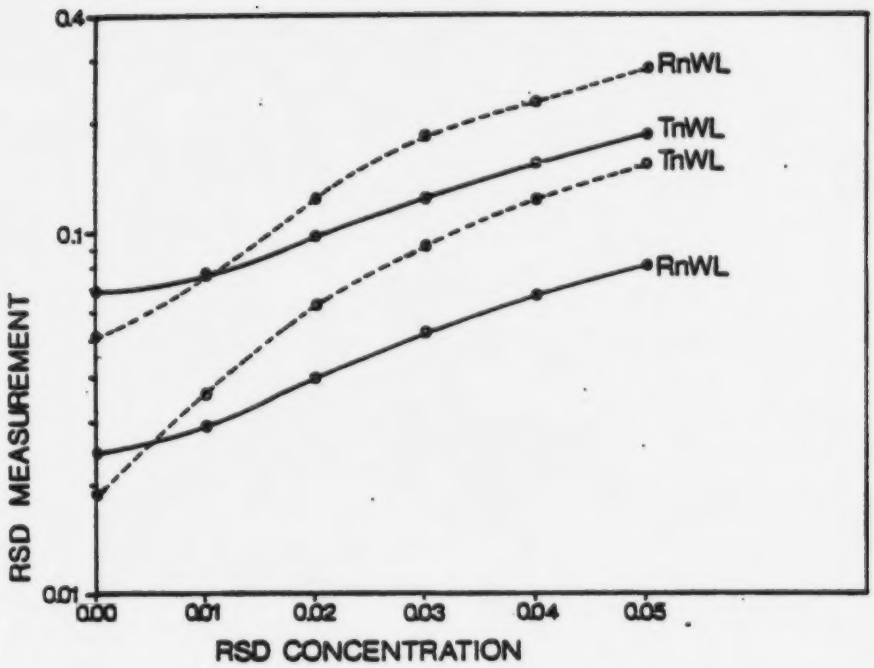

FIGURE 5. Calculated RSD measurement of radon and thoron daughter working levels vs RSD concentration for no fluctuations in flow for Harley and Pasternack's method (-----) and Khan, Busigin and Phillips' method (———).

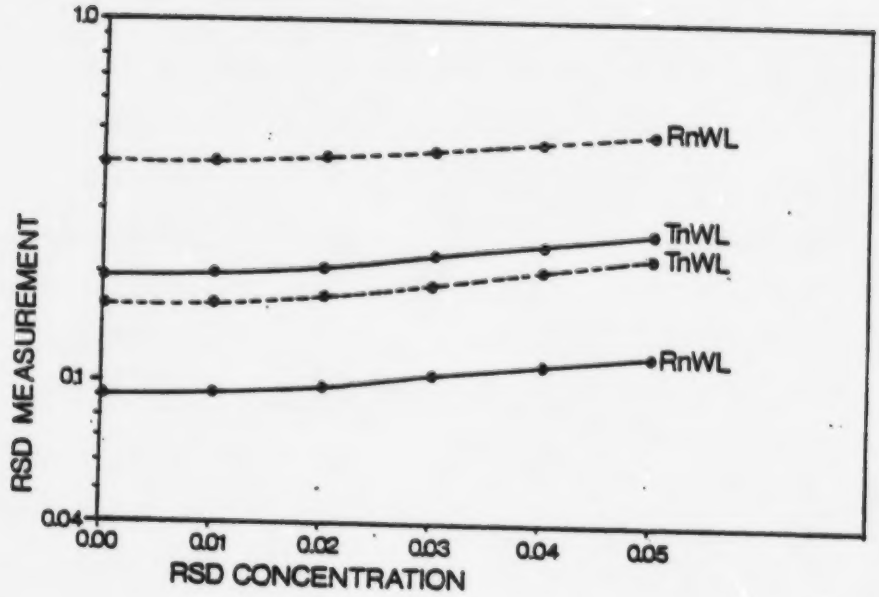

FIGURE 6. Calculated RSD measurement of radon and thoron daughter working levels vs RSD concentration for Harley and Pasternack's method (-----) and Khan, Busigin and Phillips' method (———).

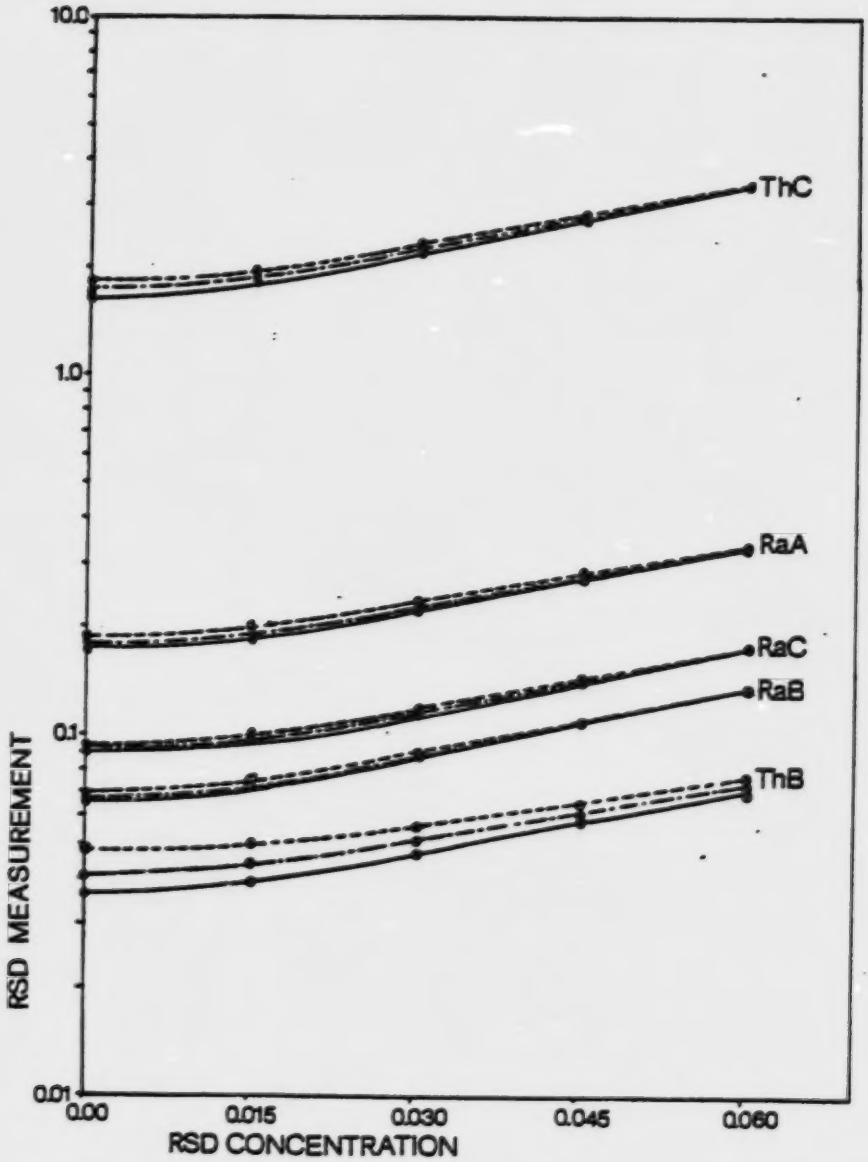

FIGURE 7. Relative standard deviations of measurement vs concentration fluctuations for 10 L/min flowrate (———), 5 L/min flowrate (—·—·—·—) and 3 L/min flowrate (– – – –) as calculated by Khan, Busigin and Phillips (in press) for 10 minute sampling - 24 hour counting.

CHAPTER 9

OPTIMIZATION OF RADON DAUGHTER MEASUREMENT TECHNIQUES

9.1 Introduction

The precision of radon daughter measurement techniques has been investigated by Martz et al. (1969) and Tremblay et al. (1979) in the case of alpha spectrometry, Raabe (1965) and Rangarajan et al. (1977) in the case of weighted least squares analysis, and Thomas (1972) and Busigin and Phillips (1980) in the case of the modified Tsivoglou method. In each of these investigations an attempt was made to optimize the precision of the measurement technique. Busigin and Phillips showed that short, widely separated counting intervals (each having fewer counts) may be better, from the point of view of precision, than longer counting intervals spaced closer together. It was also shown that optimization must be performed with respect to all the uncertainties inherent in a measurement, and not just with respect to counting statistics.

In mathematical procedures for optimizing the precision of radon daughter measurement methods, assumptions are made with respect to the independence of variables such as RaA, B and C concentration in the air (C_A, C_B, C_C) and the number of atoms of RaA, B and C (N_A, N_B, N_C) on the filter used for the air sampling, both during sampling and during the subsequent decay. The assumption of independence is made in order to be able to use the statistical "law of propagation of errors" which applies only to normally distributed, independent random variables. In the case of radon daughters, where the decay is a cascade from one radionuclide to another, one cannot in a strict sense treat the variables C_A, C_B, C_C and

N_A, N_B, N_C as independent. All previous optimizations have made this assumption of independence. Busigin and Phillips (1980) justified the assumption by using the argument that over a small range of concentration such an approximation was reasonable, at least in the case where the optimization is performed with respect to the measurement of RaA. In any case, because of the lack of any exact calculation for the precision of measurement, an approximate calculation is better than none at all. Lending further support to the assumption is the good agreement found by Busigin and Phillips between theoretical calculations and experimental results.

In principle, the errors associated with the approximation that variables such as C_A, C_B, C_C and N_A, N_B, N_C can be treated as being independent can be evaluated by comparing anlytically derived results for the precision of measurement with experimental results. In practice, however, such a comparison is difficult since the conditions under which each measurement is made must be known and be completely reproducible. Moreover, experimentation is tedious and time-consuming. In the case of the modified Tsivoglou method, 35 minutes are required for each measurement from the beginning of sampling to the end of counting.

The present work constitutes a test of the validity of the assumption of independence made in the optimization of Busigin and Phillips (1980) and employs a Monte Carlo technique rather than conventional experimentation. Monte Carlo techniques have been used successfully to simulate or carry out experiments which are otherwise tedious or even impossible to perform. Radioactive decay processes lend themselves well to Monte Carlo simulation.

9.2 Monte Carlo Simulation of Cascading Radioactive Decays

A Monte Carlo routine was set up to model the decay of RaA, RaB, and RaC. At time t = 0 min, it was assumed that the numbers of atoms of RaA, RaB and RaC present were N_A°, N_B°, N_C°. The Monte Carlo experiment was run 100 times and the numbers of atoms of RaA, RaB and RaC present at t = 1, 2, ... , 30 min ($N_A(t)$, $N_B(t)$, $N_C(t)$) were stored and then used to calculate the standard deviation in the number of atoms present at each one of these times ($\Delta N_A(t)$, $\Delta N_B(t)$, $\Delta N_C(t)$). The results of such calculations are shown in Fig. 1 for the case $N_A^\circ = 100$, $N_B^\circ = 0$, $N_C^\circ = 0$. The mean values $\bar{N}_A(t)$, $\bar{N}_B(t)$ and $\bar{N}_C(t)$ agree very well with the solutions of the Bateman equation for the system. In Fig. 1 the mean values are shown inside an envelope of 1 standard deviation.

The standard deviation in the number of atoms of RaA present as a function of time can be modelled exactly by analytical means (Friedlander et al., 1964) as

$$(\Delta N_A)^2 = N_A^\circ(1 - e^{-\lambda_A t}) e^{-\lambda_A t} \qquad (1)$$

This calculation is straightforward since the number of atoms of RaA is truly independent of the number of atoms of RaB or RaC. To model ΔN_B and ΔN_C analytically is not so straightforward since ΔN_B and ΔN_C are not independent of ΔN_A. It should be noted that equation (1) deals only with the standard deviation of the number of atoms present and does not contain any terms dealing with counting efficiency and the effect this has on the precision with which the number of atoms present at a given time can be determined. If counting efficiency, E, is less than 100% then the standard deviation in the number of atoms determined from the number of counts between 0 and t is given by (Friedlander et al., 1964):

$$(\Delta N_A)^2 = N_A^\circ(1-e^{-\lambda_A t})(1-E+E\,e^{-\lambda_A t}) \qquad (2)$$

From equation (2) it can be seen that in the case where t is much less than the half-life of the radionuclide, equation (2) reduces to

$$(\Delta N_A)^2 = N_A^\circ - \bar{N}_A(t) \qquad (3)$$

This equation is the familiar relationship where the precision of the determination of $N_A(t)$ by counting is equal to the square root of the expected number of radioactive disintegrations. It also follows from equation (3) that the standard deviation in counts is equal to the square root of the number of counts.

To show how well the Monte Carlo method agrees with equation (1), which is an exact analytical expression for RaA, the standard deviation $N_A(t)$ from Fig. 1 is compared with the calculated standard deviation in Table 1.

It can be seen that the Monte Carlo results are in good agreement with the result of equation (1). Running more than 100 Monte Carlo experiments results in even better agreement, as expected.

9.3 Application of the Monte Carlo Method to Evaluate the Precision of the Modified Tsivoglou Method

The Monte Carlo method was applied to the modified Tsivoglou method by modelling the collection and decay of radon daughters during sampling, and the decay and counting of the daughters (assuming a counting efficiency of 0.4 for α-particles) following sampling. In this way it is possible to evaluate by Monte Carlo experiment the number of counts obtained in any 3 counting intervals. These experimental counts

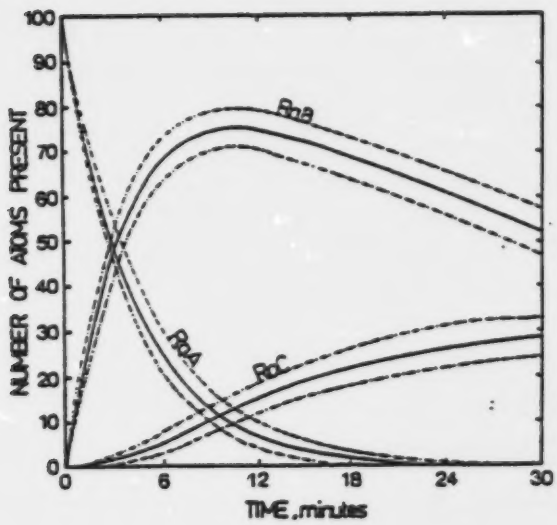

Figure 1. Decay Curves for RaA, RaB and RaC Calculated by Monte Carlo Experiments, Showing Standard Deviations ($N_A^\circ = 100$, $N_B^\circ = 0$, $N_C^\circ = 0$). Mean values (———). Envelope of on standard deviation (- - - -).

Table 1

Comparison of $N_A(t)$ Calculated by Equation (1) and Obtained from 100 Monte Carlo Experiments

Time (min)	Monte Carlo		Equation (1)	
	$\bar{N}_A$	ΔN_A	$\Delta\bar{N}_A$*	N_A
0	100	0	100	0
1	80.25	4.06	79.67	4.02
4	40.65	5.34	40.29	4.91
11	8.12	2.72	8.21	2.75
17	2.08	1.58	2.10	1.43
20	1.08	1.17	1.06	1.02
30	0.12	0.39	0.11	0.33

* $\bar{N}_A$ was calculated from $\bar{N}_A = N_A^\circ e^{-\lambda_A t}$

were then used to calculate the air concentrations C_A, C_B and C_C in order to compare them with the true mean concentration during sampling. In this way the precision of the modified Tsivoglou method was evaluated when using various counting intervals.

For the purpose of these calculations, concentration and flowrate fluctuations during a sampling time of 5 min were assumed to be zero, the air concentrations C_A, C_B and C_C were assumed to be 100, 60 and 40 pCi L^{-1} respectively, the alpha counter efficiency, E, was assumed to be 0.4 counts/disintegration, and the flowrate was assumed to be 3 L min^{-1}. A comparison of the relative standard deviations of the measured concentration of RaA, B and C as calculated by the method of Busigin and Phillips (1980) with the relative standard deviation of measurement as calculated by the Monte Carlo method from 100 Monte Carlo experiments is given in Table 2 for selected counting intervals. (With no fluctuations in flowrate and concentration during sampling, the standard deviation of the number of counts in each counting interval is assumed to be equal to the square root of the expected number of counts (Busigin and Phillips, 1980).

From Table 2 it can be seen that there is relatively good agreement for the relative standard deviation for RaA measurement, S_A, calculated by the method of Busigin and Phillips (1980) and the Monte Carlo experiments. The agreement for S_B and S_C, the relative standard deviations of RaB and RaC measurement, is poor in an absolute sense but good in a qualitative sense. The disagreement in an absolute sense probably stems from the assumption made by Busigin and Phillips about the independence of variables such as C_A, C_B, C_C during sampling and N_A, N_B and N_C during sampling and subsequent decay.

Table 2

A Comparison of Relative Standard Deviations of Measurement as Calculated by Busigin and Phillips (1980) and Monte Carlo Experiments

Counting Interval			S_A (%)		S_B (%)		S_C (%)	
			Busigin and Phillips (1980)	Monte Carlo	Busigin and Phillips (1980)	Monte Carlo	Busigin and Phillips (1980)	Monte Carlo
2-5	6-12	13-20	14.09	15.24	7.12	4.78	12.00	5.39
2-5	6-12	14-30	13.89	15.09	6.81	4.60	11.89	5.29
2-5	6-13	15-30	13.04	14.17	6.29	4.30	10.94	4.88
2-5	6-20	21-30	11.10	12.39	5.72	3.50	9.21	3.99
2-5	7-17	23-30	10.84	11.71	5.66	3.60	8.97	3.83
2-5	7-16	23-30	10.81	11.87	5.74	3.70	9.02	3.91

9.4 Conclusions

In the absence of fluctuations in flowrate and concentration during the course of measurement, the relative standard deviation of RaA measurement as calculated by the method of Busigin and Phillips (1980) agrees within 20% with Monte Carlo experiments. Their method, however, significantly overestimates the standard deviation of RaB and RaC measurement even though qualitatively there is agreement with the Monte Carlo experiments. Further work is presently under way to simulate realistic flowrate and concentration fluctuations by Monte Carlo experiment and to determine their effect on precision.

CHAPTER 10

MEASUREMENT OF CHARGED AND UNATTACHED FRACTIONS OF RADON AND THORON DAUGHTERS IN TWO CANADIAN URANIUM MINES

10.1 Introduction

The charged and unattached fractions of ^{222}Rn daughters depend upon the environmental conditions in the air in which the radon daughters are formed. To investigate the variability of the charged and unattached fractions under uranium mine conditions, measurements were made in two uranium mines at Elliot Lake, Ontario. In Mine No. 1, a non-diesel (electric) area was chosen. The area chosen was a mined out stope, downstream from a work area. The relative humidity was 100% and the temperature 13°C. No slushing was being carried out upstream. In Mine No. 2, measurements were made in the presence of diesel-operated equipment in a mined out stope having nearly stagnant air conditions. The relative humidity was 100% and the temperature 19°C.

10.2 Charged Fraction Measurements

Radon undergoes radioactive decay to form RaA (^{218}Po). A fraction of the recoil RaA atoms (approximately 30% in air at 100% relative humidity) have, upon thermalization, a positive charge (Busigin, Busigin and Phillips, 1981). Similarly, other radon and thoron daughter decay products are "born" charged. However, the charged species are neutralized through chemical and ion recombination mechanism in air (Busigin, van der Vooren, Babcock and Phillips, 1981). The charged fraction in ambient air

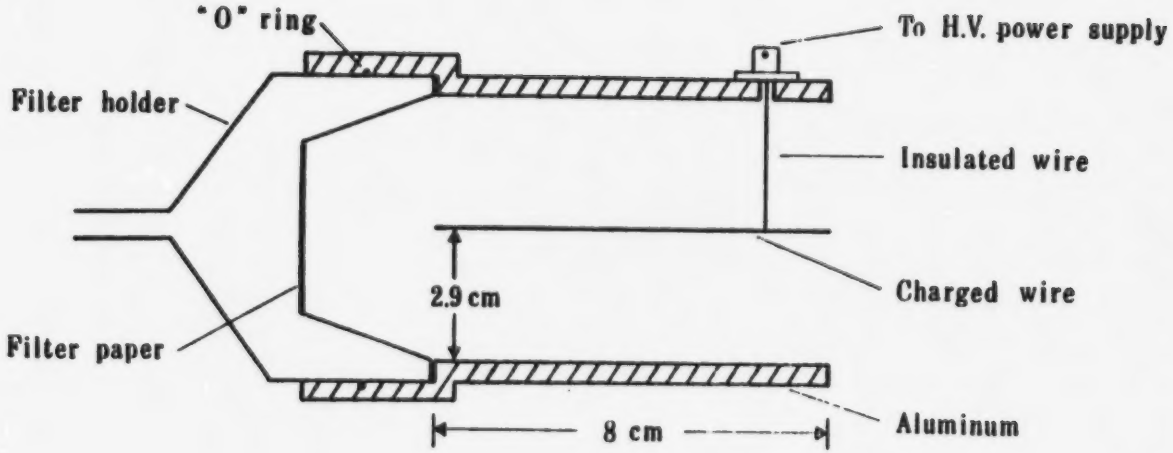

Fig. 1. Schematic diagram of cylindrical condenser used for charged fraction measurements.

will therefore depend upon the fraction of atoms that carry a charge at the end of the recoil path and the rate of neutralization in air.

For the purpose of measuring the charged fraction of radon daughters in uranium mines, two cylindrical condensers were constructed as shown in Fig. 1. Each consisted of an aluminum shell (maintained at ground potential) with an inside diameter of 5.8 cm, 8 cm long and with a wire running through the centre. To the central wire of one condenser a potential of -1000V was applied. The experiments consisted of drawing samples of air simultaneously through the two condensers (at 2 L min^{-1} for 10 min) and collecting on glass fibre filters the ^{222}Rn and ^{220}Rn daughters which passed through. The radon and thoron daughter concentrations were determined by the activity collected on the filters using an optimized modified Tsivoglou method (Busigin and Phillips, 1980). Charged fractions were determined by comparing the calculated air concentrations from the filters following the two condensers. The charged fraction measurement results for both mines are shown in Tables 1 and 2.

10.3 Unattached Fraction Measurements

The unattached fraction measurements were performed by drawing air for 10 min at a flowrate of 2 L min^{-1} through a 60-mesh wire screen backed by a glass fibre filter. The filter and the wire screen were counted in a pair of alpha-scintillation counters and the ^{222}Rn daughter concentrations determined using the optimized modified Tsivoglou method (Busigin and Phillips, 1980). ThB was determined by counting 7 to 8 hours later. For these determinations, the wire screen was assumed to collect 76% of the unattached and no attached daughters. The collection efficiency

TABLE 1

Charged Fraction Measurement Results for Mine No. 1

Date/Time	Concentration (pCi L^{-1})				Charged Fraction (%)			
	RaA	RaB	RaC	ThB	RaA	RaB	RaC	ThB
July 13th 9:12 AM	532	427	288	2.9	0.0	3.4	13.5	0.0
" " 10:30 AM	Blast occurred upstream of measurement area.							
" " 11:15 AM	550	432	353	3.4	0.0	0.0	14.5	7.2
" " 12:12 PM	403	315	214	3.2	27.0	11.1	0.0	9.7
July 14th 9:06 AM	267	224	173	2.6	0.0	6.1	9.7	22.1
" " 10:03 AM	297	247	181	2.8	16.7	11.1	0.0	20.2
" " 11:00 AM	301	208	189	2.5	10.8	2.9	1.9	3.8
" " 11:56 AM	421	217	152	2.8	13.8	3.4	4.3	6.5
Mean Value	396	296	221	2.9	9.8	5.4	6.3	10.1
Standard Deviation	114	98	73	0.3	10.4	4.3	6.2	8.5

TABLE 2

Charged Fraction Measurement Results for Mine No. 2

Date/Time	Concentration (pCi L^{-1})				Charged Fraction (%)			
	RaA	RaB	RaC	ThB	RaA	RaB	RaC	ThB
July 16th 9:50 AM	389	234	149	5.3	4.4	4.5	3.3	0.0
July 17th 7:39 AM	466	240	129	3.5	11.4	2.0	0.0	0.0
" " 8:36 AM	446	232	138	5.5	8.2	4.8	1.2	5.8
" " 9:22 AM	328	205	170	5.6	24.3	19.1	0.0	3.1
" " 10:30 AM	378	240	140	4.4	0.0	0.0	26.2	54.6
Mean Values	402	231	146	5.0	10.2	6.1	6.1	12.7
Standard Deviation	55	14	15	1.2	10.6	7.5	11.3	23.5

was determined by George (1972), by calculation assuming a particular diffusion coefficient for unattached RaA, as well as by experiments. More recent work by Busigin, Busigin and Phillips (1981), Busigin, van der Vooren, Babcock and Phillips (1981) and van der Vooren, Busigin and Phillips (1982) shows that, because of the variability of the diffusion coefficient of RaA and the collection of attached as well as unattached radon daughters by a wire screen, such measurements of unattached fraction may not be accurate to more than one significant figure.

The results of the measurements for both mines are shown in Tables 3 and 4.

10.4 Conclusions

In both diesel and electrically operated uranium mines, the charged and unattached fractions are low (<30% for charged fraction except for one measurement of ThB, and <7% for unattached fraction). Most values of the charged fraction of radon and thoron daughters were in the range 2 to 10%. Most unattached fractions were in the range of 0 to 2%. The wide scatter in the individual measurements of charged fraction reflects the difficulty of this type of measurement as well as the temporal and spatial variations in air quality conditions in uranium mines.

TABLE 3

Unattached Fraction Measurement Results for Mine No. 1

Date/Time	Concentration (pCi L^{-1})				Unattached Fraction (%)			
	RaA	RaB	RaC	ThB	RaA	RaB	RaC	ThB
July 13th 10:19 AM	308	218	152	1.3	1.6	1.1	0.9	3.4
" " 10:30 AM	Blast occurred upstream of measurement area							
" " 11:34 AM	236	192	180	1.6	3.7	0.9	0.0	0.0
" " 12:33 PM	214	150	103	1.6	1.2	0.1	1.3	0.1
July 14th 9:17 AM	218	131	68	1.2	1.8	0.9	0.9	3.9
" " 10:14 AM	122	114	84	1.3	1.1	1.6	0.4	2.5
" " 11:11 AM	161	112	84	1.2	3.9	0.4	0.0	6.7
" " 12:07 PM	234	135	68	1.3	3.2	1.4	0.0	3.1
Mean	171	150	105	1.4	2.3	0.9	0.5	2.8
Standard Deviation	83	40	43	0.2	1.2	0.5	0.5	2.3

TABLE 4

Unattached Fraction Measurement Results for Mine No. 2

Date/Time	Concentration (pCi L^{-1})				Unattached Fraction (%)			
	RaA	RaB	RaC	ThB	RaA	RaB	RaC	ThB
July 16th 10:01 AM	270	132	60	2.8	1.2	1.2	0.0	0.9
July 17th 7:50 AM	180	102	73	3.1	1.2	0.5	0.0	1.1
" " 10:41 AM	149	84	83	3.0	2.0	0.4	0.0	0.0
Mean	200	106	72	3.0	1.5	0.7	0.0	0.7
Standard Deviation	63	24	11	0.1	0.5	0.4	0.0	0.6

CHAPTER 11

THE CHEMICAL FATE OF ^{218}Po IN AIR

11.1 Introduction

The nature of the physico-chemical state of radon daughters influences their interaction with aerosols and modifies their collection characteristics and dosimetric behaviour. When ^{222}Rn gas undergoes alpha decay to form ^{218}Po (RaA), the recoil atom has initially about 110 KeV of recoil energy and is positively charged from the stripping of orbital electrons by the departing alpha particle. The recoil ^{218}Po atoms may or may not have a positive charge upon thermalization depending on the nature of the charge transfer process occurring near the end of the recoil path. After thermalization, charged species undergo neutralization reactions, and may recombine with negatively charged ions or, under certain circumstances, may remove an electron from a neutral molecule.

In this work the gas-phase chemistry of ^{218}Po is examined in terms of the collection characteristics of the charged species in an electric field. The effects of humidity on the diffusion coefficient of the neutral species, the fraction born charged, and the neutralization rate were determined in air and in argon gas-phase systems.

11.2 Experimental Investigation

A specially constructed instrument of well-defined geometry was employed to study the electrostatic collection of charged ^{218}Po species and to allow calculation of the diffusion coefficient of the neutral species, the fraction born charged and the neutralization rate and

mobility of the charged species. The instrument consisted of two parallel aluminum discs separated by a 4.4 cm thick Teflon ring of 24 cm inner diameter. The top plate was kept at ground potential and held in its centre a diffused junction silicon detector. The detector was custom designed and constructed to be flush with the plate and at ground potential on its surface in order to maintain a uniform electric field for electrostatic collection. The lower plate was operated at various electrical potentials relative to the grounded upper plate in order to collect electrostatically the positively charged species on either the upper or the lower plate. Neutral species were collected by diffusion on both plates. The instrument also contained a pressure transducer, thermometer well, septum holder and inlet and outlet valves.

The source for radon gas was a solution of radium chloride contained in a bubbler. Any gases originally present in the bubbler were initially purged using high purity (99.9995% minimum purity) argon. Extreme care was taken to avoid contamination of the instrument with impurities.

The flux of ^{218}Po species to the detector surface was measured by an alpha spectrometer, thus making it possible to separate the decays of RaA and RaC'. For each voltage studied, the count rate due to RaA was measured twice. The entire range of voltages studied was repeated at least three times in order to obtain an average value. All count rates were corrected for the decay of radon. All experiments were performed at room temperature (25-26°C). Double distilled water which had been degassed with argon to remove any O_2, etc. was injected through the septum to examine the effect of humidity.

11.3 Theoretical Model for the Collection of ^{218}Po Species in an Electric Field

The collection of ^{218}Po species in the presence of an electric field is a complex function of: E, (Vcm^{-1}), the electric field strength; H, (cm), the distance between the parallel plates; C_{Rn}, C_A, C_{A+}, (atom cm^{-3}), the concentrations of ^{222}Rn and neutral and charged ^{218}Po species; λ_{Rn}, λ_A, (s^{-1}), the decay constants of ^{222}Rn and ^{218}Po (RaA); f, the fraction of ^{218}Po species having a positive charge at the end of the recoil path; K (s^{-1}), the neutralization rate constant for positive ^{218}Po species; B, ($cm^2\ s^{-1}\ V^{-1}$), the mobility of the charged ^{218}Po species; D_A, D_{A+}, ($cm^2\ s^{-1}$), the diffusion coefficients of the neutral and charged ^{218}Po species and the temperature, pressure and chemical composition of the gaseous environment.

The transport of ^{218}Po species to the top and bottom plates occurs by both diffusive and electrostatic mechanisms. In the derivations that follow, three assumptions are made:

(i) That diffusion to the walls is negligible. (This assumption is reasonable because the distance from the centre to the walls is 12 cm, which is equal to 4.8 diffusion half lengths if one assumes a diffusion coefficient of 0.05 $cm^2\ s^{-1}$. The top and bottom plates are 0.88 diffusion half lengths away at most. The probability of a particle being able to diffuse 4.8 diffusion half lengths is 3.6%. In this case, diffusion to the top and bottom plates competes with lateral diffusion, effectively diminishing the wall effects to much less than 1%).

(ii) That diffusive transport of positive ^{218}Po species in the presence of an electric field is negligible.

(iii) That there are no negative ^{218}Po species present.

The one dimensional unsteady state transport of positively charged species in the x direction in the presence of an electric field is described by the partial differential equation:

$$\frac{\partial C_{A+}}{\partial t} = f\lambda_{Rn}C_{Rn} - \lambda_A C_{A+} - KC_{A+} + D_{A+}\left(\frac{\partial^2 C_{A+}}{\partial x^2}\right) - BE\left(\frac{\partial C_{A+}}{\partial x}\right) \qquad (1)$$

The first and second terms represent production and decay of the charged species. The third term represents neutralization of the charged species through first order reaction. The last two terms represent removal by diffusion and electrostatic collection. For positive electric fields the boundary condition which applies is: at x = 0 (lower plate); $C_{A+} = 0$.

The equation is readily solved to give:

$$C_{A+} = \frac{f\lambda_{Rn}C_{Rn}}{K + \lambda_A}\left[1 - e^{-\left(\frac{K + \lambda_A}{BE}\right)x}\right] \qquad (2)$$

The time and position dependent partial differential equation which describes the transport of the neutral species in the presence of an electric field is given by equation (3):

$$\frac{\partial C_A}{\partial t} = (1 - f)\lambda_{Rn}C_{Rn} - \lambda_A C_A + KC_{A+} + D_A\left(\frac{\partial^2 C_A}{\partial x^2}\right) \qquad (3)$$

Boundary conditions are:

At $x = 0$; $C_A = 0$

$x = H$; $C_A = 0$

Equation (3) can be solved for the steady-state situation (for positive electric fields) by substituting equation (2) and applying the above boundary conditions to yield:

$$C_A = \frac{(a_1 + a_2)\cosh\beta H - a_1 e^{-\phi H} - a_2}{\sinh\beta H} \sinh\beta x$$

$$- (a_1 + a_2)\cosh\beta x + a_1 e^{-\phi x} + a_2 \qquad (4)$$

$$\beta = \sqrt{\frac{\lambda_A}{D_A}}$$

$$\phi = \frac{K + \lambda_A}{BE}$$

$$a_1 = \frac{Kf\lambda_{Rn} C_{Rn}}{(D_A\phi^2 - \lambda_A)(K + \lambda_A)}$$

$$a_2 = \frac{Kf_{Rn} C_{Rn}}{(K + \lambda_A)\lambda_A} + \frac{(1 - f)\lambda_{Rn} C_{Rn}}{\lambda_A}$$

11.4 Calculation of Flux in a Positive Electric Field

The total flux of ^{218}Po species, N^+ (atoms cm^{-2} s^{-1}) toward the detector surface in a positive electric field is the sum of the flux of the neutral species due to diffusion and that of the charged species due to electrostatic collection:

$$N^+ = -D_A \left(\frac{dC_A}{dx}\right)_{x=H} + BE(C_{A+})_{x=H} \qquad (5)$$

Differentiation of equation (4) with respect to x and substitution of $x = H$ yields the equation for $(dC_A/dx)_{x=H}$. Substitution of this and the equation for $(C_{A+})_{x=H}$ yields the flux equation:

$$N^+ = a\sqrt{\lambda_A D_A}\ \frac{e^{-\phi H}\cosh\beta H - 1}{\sinh\beta H}$$

$$+ \frac{f\lambda_{Rn} C_{Rn}}{\phi}\left[1 - e^{-\phi H}\right] + a_1\phi D_A\, e^{-\phi H}$$

$$+ a_3 \left[\frac{\cosh\beta H - 1}{\sinh\beta H} \right] \qquad (6)$$

$$a_3 = \frac{\lambda_{Rn} C_{Rn} \sqrt{\lambda_A D_A} (K + \lambda_A - f\lambda_A)}{\lambda_A (K + \lambda_A)}$$

11.5 Calculation of Flux in a Negative Electric Field

The total flux, N^- (atoms cm^{-2} s^{-1}) of ^{218}Po species toward the detector surface in a negative electric field is due only to diffusion of neutral species and is given by equation (7):

$$N^- = -D_A \left(\frac{dC_A}{dx} \right)_{x=H} \qquad (7)$$

To obtain dC_A/dx, equation (1) must be solved for the steady state situation using the boundary condition that at $x = H$; $C_{A+} = 0$. The solution is:

$$C_{A+} = \frac{f\lambda_{Rn} C_{Rn}}{K + \lambda_A} [1 - e^{\phi(H - x)}] \qquad (8)$$

Equation (3) can be applied to the steady-state situation in a negative electric field by substituting equation (8) for C_{A+} and applying the boundary conditions:

At $x = 0$; $C_A = 0$

$x = H$; $C_A = 0$

The solution is:

$$C_A = \left[\frac{(a_1 e^{\phi H} + a_2)\cosh\beta H - a_1 - a_2}{\sinh\beta H} \right] \sinh x$$

$$- (a_1 e^{\phi H} + a_2)\cosh\beta x + a_1 e^{\phi(H - x)} + a_2 \qquad (9)$$

Differentiation of equation (9) with respect to x yields the equation for dC_A/dx. Substitution of $x = H$ into the equation for dC_A/dx provides the equation for substitution into equation (7). Thus the flux equation for negative electric fields is:

$$N^- = a_1\sqrt{\lambda_A D_A}\left[\frac{\cosh\beta H - e^{\phi H}}{\sinh\beta H} + \frac{\phi D_A}{\sqrt{\lambda_A D_A}}\right]$$

$$+\left[\frac{K\lambda_{Rn}C_{Rn} + (1-f)\lambda_{Rn}C_{Rn}\lambda_A}{\lambda_A(K+\lambda_A)}\right]\sqrt{\lambda_A D_A}\left[\frac{\cosh\beta H - 1}{\sinh\beta H}\right] \qquad (10)$$

Equation (10) can be simplified further by assuming that the neutralization rate is much higher than the decay rate, that is, $K >> \lambda_A$. This is a reasonable assumption since a typical neutralization rate constant of about 2 s^{-1} is much greater than λ_A (3.79×10^{-3} s^{-1}).

11.6 Calculation of Flux in Zero Electric Field

The total flux, N (atoms cm^{-2} s^{-1}) of ^{218}Po species toward the detector surface without an electric field is given by equation (11):

$$N = -D_A\left(\frac{dC}{dx}\right)_{x=H} \qquad (11)$$

where C is the concentration of ^{218}Po (atoms/cm^3). The diffusion coefficient for the neutral species is assumed to apply in this case. This assumption is reasonable since movement due to diffusion of charged species would be negligible. A neutralization rate constant of 2 s^{-1} corresponds to a neutralization half-life of about 0.35 s; thus predominantly neutral species are present under these conditions.

The unsteady state transport of ^{218}Po is given by:

$$\frac{\partial C}{\partial t} = D_A\left(\frac{\partial^2 C}{\partial x^2}\right) + \lambda_{Rn}C_{Rn} - \lambda_A C \qquad (12)$$

Boundary conditions are:

At $x = 0$; $C = 0$

At $x = H$; $C = 0$

The solution for the steady state situation is:

$$C = \frac{\lambda_{Rn}C_{Rn}}{\lambda_A}\left[\frac{\sinh\alpha H - \sinh(H - x)\alpha - \sinh x}{\sinh\alpha H}\right] \qquad (13)$$

where $\alpha = \sqrt{\frac{\lambda_A}{D_A}}$

Differentiation of equation (13) with respect to x and substitution of $x = H$ yields the equation for $(dC/dx)_{x=H}$. Substitution into equation (11) yields the flux equation for $E = 0$ V cm^{-1}:

$$N = \frac{\lambda_{Rn}C_{Rn}}{\alpha\sinh\alpha H}\left[\sinh^2\alpha H + (\cosh\alpha H)(1 - \cosh\alpha H)\right] \qquad (14)$$

Since flux is directly proportional to count rate, the three relationships between flux and electric field can be employed to calculate D_A, f, K/B and C_{Rn}. A non-linear least squares fitting routine in four dimensions is used to fit the theoretical curve to the experimental data.

11.7 Calculation of Electric Mobility

Since the flux equations are dependent on the ratio of K to B, the mobility of the positive species must be estimated in order to obtain an

approximate value for K. A value for B can be deduced using the results of Tyndall (1938) on the mobility of positive ions in gases. Mobility is found to be proportional to the mass term

$$\left(1 + \frac{m}{M}\right)^{1/2}$$

where M and m are the masses of the ion and gas molecule respectively. The proportionality holds for monomolecular ions in the absence of electron transfer. For thallium ions (204 amu) in argon, B = 2.05 $cm^2\ s^{-1}\ V^{-1}$. Consequently, ^{218}Po ions in argon may be estimated to have a mobility of 2.04 $cm^2\ s^{-1}\ V^{-1}$. To estimate the mobility in air, the data of Tyndall for Tl ions in N_2 can be used. Tl ions have a mobility of 2.17 $cm^2\ s^{-1}\ V^{-1}$ in N_2; consequently ^{218}Po ions in air may be estimated to have a mobility of 2.17 $cm^2\ s^{-1}\ V^{-1}$.

The presence of polar molecules such as water results in the formation of clusters by the attachment of polar molecules to the ^{218}Po ion. This clustering may reduce the mobility of the ^{218}Po ion. However, Munson and Tyndall (1939) found that the mobility of Cs (133 amu) in argon decreased only 2% in the presence of water vapour. Since ^{218}Po is a much larger ion, polar molecules will have a weaker attraction and a smaller effect on the mobility.

It should be noted that these mobility values are only estimates and that B should ideally be determined experimentally. If the positive ^{218}Po species is a molecular species (such as PoO_2^+) then the molecular radius will be substantially different and the proportionality will not hold.

11.8 Experimental Results

The effect of water vapour was studied in two gas phase systems: argon (99.9995% minimum purity) and air. Figure 1 shows the different curves obtained for various water concentrations in argon. The curves obtained for air were similar.

It is apparent from Figure 1 that the positive parts of the curves have lower plateaus at higher humidities. This result indicates that the fraction born charged decreases with increasing humidity.

The theoretical model was fitted to the experimental data as discussed previously. An example of the fit obtained is illustrated in Figure 2 using data from the ^{218}Po-air (zero water content) gas phase system. The relative standard deviation between experimental points and the theoretical curve is typically 0.80%.

Values of the diffusion coefficient for the neutral species, the fraction born charged, the ratio K/B, the approximate value for the rate constant, and the radon concentration for each gas phase system are tabulated in Table 1.

In order to determine the accuracy which can be assigned to each of the four parameters, a numerical simulation was undertaken. A control set of data (count rates) was chosen and for each count rate (which corresponded to a particular voltage), a normally distributed random number was generated assuming the standard deviation of N counts to be $\sqrt{N}$. These numbers were then made the input of the least squares fitting program. The resulting best fit values for D_A, f, K/B and C_{Rn} were recorded and the entire procedure was repeated fifty times. The standard deviation of 51 runs was used along with the mean in order to calculate

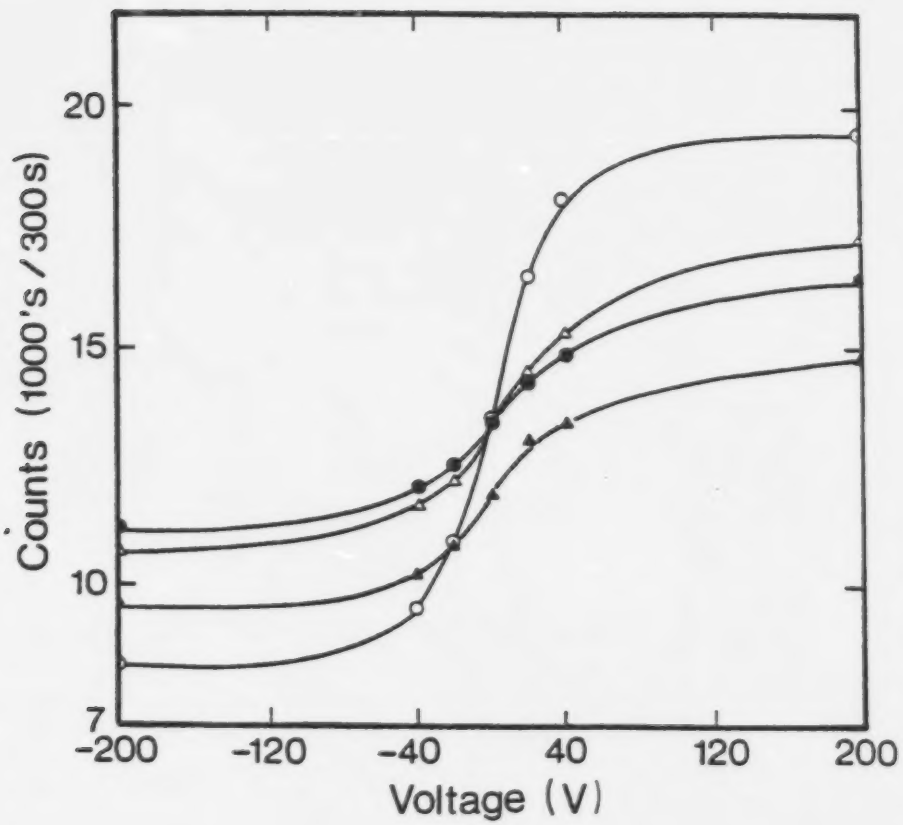

Fig. 1. The effect of water vapour in the ^{218}Po-Ar-H O gas phase system.

O - pure argon; Δ - 8% relative humidity; ● - 15% relative humidity; ▲ - 100% relative humidity.

Points shown are experimental results.

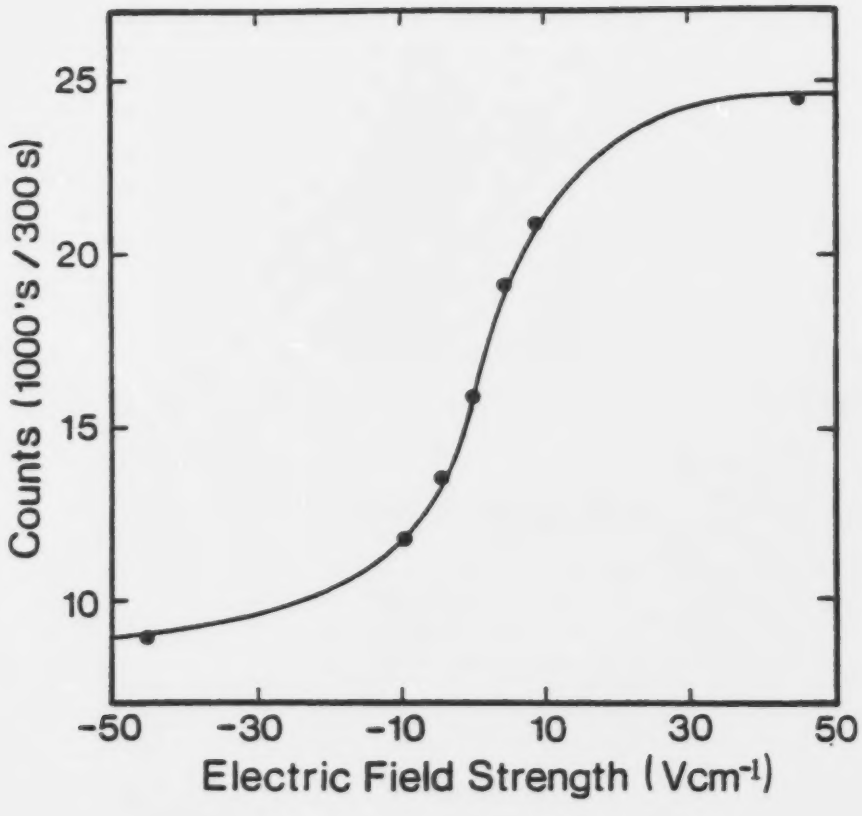

Fig. 2. Theoretical and experimental data for the ^{218}Po-Air gas phase system.

Table 1. Results of Weighted Least-Squares Fitting of Theoretical Curves to Experimental Data

Gas	H_2O Partial Pressure (mm Hg)	D_A ($cm^2\ s^{-1}$)	f	K/B ($V\ cm^{-2}$)	K* (s^{-1})	C_{Rn} (atoms cm^{-3})
Argon (99.9995% minimum purity)	0	0.101	0.405	6.05	12.34	1.069×10^6
	2.02	0.028	0.245	6.03	12.30	3.802×10^6
	3.78	0.043	0.203	6.02	12.28	2.973×10^6
	25.21	0.046	0.230	4.93	10.06	1.430×10^6
Air	0	0.048	0.513	5.54	12.03	5.297×10^6
	2.02	0.035	0.353	7.45	16.17	4.453×10^6
	3.78	0.065	0.298	5.48	11.89	2.451×10^6
	25.21	0.076	0.298	3.71	8.05	1.657×10^6

* Estimated from K/B where B = 2.04 $cm^2\ s^{-1}\ V^{-1}$ in argon and 2.17 $cm^2\ s^{-1}\ V^{-1}$ in air.

the relative standard deviation for each parameter. The resulting relative standard deviations are as follows:

f, 3.73%

D_A, 34.43%

K/B, 6.02%

C_{Rn}, 5.14%

The experimentally determined values are therefore likely to be within two standard deviations at 95% confidence.

11.9 Discussion

From the data presented in Table 1, it is apparent that the fraction born charged decreases with increasing humidity in both argon and air gas phase systems. This result indicates that neutralization must occur at or just before the end of the recoil path of the ^{218}Po ion.

Values of the ratio K/B in Table 1 may be used to examine the mechanism of the neutralization reaction. If it is assumed that neutralization of $^{218}Po^+$ species occurs primarily through recombination with negative small ions, then the neutralization rate constant, K (s^{-1}), should be proportional to the negative small ion concentration. The negative small ion concentration depends on the ionization rate within the gas phase which in turn depends on the radon concentration. The negative small ion concentration in a given volume can be determined from the solution of the following equation

$$\frac{dC_-}{dt} = \xi C_{Rn} - \gamma C_+ C_- \qquad (15)$$

where γ is the recombination coefficient of negative and positive small

ions and C_{Rn} is the production rate of negative small ions. If it is assumed that $C_+ \sim C_-$ then:

$$C_- = C_+ = \sqrt{\frac{\xi C_{Rn}}{\gamma}} \qquad (16)$$

Equation (16) implies that the negative small ion concentration C_-, and, hence, the neutralization rate, K, of $^{218}Po^+$ species should be proportional to $\sqrt{C_{Rn}}$. Therefore, assuming no change in mobility, the ratios K/B at two different radon concentrations should be related by:

$$\frac{(K/B)_o}{(K/B)_i} = \sqrt{\frac{C_{Rn,o}}{C_{Rn,i}}} \qquad (17)$$

If $C_{Rn,o}$ is fixed, then $(K/B)_i \sqrt{\frac{C_{Rn,o}}{C_{Rn,i}}}$ should be a constant if B does not change.

Figure 3 shows a plot of $(K/B)_i \sqrt{\frac{C_{Rn,o}}{C_{Rn,i}}}$ versus humidity for the argon and air gas phase systems.

Figure 3 shows that equation (17) is obeyed reasonably well at relative humidities greater than 15-20%. At lower relative humidities, this equation is not obeyed, suggesting either that the mechanism for neutralization is different, or that the mobility of the $^{218}Po^+$ species is substantially different at low humidities than at high humidities.

11.10 Conclusions

Many workers have investigated the diffusion coefficient of ^{218}Po. A recent review of the subject has been published by Busigin, van der Vooren, Babcock and Phillips (1981). The present work is an extension of that work: the diffusion coefficient of the neutral species is measured

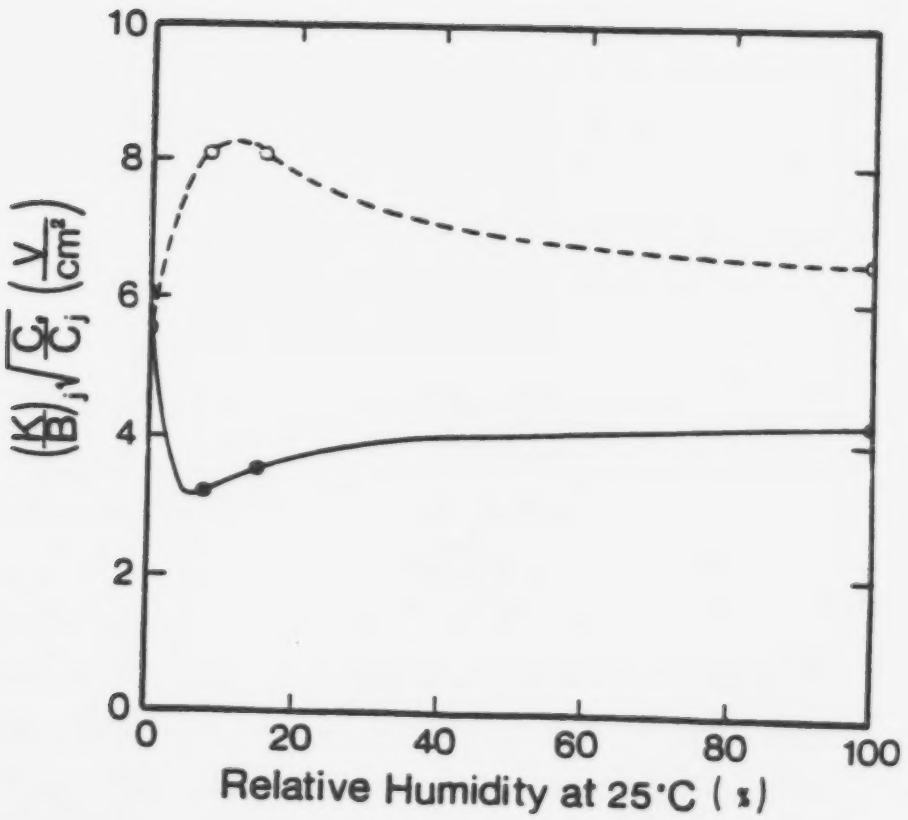

Fig. 3. Variation of $(K/B)_i \sqrt{\frac{C_{Rn,o}}{C_{Rn,i}}}$ with relative humidity. Argon (———), air (– – –).

separately from that of the charged species. A deficiency of previous work is that the neutralization rate has been discussed, but the importance of the fraction born charged has been overlooked. In the present work, the neutralization rate and the fraction born charged are determined independently.

The neutralization rate has been found to correspond to ion-ion recombination at relative humidities above 15-20% (25°C). At lower humidities, either the neutralization occurs by some different mechanism, or the mobility of charged species is substantially different. Also, the fraction born charged is highest at 0% relative humidity and decreases as the relative humidity increases.

REFERENCES FOR CHAPTER 1

Busigin, A., van der Vooren, A.W. and Phillips, C.R., 1980, "A Technique for Calculation of Aerosol Particle Size Distributions from Indirect Measuremants", Aerosol Science, Vol. 11, pp. 359-366.

Busigin, A., van der Vooren, A.W. and Phillips, C.R., 1981, "Measurements of the Total and Radioactive Aerosol Size Distributions in a Canadian Uranium Mine", Amer. Industrial Hygiene Assoc. J., Vol. 42, pp. 310-314.

Friedlander, S.K., 1977, Smoke, Dust and Haze, John Wiley and Sons. Inc., New York.

Holub, R.F. and Droullard, R.F., 1979, "The Reduction of Airborne Radon Daughter Concentration by Plate-out on an Air Mixing Fan", Health Physics, Vol. 36, pp. 497-504.

Holub, R.F. and Droullard, R.F., 1980, "Role of Plate-out in Radon Daughter Mixture Distributions in Uranium Mine Atmospheres", Health Physics, Vol. 17, pp. 761-772.

Lévêque, J., 1928, Ann. Mines, (12), Vol. 13, pp. 201-381.

Raabe, O.G. and Wrenn, M.E., 1969, "Analysis of the Activity of Radon Daughter Samples by Weighted Least Squares", Health Physics, Vol. 17, pp. 593-605.

van der Vooren, A.W., Busigin, A. and Phillips, C.R., in press, "An Evaluation of Unattached Radon Daughter Measurement Techniques, Health Physics.

REFERENCES FOR CHAPTER 2

Booth, L.F., Johnson, T.L. and Attix, F.H., 1972, "Lithium Fluoride Glow-Peak Growth Due to Annealing", Health Physics, Vol. 23, pp. 137-142.

Cooke, D.W., 1978, "The Thermoluminescence Mechanism in LiF (TLD-100): Extension of the Mayhugh-Christy Model", Journal of Applied Physics, Vol. 49, No. 7, pp. 4206-4215.

Deward, L.A. and Stoebe, T.G., 1972, "The Emission Spectrum of LiF (TLD-100) at Low and High Exposures", Physics in Medicine and Biology, Vol. 17, No. 2, pp. 187-192.

Fairchild, R.G.F., Mattern, P.L., Lengweiber, K. and Levy, P.W., 1978a, "Thermoluminescence of LiF-100: Emission Spectra Measurements", Journal of Applied Physics, Vol. 49, No. 8, pp. 4512-4522.

Fairchild, R.G., Mattern, P.L., Lengweiber, K. and Levy, P.W., 1978b, "Thermoluminescence of LiF TLD-100: Glow Curve Kinetics", Journal of Applied Physics, Vol. 49, No. 8, pp. 4523-4533.

Garlick, G.F.Y., 1949, "Luminescent Materials:, Oxford University Press, London.

Gorbics, S.G., Attix, F.H. and Pfaff, J.A., 1967, "Temperature Stability of CaF_2:Mn and LiF (TLD-100) Thermoluminescent Dosimeters", International Journal of Applied Radiation and Isotopes, Vol. 18, pp, 625-630.

Grant, R.M. and Cameron, J.R., 1966, "Effects of Preirradiation Annealing on the Thermoluminescence and Dielectric Loss of LiF:Mg", Journal of Applied Physics, Vol. 37, No. 10, pp, 3791-3795.

Halperin, A., Leibovitz, M. and Schlesinger, M., 1962, "Evaluation of Thermal Activation Energies from Glow Curves", Review of Scientific Instruments, Vol. 33, pp. 1168-1174.

Harris, A.M. and Jackson, J.H., 1970a, "On the Low Temperature Aneealing of TLD-LiF", Health Physics, Vol. 18, pp. 162-164.

Harris, A.M. and Jackson, J.H., 1970b, "Rapid Scanning Spectrometer for the Region 200-850 nm Application to Thermoluminescence Emission Spectra", Journal of Applied Physics D: Applied Physics, Vol. 3, pp. 624-629.

Hickmott, T.W., 1972, "TL and Color Centres in re-Sputtered SiO_2 Films", Journal of Applied Physics, Vol. 43, pp. 624-629.

Hill, J.J. and Schweck, P., 1955, "Experimental Study of the Mechanism of Thermoluminescence in Irradiated Sodium Chloride", The Journal of Chemical Physics, Vol. 23, No. 4, pp. 652-658.

Jackson, J.H. and Harris, A.M., 1970, "Annealing Effects and Optical Absorption of TL LiF", British Journal of Physics C: Solid State Physics, Vol. 3, pp, 1967-1970.

Klick, C.C., Chaffy, E.W., Gorbics, S.G., Attix, F.H., Shulman, J.H. and Allard, Y.G., 1967, "Thermoluminescence and Color Centers in LiF:Mg", Journal of Applied Physics, Vol. 38, No. 10, pp. 3867-3874.

Mason, E.W., McKinley, A.F. and Clark, I., "Cooling Rate Effects in Thermoluminescence Dosimetry Grade Lithium Fluoride. Implications for Practical Dosimetry", Physics in Medicine and Biology, Vol. 21, No. 1, pp. 60-66.

Mayhugh, M.R., Christy, R.W. and Johnson, N.M., "Thermoluminescence and Color Center Correlations in Dosimetry LiF", Journal of Applied Physics, Vol. 41, No. 7, pp. 2968-2976.

Milroy, P., Orton, C.G. and Seibert, J., 1973, "Low Temperature Response of LiF-Teflon Dosimeters", Radiation Research, Vol. 56, pp. 232-237.

Moran, P.R. and Podgorsak, E.B., 1971, *SAEC Report No. C001005-164.

Nicholas, K.H. and Woods, J., 1964, "The Evaluation of Electron Trapping Paramaters from Conductivity Glow Curves in Cadmium Sulphide", British Journal of Applied Physics, Vol. 15, pp. 783-795.

Pearson, D.W. and Cameron, J.R., 1966, USAEC Report No. C00-1105-123.

Podgorsak, E.B., Moran, P.R. and Cameron, J.R., 1971, "Thermoluminescent Behaviour of LiF(TLD-100) from 77° to 500°K", Journal of Applied Physics, Vol. 42, No. 7, pp. 2761-2767.

Randall, J.T. and W lkins, M.H.F., 1945, "The Study of Trap Distributions" Proceedings of the Royal Society (London) A, Vol. 84, pp. 366-390.

Townsend, P.D., Clark, C.D. and Levy, P.W., 1967, "Thermoluminescence in Lithium Fluoride", Physics Review, Vol. 155, No. 3, pp. 908-917.

Webb, G.A.M., 1967, "Fading in Thermoluminescent Lithium Fluoride after Irradiation with Low Doses", British Journal of Applied Physics, Vol. 18, pp. 7-11.

Zimmerman, D.W. and Cameron, J.R., 1964, "Determination of Trap Depths and Frequency factors for TLD-100 and 1963 Harshaw Optical Grade LiF Using Isothermal Decay of TL", TID-25160.

Zimmerman, D.W. and Cameron, J.R., 1965, "Trap Depths and Frequency Factors of Thermoluminescence Glow Peaks of Optical Grade LiF and TLD-100", USAEC Report Conf-650637.

Zimmerman, D.W., Rhymer, C.R. and Cameron, J.R., 1966, "Thermal Annealing Effects on the Thermoluminescence of LiF", Health Physics, Vol. 12, pp. 525-531.

Ziniker, W.H., Rusin, J.M. and Stoebe, T.G., 1973, "Thermoluminescence and Activation Energies in Al_2O_3, MgO and LiF (TLD-100), Journal of Materials Science, Vol. 8, pp. 407-412.

REFERENCES FOR CHAPTER 3

Christy, R.W. and Mayhugh, M.R., 1972, "TL Mechanism in Dosimetry LiF", Journal of Applied Physics, Vol. 43, pp. 3216-3217.

Gorbics, S.G. et al., 1969, "Thermal Quenching of LiF TLD Phosphors", International Journal of Applied Radiation Isotopes, Vol. 20, pp. 829-861.

Klick, C.C. Chaffy, E.W., Gorbics, S.G., Attix, F.H., Shulman, J.H. and Allard, Y.G., 1967, "Thermoluminescence and Color Centers in LiF: Mg", Journal of Applied Physics, Vol. 38, pp. 3867-3874.

Miller, L.D. and Bube, R.H., 1970, "Luminescence Trapping and F Centers in LiF Centers in LiF Crystals", Journal of Applied Physics, Vol. 41, pp. 3687-3697.

Mourad, R. and Phillips, C.R., 1981, "Investigation of Trapping Centres in Thermoluminescent Dosimetry Materials with Application to LiF:Mg", Proc. of International Conference on Radiation Hazards in Mining: Control, Measurement, and Medical Aspects, Society of Mining Engineers of AIME, Golden, CO, October 4-9, 1981 pp. 887-899.

REFERENCES FOR CHAPTER 4

Becker, K., 1972, "The Future of Personal Dosimetry", Health Physics, vol. 23, pp. 729-737.

Chapuis, A.M. Dajlevic, D., Duport, Ph. and Soudain, G., 1972, "Dosimetrie du Radon", communication presentee au Congres de Bucarest.

Jacobi, W., Haider, B., Huber, J. and Regulla, D., 1981, "A Sensitive TL-Detector for Radon Daughter Monitoring", Proc. of Int. Conf. Radiation Hazards in Mining: Control, Measurement, and Medical Aspects, pp. 846-847, Golden, CO, Oct. 4-9, 1981.

McCurdy, D.E., Schiager, K.J. and Flack, E.D., 1969, "Thermoluminescent Dosimetry for Personal Monitoring of Uranium Mines", Health Physics, vol. 17, pp. 415-422.

Pai, H.L., Jokura, K. and Phillips, C.R., 1981, "Mine Test of Thermoluminescent and Energy Discriminatory Track Etch Personal Dosimeters in Uranium Mines having Nearly Equal Concentrations of Radon and Thoron Daughters, Radiation Protection Dosimetry, vol. 1, no. 2, pp. 117-123.

Pai, H.L. and Phillips, C.R., 1977, "Design of a Personal Working Level Monitor for Use in Uranium Mines for both Radon and Thoron Daughters", in CONF-771072, Nuclear Methods in Environmental and Energy Research, pp. 441-443, Proc. of Third International Conference, October 10-13, 1977.

Phillips, C.R., Pai, H.L. and Stocker, H., 1978, "Laboratory and Uranium Mine Evaluation of the CEA Track Etch Personal Alpha Dosimeter", in Radon Monitoring, pp. 69-85, Proc. of NEA Specialist Meeting on Personal Dosimetry and Area Monitoring Suitable for Radon and Daughter Products, Paris, France, November 20-22, 1978.

Tochilin, E., Goldstein, N. and Lyman, J.T., 1968, "The Quality and LET Dependence of Three Thermoluminescent Dosimeters and Their Potential Use as Secondary Standards", in Proc. Sec. Int. Symp. Luminescence Dosimetry, Conf-680920, 1968, 424.

Zimmerman, D.W., 1972, "Relative Thermoluminescent Effects of Alpha and Beta Radiation", Radiation Effects, Vol. 14, pp. 81-92.

REFERENCES FOR CHAPTER 5

Burgkhardt, B., Herrera, R. and Piesch, E., 1976, "Fading Characteristics of Different Thermoluminescent Dosimeters", Nuclear Instruments and Methods, Vol. 137, pp. 41-47.

Weast, R.C., Handbook of Chemistry and Physics, 58th edition, CRC Press Inc., Ohio (1978).

REFERENCES FOR CHAPTER 6

Cote, P. and Townsend, M.G., 1981, "Mixtures of Radon and Thoron Daughters in Underground Atmospheres", Health Physics, Vol. 40, pp. 5-17.

Department of Science and the Environment, Australia, 1980, "Code of Practice on Radiation Protection in the Mining and Milling of Radioactive Ores".

Duggan, M.H., 1973, "Some Aspects of Hazard from Airborne Thorong and its Daughter Products", Health Physics, Vol. 24, pp. 301-310.

Jacobi, W., 1972, "Activity and Potential α-Energy of Radon and Thoron Daughters in Different Air Atmospheres", Health Physics, Vol. 22, pp. 441-450.

Kawaji, M., Pai, H.L. and Phillips, C.R., 1981, "Use of Gross Filter Activities in a Continuous Working Level Monitor", Health Physics, Vol. 40, pp. 543-548.

Ogden, T.L., 1974, "A Method for Measuring the Working Level Values of Mixed Radon and Thoron Daughters in Coalmine Air", Annals of Occupational Hygiene, Vol. 17, pp. 23-24.

Ogden, T.L., 1977, "Radon and Thoron Working Levels from Ordinary Industrial Hygiene Dust Samples:, Annals of Occupational Hygiene, Vol. 20, pp. 49-53.

Pai, H.L. and Phillips, C.R., 1977, "Design of a Personal Working Level Monitor for Use in Uranium Mines for Both Radon and Thoron Daughters" in CONF-771072, Nuclear Methods in Environmental and Energy Research, pp. 441-443, Proc. of Third International Conference, Oct. 10-13, 1977.

Pai, H.L. Jokura, K. and Phillips, C.R., 1981, "Mine Test of Thermoluminescent and Energy Discriminatory Track Etch Personal Dosimeters

in Uranium Mines having Nearly Equal Concentrations of Radon and Thoron Daughters", Radiation Proctection Dosimetry, Vol. 1, No. 2, pp. 117-123.

Phillips, C.R., Pai, H.L. and Stocker, H., 1978, "Laboratory and Uranium Mine Evaluation of the CEA Track Etch Personal Alpha Dosimeter", in Radon Monitoring, pp. 69-85, Proc. of NEA Specialist Meeting on Personal Dosimetry and Area Monitoring Suitable for Radon and Daughter Products, Paris, France, November 20-22, 1978.

REFERENCES FOR CHAPTER 7

Busigin, A., van der Vooren, A.W. and Phillips, C.R., 1978, "Attached and Unattached Radon Daughters: Measurements and Measurement Techniques in Uranium Mines and in the Laboratory", report to the Atomic Energy Control Board, AECB 1169, Dec. 1978.

Busigin, A. and Phillips, C.R., 1980, "Uncertainties in the Measurement of Airborne Radon Daughters", Health Phys., Vol. 39, p. 943.

Cote, P., Leclerc, A., Townsend, M.G. and Tremblay, R.J., 1978, "Optimization of Radon and Thoron Daughter Counting Procedures" in Radon Monitoring, pp. 109-116, Proc. of NEA Specialist Meeting on Personal Dosimetry and Area Monitoring Suitable for Radon and Daughter Products, Paris, November 20-22, 1978.

Duggan, M.H., 1973, "Some Aspects of the Hazards from Airborne Thoron and its Daughter Products", Health Phys., Vol. 24, p. 301.

Harley, N.H. and Pasternack, B.S., 1973, "Experimental Absorption Applied to Lung Dose from Thoron Daughters", Health Phys., Vol. 24, p. 379.

Pai, H.L. and Phillips, C.R., 1977, "Design of a Personal Working Level Monitor for Use in Uranium Mines for both Radon and Thoron Daughters", in CONF-771072, Nuclear Methods in Environmental and Energy Research, pp. 441-443, Proc. of Third Int. Conf., Oct. 10-13, 1977.

Phillips, C.R., Pai, H.L. and Stocker, H., 1978, "Laboratory and Uranium Mine Evaluation of the CEA Track Etch P rsonal Alpha Dosimeter", in Radon Monitoring, pp. 69-85, Proc. of NEA Specialist Meeting on Personal Dosimetry and Area Monitoring Suitable for Radon and Daughter Products, Paris, November 20-22, 1978.

Rock, R.L., 1975, "Sampling Mine Atmospheres for Potential Alhpa Energy due to the Presence of Thoron Daughters", Report IR 1015, U.S. Dept. of Interior (Mining Enforcement and Safety Administration).

Thomas, J.W., 1970, "Modification of the Tsivoglou Method for Radon Daughters in Air", Health Phys., Vol. 19, p. 691.

Thomas, J.W., 1972, "A Measurement of Radon Daughters in Air", Health Phys., Vol. 23, p. 783.

REFERENCES FOR CHAPTER 8

Bigu, J., 1980, "Radiation, Ventilation and Dust Studies at Denison Mines", EMR-Division Report MRP/MRL 80-114.

Busigin, A. and Phillips, C.R., 1980, "Uncertainties in the Measurement of Airborne Radon Daughters", Health Physics, Vol. 39, pp. 943-955.

Harley, N.H. and Pasternack, B.S., 1973, "Experimental Absorption Applied to Lung Dose from Thoron Daughters", Health Physics, Vol. 24, pp. 379-386.

Khan, A., Busigin, A. and Phillips, C.R., in press, "An Optimized Scheme for Measurement of the Concentration of the Decay Products of Radon and Thoron", Health Physics.

Loysen, P., 1969, "Errors in Measurement of Working Level", Health Physics, Vol. 16, pp. 6290635.

Pai, H.L. and Phillips, C.R., 1977, "Design of a Personal Working Level Monitor for Use in Uranium Mines for both Radon and Thoron Daughters", in CONF-771072, Nuclear Methods in Environmental and Energy Research, pp. 441-443, Proc. of 3rd International Conference, October 10-13, 1977.

Pai, H.L., Jokura, K. and Phillips, C.R., 1981, "Mine Test of Thermoluminescent and Energy Discriminatory Track Etch Personal Dosimeters in Uranium Mines Having Nearly Equal Concentrations of Radon and Thoron Daughters", Radiation Protection Dosimetry, Vol. 1, No. 2, pp. 117-123.

Strander, E., 1980, "Thoron and Radon Daughters in Different Atmospheres", Health Physics, Vol. 38, pp. 777-785.

REFERENCES FOR CHAPTER 9

Busigin, A. and Phillips, C.R., 1980, "Uncertainties in the Measurement of Airborne Radon Daughters", Health Physics, Vol. 39, pp. 943-955.

Friedlander, G., Kennedy, J.W. and Miller, J.M., 1964, "Nuclear and Radiochemistry", 2nd edition, John Wiley, N.Y., p. 175.

Martz, D.E., Hollemann, D.F., McCurdy, D.E. and Schiager, K.H., 1969, "Analysis of Atmospheric Concentrations of RaA, RaB and RaC by Alpha Spectroscopy", Health Physics, Vol. 17, pp. 131-138.

Raabe, O.G. and Patterson, F.S., 1965, "A Method of Analysis of Air Sampling Data for Particulate Alpha Emitters in a Radon-Thoron Daughters Atmosphere", USAEC Rapt. UR 658.

Rangarajan, C. Gopalakrshihnan, S. and Eapen, C.D., 1977, "The Application of Least Squares Analysis for the Estimation of Low Atmospheric Concentration of Short-Lived Radon Daughters and Studies on their Disequilibrium", Pageoph, Vol. 115, pp. 513-522.

Thomas, J.W., 1972, "Measurement of Radon Daughters in Air", Health Physics, Vol. 23, pp. 783-791.

Tremblay, R.J., LeClerc, A., Mathieu, C. and Pepin, R., 1979, "Measurement of Radon Progeny Concentrations in Air by α-Particle Spectrometric Counting During and After Sampling", Health Physics, Vol. 36, pp. 401-411.

REFERENCES FOR CHAPTER 10

Busigin, C.J., Busigin, A. and Phillips, C.R., 1981, "The Chemical Fate of ^{218}Po in Air", Proc. of Int. Conf. on Radiation Hazards in Mining: Control, Measurement and Medical Aspects, Golden, CO, Oct. 4-9.

Busigin, A., van der Vooren, A.W., Babcock, J.C. and Phillips, C.R., 1981, "The Nature of Unattached RaA (^{218}Po) Particles", Health Physics, Vol. 40, p. 333.

Busigin, A. and Phillips, C.R., 1980, "Uncertainties in the Measurement of Airborne Radon Daughters", Health Physics, Vol. 39, p. 943.

George, A.C., 1972, "Measurement of the Uncombined Fraction of Radon Daughters with Wire Screens", Health Physics, Vol. 23, p. 390.

van der Vooren, A.W., Busigin, A. and Phillips, C.R., 1982, "An Evaluation of Unattached Radon Daughter Measurement Techniques", Health Physics, in press.

REFERENCES FOR CHAPTER 11

Busigin, A., van der Vooren, A.W., Babcock, J.C. and Phillips, C.R., 1981, "The Nature of Unattached RaA (^{218}Po) Particles", Health Physics, Vol. 40, March, pp. 333-343.

Munson, R.J. and Tyndall, M.A., 1939, "The Mobility of Alkali Ions in Gases. I. The Attachment of Water Molecules to Alkali Ions in Gases", Proc. Royal Soc. A., Vol. 172, pp. 28-42.

Tyndall, R.J., 1938, The Mobility of Positive Ions in Gases, Cambridge University Press, London, pp. 36-39.

ACKNOWLEDGEMENTS

This report contains the contributions of many individuals. Major contributions were made by H. Leung (Chapters 1, 4, 5 and 6), M. Fu (Chapter 1), R. Mourad (Chapters 2 and 3), A. Khan (Chapters 7 and 8), A. Busigin (Chapters 7, 9, 10 and 11), S. Pogorski (Chapters 8 and 9) and C. Busigin (Chapters 10 and 11).

Valuable contributions were also made by R. Luymes, D. Chin and N. Busigin, particularly with respect to experimental work.

The cooperation of Denison Mines and Rio Algom mines for certain experimental work is gratefully acknowledged.

The scientific liaison of Dr. Harold Stocker of the Atomic Energy Control Board of Canada is gratefully acknowledged.